DM

Carboxylated and Aminated Carbon dots
Hydrothermal synthesis, photostability and DNA interaction studies

MASTER DISSERTATION

Ivo José Viveiros Martins
MASTER IN NANOCHEMISTRY AND NANOMATERIALS

UNIVERSIDADE da MADEIRA
A Nossa Universidade
www.uma.pt

February | 2018

Carboxylated and Aminated Carbon dots
Hydrothermal synthesis, photostability and DNA interaction studies

MASTER DISSERTATION

Ivo José Viveiros Martins
MASTER IN NANOCHEMISTRY AND NANOMATERIALS

SUPERVISOR
João Manuel Cunha Rodrigues

CO-SUPERVISOR
Helena Maria Pires Gaspar Tomás

Carboxylated and Aminated Carbon dots: hydrothermal synthesis, photostability, and DNA interaction studies

Dissertation submitted to the University of Madeira in fulfillment of the requirements for the degree of Master in Nanochemistry and Nanomaterials

by Ivo José Viveiros Martins

Work developed under the supervision of Professor João Manuel Cunha Rodrigues and co-supervised by Professor Helena Maria Pires Gaspar Tomás

Faculdade de Ciências Exatas e de Engenharia
Centro de Química da Madeira
Campus Universitário da Penteada
Funchal–Portugal

February 2018

Declaration

I hereby declare that this thesis is the result of my own work, is original and was written by me.

I also declare that its reproduction and publication by Madeira University will not break any third-party rights and that I have not previously (in its entirely or in part) submitted it elsewhere for obtaining any qualification or degree.

Furthermore, I certify that all sources of information used in the thesis were properly cited.

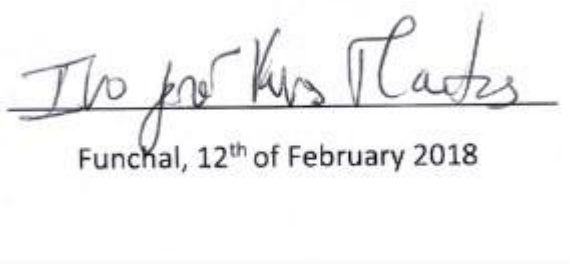

Funchal, 12th of February 2018

Contributions:

- **Oral Communications:**

1. Ivo J. Martins, Helena Tomás, and João Rodrigues. *Carboxylated and Aminated fluorescent carbon dots: Synthesis and Characterization*. Presented at the 4th CQM Annual Meeting from 3-4 February 2017 held at Madeira University, Madeira Island, Portugal and organized by CQM-Centro de Química da Madeira.

2. Ivo J. Martins, Helena Tomás, and João Rodrigues. *Aminated fluorescent carbon dots: Synthesis and Characterization*. Presented at the *1ª Reunião do Grupo do Carbono* from 12-13 June 2017 held at Biblioteca Almeida Garrett, Porto, Portugal and organized by SPQ-Sociedade Portuguesa de Química.

3. Ivo J. Martins, Helena Tomás, and João Rodrigues. *Carbon dots based on ascorbic acid: synthesis and characterization.* Presented at the 5th CQM Annual Meeting 1-3 February 2018 held at Madeira University, Madeira Island, Portugal and organized by CQM-Centro de Química da Madeira.

- **Poster Communication:**

1. Ivo Martins, João Rodrigues, and Helena Tomás. *DNA delivery and intracellular imaging nano platform based on fluorescent carbon dots and PAMAM dendrimers*. Presented at MAD-NANO16: Madeira International Conference on Emerging Trends and Future of Nanomaterials for Human Health held at Madeira Island, Portugal from 17-20 November 2016, organized by CQM-Centro de Química da Madeira.

Acknowledgements

- I acknowledge the Madeira Chemistry Research Center (CQM) for the support in the development of this Master thesis providing lab facilities, chemicals, and instrumentation. Dra. Isabel Nogueira from the MicroLab (IST) is also acknowledged for the characterization by TEM and the obtained high-quality TEM images.

- I would like to extend my thanks to the Fundação para a Ciência e a Tecnologia (FCT) through the CQM Strategic Project PEst-OE/QUI/UI0674/2013 and also ARDITI-Agência Regional para o Desenvolvimento da Investigação Tecnologia e Inovação through the project M1420-01-0145-FEDER-000005 - Centro de Química da Madeira - CQM^{+} (Madeira 14-20 Program).

- A personal acknowledgement to my supervisor Professor João Rodrigues and Professor Helena Tomás for the orientation and critical review of my work.

- I am also thankful for the team members of the Molecular Materials Research Group that helped directly or indirectly during my master thesis. A personal acknowledgement to my master colleague Gina Tavares and researcher Filipe Olim for the help and support in some of the experiments performed.

Abstract

Carbon dots (CDs) are a class of zero-dimensional nanomaterials that were discovered in 2004. Being composed mainly by carbon, spherical in shape, and with a size ranging between 1-10 nm, hold very interesting properties, such as excellent photostability, low cytotoxicity, surface functionalization and high quantum yields when compared to other fluorophores. Regarding applications, CDs already have a considerable array being used for solar cells, chemical sensing, drug and gene delivery. Specifically, CDs have demonstrated their ability to condense and transfect DNA, as demonstrated by previous works.

PAMAM dendrimers are globular molecules that hold very interesting properties for biomedical applications, especially for gene delivery. One of their versatilities is their ability to interact electrostatically with other structures, and results have shown their ability to condense and transfect DNA efficiently.

The combination between CDs and PAMAM dendrimers is not broadly considered. Therefore the preparation of a complex between CDs-PAMAM and DNA would be of great interest. The capacity of CDs to act as a fluorescent probe and to condense DNA, combined with PAMAM dendrimers to efficiently guide the complex towards the interior of the cells, could provide an interesting platform for gene delivery applications. Nonetheless, the preparation of this type of complex is highly dependent on the capacity of CDs to maintain its fluorescent properties after complexation with DNA and PAMAM, and so the impact of these interactions on the fluorescence properties should be extensively studied.

Here in, we report the synthesis of carboxyl and amine terminated carbon dots, using folic, ascorbic, and oxaloacetic acid as the main starting materials, and the hydrothermal approach as the method of synthesis. Further studies comprising quenching, pH, fluorescence stability over time, and DNA condensation were also performed. The interaction between CDs-DNA and CDs-PAMAM-NH_2 was also tested, aiming at studying the impact on the fluorescence properties of the dots. The results obtained, particularly TEM, confirm the success of CDs synthesis, and based on FT-IR and ξ-potential, two different amine-type and one carboxyl-terminated carbon dots were prepared. The carboxyl-CDs in contrast with the other two are relatively photostable and can transfect DNA almost completely. The results from the CDs-DNA interaction based on fluorescence spectroscopy, confirm the quenching effect by DNA. Lastly, the CDs-PAMAM interaction was tested using carboxyl-terminated carbon dots, and the results obtained also confirm a quenching effect by the G5 PAMAM-NH_2 on the fluorescence of CDs, and interestingly G5 PAMAM-NH_2 was able to enhance the fluorescence between 400-500 nm excitation when compared to the control.

Keywords: Carbon dots, hydrothermal synthesis, photostability, and DNA interaction

Resumo

Os pontos de carbono são uma classe de nanomateriais zero-dimensionais que foram descobertos em 2004. Sendo compostos maioritariamente por carbono, de forma esférica, e com um tamanho entre 1-10 nanometros, apresentam propriedades muito interessantes. As propriedades mais relevantes dos CDs são: excelente fotoestabilidade, baixa citotoxicidade, funcionalização de superfície e rendimento quântico muito superiores a outros fluoróforos. Em termos de aplicações, os CDs já têm uma grande diversidade, sendo usados para aplicações em células solares, sensores químicos, e para entrega de genes e fármacos. Especificamente, os CDs têm a capacidade para condensar e transfetar DNA, como demonstrado por trabalhos antecedentes. Os dendrímeros PAMAM são moléculas globulares com aplicações biomédicas, nomeadamente na entrega de genes. Uma das suas características é a capacidade de interagir electrostaticamente com outras estruturas. Resultados anteriores demonstraram que também podem condensar e transfetar DNA. A combinação entre os CDs e os PAMAM não tem sido muito estudada, pelo que a preparação de um complexo entre CDs-PAMAM-DNA é de grande interesse. No entanto, a preparação deste tipo de sistemas é altamente dependente da capacidade dos CDs em manterem as suas propriedades de fluorescência, visto que vão atuar como sonda fluorescente e, também condensar o DNA. O PAMAM irá funcionar como vetor não viral para guiar o complexo até o interior das células. Sendo assim, o impacto do DNA e dos dendrímeros do tipo PAMAM nas propriedades de fluorescência dos CDs deve ser bem estudada.

Neste trabalho, a síntese de CDs com periferia aminada e carboxílica foi feita utilizando materiais de partida como o acido fólico, o acido ascórbico e o ácido oxaloacetico, usando o método hidrotérmico. Para a sua caracterização, foram ainda realizados estudos de "quenching", pH, estabilidade da fluorescência com o tempo, e condensação de DNA. A interação entre os CDs-DNA e os CDs-PAMAM foi também ensaiada, com o objetivo de estudar o impacto desta na fluorescência dos CDs. Os resultados obtidos, particularmente de TEM, confirmam o sucesso na síntese de CDs. Com base nos resultados de FT-IR e Zeta-potencial, confirmou-se a formação de três tipos de nanopartículas de carbono, nomeadamente duas com periferia aminada e outra de superfície carboxílica. Os CDs de periferia rica em grupos carboxílicos têm maior fotoestabilidade comparativamente aos restantes e, também podem condensar o DNA quase completamente. Relativamente aos resultados obtidos da interação CDs-DNA, confirmou-se um efeito de "quenching" por parte do DNA. O mesmo resultado foi observado para a interação CDs-PAMAM (CDs com superfície carboxílica). Neste caso, o dendrímero PAMAM conseguiu diminuir a fluorescência dos CDs, confirmando a sua interação com este. Finalmente é de realçar a melhoria de fluorescência entre 400-500 nm de excitação comparando com o controlo.

Palavras-chave: Pontos de carbono, síntese hidrotérmica, fotoestabilidade, e interação DNA

Contents

List of figures

List of tables

List of Abbreviatures and Symbols

ξ- Zeta-potential
ν- Stretching vibration
δ- Bending mode
°C- Degree Celsius
0D- Zero-dimensional
1D- One-dimensional
2D-Two-dimensional
3D- Three-dimensional
AA- Ascorbic acid
ATR- Attenuated total reflectance
a.m.u.- Atomic mass units
a.u.- Arbitrary units
BSA- Bovine serum albumin
CB- Covalent bond
CDs- Carbon dots
CDs-AA- Carbon dots based on ascorbic acid
CDs-AA + 1,6-HXDA- Carbon dots based on ascorbic acid and 1,6-hexadiamine
CDs-FA- Carbon dots based on folic acid
CDs-OA- Carbon dots based on oxaloacetic acid
CDs-OA + 1,6-HXDA- Carbon dots based on oxaloacetic acid and 1,6-hexanediamine
CNs- Carbon nanostructures
CNDs- Carbon nanodots
CNHs- Carbon nanohorns
CNTs- Carbon nanotubes
CQDs- Carbon quantum dots
Da- Dalton
DMSO- Dimethyl sulfoxide
DNA- Deoxyribonucleic acid
DOX- Doxorubicin
dsDNA- Double-strained deoxyribonucleic acid
ECM- Extracellular matrix
EDTA- Ethylenediaminetetraacetic acid
Em- Emission
EPI- Epirubicin
FI- Fluorescence intensity
FRET- Förster resonance energy transfer
FT-IR- Fourier-transform infrared
g- Gram
G- Generation
G-C- Guanosine-Cytosine
GFP- Green fluorescent protein
GO- Graphene oxide
GPa- GigaPascal
GQDs- Graphene quantum dots
h- Hours
HOMO- Highest occupied molecular orbital

HXDA- Hexanediamine
LUMO- Lowest unoccupied molecular orbital
m- Meta
mmol- Millimole
Max- Maximum
MHz- Megahertz
Min- Minute
MWCT- Multi-walled carbon nanotube
MWCO- Molecular weight cut-off
NDs- Nanodiamonds
nm- Nanometer
NMR- Nuclear magnetic resonance
NPs- Nanoparticles
OA- Oxaloacetic acid
o- orto
OD- Optical density
p- para
PAMAM- Polyamidoamine
pDNA- Plasmid DNA
PDs- Polymer dots
PEI- Polyethyleneimine
PG- PicoGreen
pH- Potential of hydrogen
PL- Photoluminescence
PLL- Polylysine
POMAM-Polymethyleneamine
POPAM- Polypropyleneamine
Ppm- Parts per million
QY- Quantum yield
RF- Radiofrequency
RM- Reaction mixture
ROS- Reactive oxygen species
Rpm- Rotations per minute
RT- Room temperature
ssDNA- Single strain deoxyribonucleic acid
SQDs- Semi-conductor quantum dots
TE- Tris-EDTA: tris-ethylenediaminetetraacetic acid
UP- Ultrapure
UV-vis- Ultraviolet visible
V- Volts
VB- Valence band
XPS- X-ray photoelectron spectroscopy
ZP- Zeta-potential

Chapter 1- Introduction

Chapter 1- Introduction

1. Carbon Nanostructures and Dendrimers

This chapter is devoted to the main types of carbon nanostructures, their history, and developments as well as their composition, structure, and properties. A detailed section is dedicated to carbon dots, their discovery, description as carbon dots, composition, structure, properties, fluorescence mechanism, methods of synthesis, starting materials, types of reaction, reaction mechanism, and general applications. The field of dendrimers is also discussed with a focus on the developments, properties, and applications. The combination of PAMAM dendrimers, DNA and CDs is also discussed supported by examples from the literature. In addition, the main goals of this thesis are presented.

1.1 History and Developments of Carbon Nanostructures

The origins of Carbon Nanostructures (CNs) are related to the discovery of fullerenes in 1985 by H. Kroto, R. Smalley, and R. Curl,[1] culminating in the attribution of a Nobel Prize in Chemistry in 1996. Carbon Nanostructures refer to a wide variety of carbon allotropes that organize in different structures. Allotropy is the property of an element to arrange in two or more different forms, in the case of "carbon", it is possible for this to organize in a variety of ways. The capacity of carbon atoms to organize differently is directly related to the possibility of changing its hybridized state (sp^3, sp^2, and sp)[2]**.** CNs have fascinating properties, for instance: electric conductivity, absorption/emission of light, magnetic, and mechanical properties[3]**.** A wide range of potential applications are also ascribed: electronics, optronics, chemical sensing, catalysis, and biomedicine[4]**.**

Besides carbon nanotubes (CNTs) and fullerenes, there are other types of carbon nanostructures, *e.g.* carbon nanohorns (CNHs), nanodiamonds (NDs), graphene oxide (GO), and carbon dots (CDs). In 1952, Radushkevich and Lukyanovich published a paper describing the existence of carbon fibers (50 nm) with a hollow structure[5]. Sumio Iijima and co-workers later while working at NEC Corporation synthesized hollow carbon nanostructures and determined their crystal structure for the first time and named it carbon nanotubes[6]. In 1962, graphene was first observed by Boehm *et al.*[7] and rediscovered, isolated, characterized and described as graphene by Novoselov and co-workers in 2004, being later awarded the Nobel Prize in Physics for this achievement. Fullerenes were discovered as referred above by H. Kroto, R. Smalley, and R. Curl in 1985, the Nobel Prize in Chemistry was given 11 years later for their success[1].

1.2 Composition, Structure, and Properties

Fullerene is also known as *Buckminsterfullerene* after Richard Buckminster Fuller, a notable architect, designed a geodesic dome for Expo 67 (Montreal, Canada). The naming was appropriate since fullerene presented a similar shape. The first fullerene (the C_{60}) was discovered by H. Kroto, R. Smalley, and R. Curl in 1985 while developing a carbon project in which they believed fullerene had applications strictly in astronomy. They prepared carbon clusters through vaporization of graphite using laser irradiation, characterized by time of flight mass spectrometry and noted that a peak at 720 a.m.u (atomic mass units) had a peculiar behaviour, the peak was later attributed to C_{60} species[8]**.** Concerning the structure, fullerene is a truncated icosahedron composed of 60 atoms of carbon, with 60 vertices, 12 pentagonal faces and 20 hexagonal faces in a total of 32 faces. Each carbon atom is bonded to three others with sp^2 hybridization, giving rise to this stable cluster.

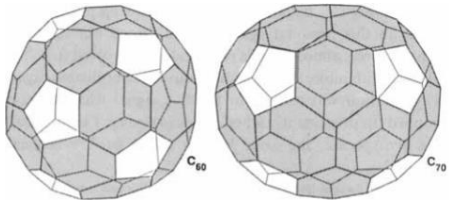

Figure 1. Fullerenes in the form of C_{60} and C_{70}. Both have a combination of hexagon and pentagon arrangements[8].

Fullerenes can be found in the form of C_{60} (most common), C_{70}, C_{76}, C_{82}, C_{84}, and C_{20} being this the smallest member of the family[9]. The properties of fullerenes are related with their unique structure and atom organization, they can act as semiconductors under specific conditions, ability to retain substances inside the cage, adsorption of free radicals, and are relatively safe and inert. Regarding applications, Jansen and co-workers[10] reported the use of fullerenes for photovoltaic solar cells. Fullerenes were paired with polymers to build a bulk heterojunction solar cell; fullerene acted as an *n*-type semiconductor (electron acceptor) and the polymer as a *p*-type (electron donor). Fullerenes might be used as catalysts for hydrogenation and hydrodealkylation as these carbon allotropes proved to be highly effective in the growth of hydrocarbon chains[11]**.** Once they can react with free radicals and decrease cell damage, fullerenes have antioxidant activity[12] and can be used to generate new copolymers with improved and specific physical and mechanical properties[13]**.**

Carbon nanotubes are cylindrical hollow nanostructures observed by Sumio Iijima in 1991[6]**.** Carbon nanotubes are composed of elemental carbon in the sp^2 form and are organized in two possible structures, single-walled carbon nanotubes (SWCNT) and multi-walled carbon nanotubes (MWCNT). Single-walled carbon nanotubes have a diameter of 1 nm, and a tube length that goes from thousands to millions of times longer. The structure of an SWCNT can be imagined as a single sheet of graphene shaped like a cylinder. The multi-walled carbon nanotubes are labeled by two distinct models: the Russian doll model and the Parchment model. The Russian doll model states that the sheets composing graphite are arranged in concentric cylinders, *e.g.,* two single-walled carbon nanotubes inside one another, as the Parchment model corresponds to graphite rolled up into herself, like rolling a newspaper[14]**.**

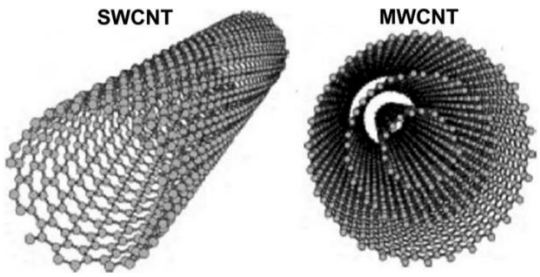

Figure 2. Structures of single-walled carbon nanotubes (SWCNT) and multi-walled carbon nanotubes (MWCNT). SWCNT corresponds to a single hollow nanotube while MWCNT to several nanotubes within different diameters[14].

A variety of properties such as: mechanical, electrical, thermal, chemical, and optical are associated to their unique structure. The mechanical properties of CNTs are related to the atomic organization, C=C bond has a large Young´s modulus in its axial direction, the value for an SWCNT is between 1-1.8 TPa, making CNTs the strongest and stiffest material yet discovered regarding tensile and elastic strength. Besides the mechanical properties, CNTs present very appealing electrical properties, the structure makes them suitable for the conduction of electricity, acting as "metal semi-conductors". The chemical properties are linked to the degree of hybridization of carbon atoms, increased curvature of a nanotube will lead to a bigger π-orbital mismatch, thus increasing the reactivity of CNTs and the covalent chemical modification increases the solubility of CNTs. Optical properties are also attributed due to theoretical studies that indicate that optical activity of chiral nanotubes disappears by increasing the nanotubes size[15]**.** Carbon nanotubes have broad applications, from catalysis and sensors to biomedical applications[16 - 18]**.**

Graphene is another carbon nanostructure with a 2D sheet of sp^2 carbon, described in the literature as the honeycomb network and the building block of 3D graphite, 1D nanotubes, and 0D fullerenes. The atomic organization in graphene allows the existence of mechanical and electrical properties. The mechanical properties of graphene are linked to the strength of the carbon bonds; graphene is the strongest material ever discovered with a tensile strength of 130 GPa, superior to the 4 GPa of A36 steel[19]**.** Graphene's electronic properties are allied with the existence of π-electrons located above and below the graphene sheet, thus making graphene an electronic conductor, ideal for applications such as photovoltaic cells and energy storage in addition to composite materials and ultrafiltration[20 - 23].

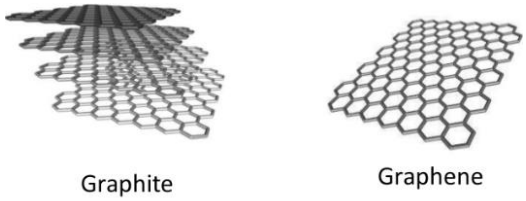

Figure 3. Structures of graphite and graphene. Graphene is a single sheet of carbon atoms organized in a hexagonal arrangement while graphite corresponds to various parallel layers of graphene interacting through Van der Waals forces[19].

Besides fullerene, carbon nanotubes, and graphene, other types of carbon nanostructures are already being explored, essentially: nanodiamonds, graphene oxide, and carbon dots. Distinctively, the latter has been receiving increased attention since its discovery in 2004.

1.3 Carbon Dots

1.3.1 Discovery and description as Carbon Dots

Carbon dots are a class of zero-dimensional nanomaterials that were first discovered in 2004 by Xu *et al.*[24] and described as quantum-sized carbon dots in 2006 by Sun and co-workers[25]**.** These carbon nanoparticles were observed in 2004 at the University of South Carolina, as SWCNTs were purified by gel-electrophoresis. The SWCNTs fragments were being separated; when they noted that a fraction of those fragments was fluorescent, after further characterization they recognized the potential of the so-called "fluorescent carbon". In 2006, Sun and associates named the fluorescent carbon as "carbon dots", important developments were also performed in understanding the possible quantum-size effects, as particles with 30-50 nm were less fluorescent than particles with a smaller size.

Carbon dots emerged as a new field since its discovery, and over the years quite a few research groups focused their work in trying to synthesize carbon dots with new methods and cheap starting materials. Meaningful advances on both reaction and fluorescence mechanisms and a growing understanding of their properties led to a new set of applications.

Carbon dots (CDs) can be found under the form of three distinct structures: graphene quantum dots (GQDs), carbon quantum dots (CQDs), and carbon nanodots (CNDs); even though the nomenclature needs to be defined, not only the nomenclature but also the type of carbon-based dot mentioned in the literature. Occasionally, researchers assume a specific structure while the characterization needs clarification. Therefore, to avoid controversies and confusion, regarding nomenclature and structure distinction, this thesis will follow the nomenclature and definitions provided by Cayuela *et al.*[26].

1.3.2 Structure, Composition, and Properties

Graphene quantum dots, carbon quantum dots, and carbon nanodots are distinct regarding structure, fluorescence mechanism, methods of preparation, and properties. Regarding structure, GQDs consist on a single crystalline sheet of graphene with sizes between 2-20 nm, shaped as a disc (quite like graphene oxide) where the internal structure is composed of sp^2 hybridized carbon and the functional groups are positioned at the surface. Regarding the structure of CQDs, they have a crystalline structure with sp^2/sp^3 carbon with a quasi-spherical shape, the range of size goes from 1-10 nm. Lastly, carbon nanodots, also recognised as polymer dots (PDs), have mostly sp^3 hybridized carbon randomly organized with an amorphous carbon core[26].

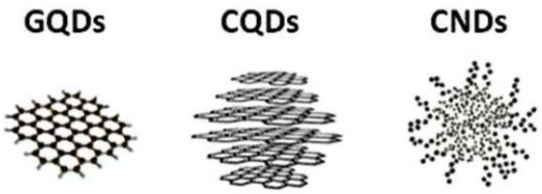

Figure 4. Graphene quantum dots (GQDs), carbon quantum dots (CQDs), and carbon nanodots (CNDs)[26].

Carbon is the key element for these nanostructures, but a certain amount of oxygen, nitrogen, and other heteroatoms like sulfur and phosphorus can also make part of the composition. The different elements that compose CDs allow the possibility of having different functional groups at the surface, *e.g.* carboxyl (-COOH), hydroxyl (-OH), amino ($-NH_2$), amide ($CO-NH_2$) and even sulfhydryl (-SH) and phosphorous ($-PO_3$) groups. Over the years, numerous research groups reported CDs with different functional groups and the importance of these in their properties[27,28].

The fascinating properties of carbon dots are related with their composition, structure, and surface defects. The properties of CDs are photostability, biocompatibility, low cytotoxicity, surface functionalization, water solubility, and high quantum yields when compared to other organic molecules, making these versatile for a diversity of applications. One of the key features of CDs is their photoluminescence(PL), although the origin and mechanism are not profoundly understood vital developments have been made to comprehend it fully[29 - 31]. The three main possibilities for their PL origins are summarized in the next section.

1.3.3 Fluorescence Mechanisms

The photoluminescence mechanism of the metal semi-conductor quantum dots is well known; it explains an electron being promoted to higher levels of energy, from the valence band to the conduction band, the succeeding results in the emission of fluorescence when the electron returns to his ground state. This type of mechanism is based on the principle that no defects or impurities bring new interstates in the bandgap. For the carbon based-dots the fluorescence mechanism is different, and two distinct mechanisms are possible. For GQDs and CQDs, an electron when returning to its ground state suffers emission trap-states, these come from the heterogeneity (different functional groups) of the particle surface as well as from surface defects. The PL mechanism for CNDs is slightly different, it comes from the superposition of assembled individual emitters, *e.g.* small fluorescent molecules that are localized at the nanoparticle surface[26]. Graphene quantum dots, and carbon quantum dots have quantum confinement, but the size-dependent PL is not fully clear. In the case of carbon nanodots, no quantum confinement is ascribed, as well as size-dependent PL. One of the aspects of CNDs is their typical broad emission bands, because of different individual emitters localized predominantly at the surface[26].

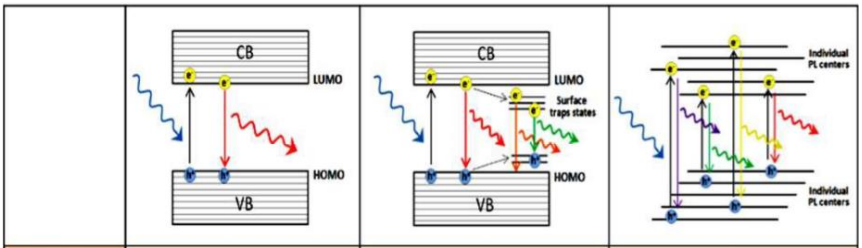

PL scheme	I	II	III
Nanodot Type	SQDs	CQDs / GQDs	CNDs
Characteristics	Quantum confinament	Quantum confinament	No quantum confinament
	Size-dependent PL	Size-dependent PL (no clear)	Size-independent PL
	Excitation-independent PL	Excitation-dependent PL	Excitation-dependent PL
	Narrow PL band	Broad PL band	Very broad PL band
	Long lifetimes	Medium lifetimes	Short lifetimes

Figure 5. Scheme of the different photoluminescence mechanisms for semi-conductor quantum dots (SQDs), carbon quantum dots (CQDs), graphene quantum dots (GQDs), and carbon nanodots (CNDs) and their common characteristics[26].

1.3.4 Methods of Synthesis and Starting Materials

The synthesis of GQDs, CQDs, and CNDs relies on a diversity of methods either from the top-down or bottom-up approach. The top-down methods for CDs synthesis are typically: laser ablation[32], electrochemical method[33], and plasma treatment[34]**.** Using the bottom-up approach, different methods, *e.g.,* pyrolysis, microwave, ultrasounds, combustion, and reverse micelle method, including the hydrothermal and the solvothermal method, are used[35 - 41]. The methods of synthesis are frequently chosen based on the type of carbon-based dot desired. GQDs can be obtained mainly by using top-down approaches with graphite-based constituents as the starting materials. CQDs can be synthesized mostly by using the bottom-up approach (hydrothermal and pyrolysis) with small organic molecules subjected to elevated temperatures (over 200 ^{o}C), whereas CNDs (polymer dots) synthesis relies on temperatures between 100-200 ^{o}C and using small organic compounds as starting materials.

Regarding starting materials, a considerable diversity of compounds is used for CDs synthesis. The typical compounds in our laboratory shelves can be used, as well as ‘‘natural’’ starting materials (table 1).

Table 1. Starting materials used for the synthesis of CDs (top-down and bottom-up approach).

Synthetic route	Precursor	Synthetic method/General conditions
Top-down	Solid Carbon	Laser ablation: with 1064, 532, and 355 nm[32]
	Graphite rod	Electrochemical exfoliation: 60 V potential[33]
	D-fructose	Plasma treatment[34]
Bottom-up	PAMAM dendrimers	Hydrothermal: 200 ^{o}C for 5 hours[42]
	Citric Acid/PEI	Hydrothermal: 100 ^{o}C for 2 hours[43]
	Chitosan	Pyrolysis: 300 ^{o}C for 2 hours (heating rate 5 ^{o}C/ min, N_2 atmosphere)[44]
	Phenylenediamine (o, m, p)	Solvothermal: 180 ^{o}C for 12 hours[45]
	Papaya	Hydrothermal: 200 ^{o}C for 5 hours[46]
	Date molasses	Microwave: 1000 W for 3 minutes[47]
	Urine	Pyrolysis: 200 ^{o}C for 12 hours[48]
	Potatoes	Hydrothermal: 170 ^{o}C for 12 hours[49]
	Orange juice	Hydrothermal: 120 ^{o}C for 150 minutes[50]
	Cow manure	Reflux: in Nitric Acid for 72 h[51]
	Pomegranate	Hydrothermal: 170 ^{o}C for 12 hours[52]
	Hair	Pyrolysis: 200 ^{o}C for 24 hours[53]

1.3.5 Types of Reaction

CDs synthesis relies on a diversity of methods, and according to the starting material and method, the formation of carbon dots may experience varied steps.

The top-down approach usually relies on large starting materials, *e.g.,* graphite, charcoal, and candle soot, these are decomposed, exfoliated, and mechanically disturbed until reaching a nanoscale size. For instance, carbon dots can be produced from graphite rods through electrochemical exfoliation in water. In this case, water acted as an electrolyte by applying a 60 V potential to the graphite rods solution. Positively and negatively charged ions were inserted inside graphite leading to the release of single and few layers of graphene with sizes ranging between $2 - 20$ nm, the so-called graphene quantum dots (GQDs)[33]**.** In another approach, and applying the laser ablation method, a carbon target was inserted in pure acetone, and a laser with 1064, 532, and 355 nm was activated for a certain time, thus producing CDs. Concretely, the laser beam allowed the ablation of the carbon target, the target surface absorbed the energy of the incident beam, heating and removing small fragments of carbon through evaporation, the small particles were collected in solution[32]**.**

The synthesis of carbon dots from the bottom-up approach relies on small molecular precursors, *e.g.,* aromatic, aminated, carboxylated, and hydroxylated compounds. The hydrothermal method is the most

common method and consists on water as a solvent and takes advantage of the closed system for the reaction to occur in harsh conditions, regarding pressure and temperature. Zhu *et al.*[54] synthesized carbon dots using citric acid and ethylenediamine, the formation of CDs was achieved due to a condensation reaction between the citrate ion and the amine precursor, with further polymerization and carbonization at 200 ^{o}C for 5 hours[54]. In another approach using the same method, with citric acid and amine precursors as the starting compounds, it was possible to generate N-doped GQDs. The formation of N-GQDs occurred due to the formation of a graphene structure (by dehydration reaction), followed by doping of the amine precursors on the surface. These amine precursors interacted with carboxylated and hydroxylated groups, generating amide and pyrrolic structures[55]. Using the same method, the synthesis of S-CDs was possible due to a polymerization reaction of thioacetamide precursors, followed by a nucleation process and growth of the CDs doped with sulphur atoms[56].

1.3.6 General Applications

Carbon dots have an impressive set of applications which are associated with their unique and astonishing properties. CDs are used for chemical sensing, biomedical applications, and supercapacitors. Aiming supercapacitor applications, a nanocomposite between CDs and RuO_2 was developed, and the results showed an excellent rate capability and interesting cycling stability. The hybrid network allowed the rapid charge transport and ionic motion during the charge-discharge process, resulting in rapid redox reactions[57].

Chemical sensing applications are particularly focused on heavy metal and chlorine detection. Monitoring the fluorescence intensity before and after quenching allows assuming the sensing properties. A considerable amount of work is mainly devoted to the detection of unwanted species in water, heavy metal and halogen detection is of great interest since these are related with several health problems[58 - 59]**.** Ding and co-workers[60] announced the use of CD-Rhodamine B conjugates to detect chlorine in water, the decrease in fluorescence intensity and significant color changes were indicative of chlorine detection[60]. Cobalt, and mercury ions were also sensed by CDs and tested in real lake and tape water[61,62].

Among the applications in chemical sensing, a considerable amount of work is dedicated to biomedical applications, expressly for gene and drug delivery as well as biosensing. Carbon dots have been used for gene delivery purposes, as it was reported the conjugation between CDs and PEI with the purpose of DNA delivery[63]. In addition to gene delivery, carbon-based dots can also be used for drug delivery applications. Doxorubicin (an anti-cancer drug) was combined with CDs and bovine serum albumin (BSA) to build a drug delivery system; the loading of DOX into CDs was 86 %, and the release was pH-dependent, the results exposed a 4% and 12% release for pH 5.8 and 7.2, respectively[64].

Biological sensing is related to the detection of metal ions, proteins, sugars, DNA, and others in biological systems. In that sense, Li *et al.*[65] used CDs to hybridize with ssDNA and generate dsDNA[65]. Reactive oxygen species (ROS) were also sensed by CDs, namely NO species. Concretely, CD-based sensor accepted energy leading to a fluorescence color change from blue to green[66]. The examples reported for gene, drug, and biosensing applications serve as examples from the hundreds already published.

1.4 Dendrimers

1.4.1 History and Developments

Dendrimers are polymers which were first synthesized by Fritz Vögtle in 1978 through a divergent method. These special polymeric molecules are globular in shape and exhibit a certain number of functional groups at the surface according to its generation.

The synthesis of dendrimers by Vögtle was achieved by starting with primary monoamines and diamines reacting with acrylonitrile, this led to the formation of a dinitrile, with further hydrogenation and resulting in a diamine[67].

Dendrimers have their own system of classification and nomenclature, the ‘‘Newkome rules’’[68], and three distinct types of dendritic molecules are possible: dendrimers, cascadanes, and hyperbranched molecules. Dendrimers have an ‘‘almost perfect’’ structure, while cascadanes are regularly branched and

regarding structure are defect-free; lastly, the hyperbranched molecules are not perfect structures and show a considerable polydispersity regarding molecular weight.

Dendritic molecules are molecular architectures characterized by the following terms: core, which is the central unit and the building block of the dendrimer; generation, regular layers like onion skins; dendron, branched structures linked in the form of segments to the central unit, and end groups (surface functional groups) which are located at the surface of the dendrimer. The chemical nature of the terminal groups determines the shape, stability, conformational flexibility, and viscosity. If the number of generations increases, the number of end groups increments, and the viscosity declines when compared to lower generations. This phenomenon is related with the globular shape that the dendrimers adopt at bigger generations, while the smaller generations of dendrimers have an open-branched structure, decreasing the capacity of solubility[67].

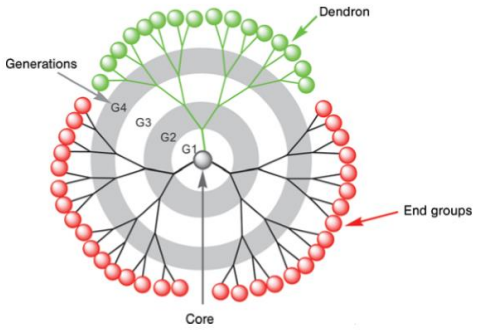

Figure 6. Dendrimer nanoarchitecture, composed of three dendrons, 4 generations, and 48 terminal groups[67].

Quite a few approaches can be used to synthesize dendritic molecules, but the divergent and convergent methods are the most widely used. Employing the divergent method (core-periphery), a core building block reacts with a small dendritic branch, these dendritic branches are further activated to serve as new reactive sites for further branching units. In the case of the convergent method (periphery-core), the branching units are synthesized separately from the core (growing in terminal groups), with the last step belonging to the attachment of the branching units to the core building block[67].

1.4.2 Main types of dendrimers families (PAMAM)

Numerous types of dendrimers, *e.g.,* polypropyleneamine (POPAM), polyamidoamine (PAMAM), polymethyleneamine (POMAM), Polylysine, among others, compose the dendrimers family. Particularly, PAMAM (polyamidoamine) dendrimers are composed of a trifunctional core unit, nitrilotripropionamide, and have tertiary amines, amide groups, and peripheral primary amines in their structure. PAMAM dendrimers have an average size between 2-10 nm depending on the dendrimer generation. The properties of PAMAM dendrimers are uniform size, controlled molecular weight (different generations), water solubility, surface functionality, and empty internal cavities. These properties allow a set of applications[67].

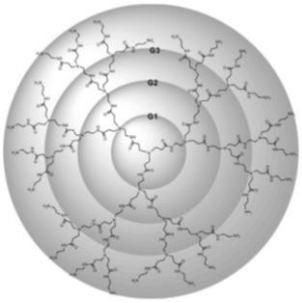

Figure 7. G3 PAMAM dendrimer. (3 generations and 24 primary amine end groups)[67].

Applications involving dendrimers are majorly for biomedical purposes, with focus on gene and drug delivery[69]. Concretely, two distinctive characteristics of PAMAM dendrimers are often seen has crucial for gene and drug delivery: the surface functionality (electrostatic interaction or covalent bonds) and the capacity of PAMAM dendrimers to carry cargo in the interior and on the periphery, these modifications are essential to decrease the surface positivity of the dendrimers and consequently attenuating the toxicity towards cells.

1.5 Carbon Dots-PAMAM and DNA interaction

As mentioned in sections 1.3.2 and 1.4, CDs and dendrimers carry unique properties that can be used for a diversity of applications, including biomedical applications, with emphasis on gene delivery. CDs are fluorescence emitters, show low cytotoxicity and high surface functionality in addition to other properties. Likewise, PAMAM dendrimers show surface functionality, among their capacity to load cargo either in the interior or periphery.

Carbon dots can be easily functionalized as demonstrated by diverse research groups[70]**.** Along with their synthesis, various moieties are attached to the carbon core, thus presenting a certain degree of functionalization. Varied types of surface functional groups, *e.g.,* carboxyl, hydroxyl, amide, primary amines, phosphate, and even sulfhydryl groups, could be on the edge of CDs, depending on the application. Other types of structures were also reported on the surface, for instance: polymers, proteins, and DNA[71]. Based on the characteristics and versatility of these two nanomaterials, the interaction between carbon dots and PAMAM dendrimers constitutes a research opportunity. The interaction will depend on the CDs surface functional groups since PAMAM dendrimers are positively charged once they are amine-terminated. CDs-PAMAM interaction would be of electrostatic nature, negatively charged CDs, with -COOH or -OH surface groups, would interact electrostatically with the positively-charged amine PAMAM groups.

Based on the large experience achieved by our group on the dendrimers field, namely for drug and gene delivery[72,73], is normal to have as our main goals, the conjugation of PAMAM dendrimers and CDs for biomedical applications (*e.g.* gene delivery). Also, we guess it would also be possible the use of positively or negatively-charged carbon dots to build the complex. The role of CDs would be to operate as a fluorescent probe and to condense DNA, a key component, acting as a linker by electrostatic interaction. DNA-CDs and PAMAM dendrimers would then build the final conjugate, with PAMAM acting as a non-viral vector to guide the complex towards the interior of the cells.

Importantly, when considering the interaction between carbon dots-DNA and carbon dots-PAMAM is the impact on the fluorescence properties. Regarding carbon-DNA conjugation, the interaction between a carbon nanomaterial and DNA is governed by distinct types of forces, *e.g.* π-π conjugation, hydrogen bonding, and van der Waals forces. The nucleobases tend to lie parallel to the carbon rings of graphene sheets and CNTs through π-π interaction[74]. Another aspect when dealing with DNA is the fact that is of polymeric nature, and so, steric effects may hinder the interaction of the nucleobases with the carbon rings.

In the literature, the conjugation between carbon dots and DNA has been studied, as Feng and co-workers[75] used photoluminescent spermine-carbon dots to induce B-Z DNA transition under specific salt conditions**.** They also found that spermine terminated carbon dots would preferentially bind to the G-C pair. In another work, Qian[76] and associates built a DNA sensor based on graphene quantum dots and carbon nanotubes, the effective nanosensor was based on the FRET and distinguished complementary and single-based mismatch nuclei acid sequences**.** Lu *et al.*[77] studied the complexation and intercalation between graphene quantum dots and DNA and found that GQDs would intercalate in the base pairs of DNA. The reported papers serve as examples from some already published. Meaningfully, the graphene quantum dots seem to be the preferred for DNA interaction, in contrast to the carbon quantum dots and carbon nanodots structure. The GQDs are favoured because they possess a crystalline single-sheet like graphene, and therefore are ideal for π-π conjugation, the others are spherical, and the interaction with DNA would be highly dependent on the type of functional groups on the surface. Since one of our objectives is the preparation of

spherical carbon dots with amine and carboxyl terminations, we wonder if the dots can complex with DNA, and what impact would have the complexation on the fluorescent properties.

Concerning CDs-PAMAM interaction, a few research groups already studied the complex formation and their properties. For instance, Zong *et al.*[78] reported that the combination of CDs with PAMAM dendrimers and AuNPs, enhancing the photoluminescence of carbon dots, as PAMAM dendrimers served as a spacer between AuNPs and CDs, the interlayer distance allowed the PL improvement of the CDs. In another study, Matai and co-workers[79] merged PAMAM dendrimers with CDs for drug delivery applications. The PAMAM-CDs conjugates served as a platform for the delivery of an anticancer-drug EPI (Epirubicin, a DNA intercalator). More recently, Campos *et al.*[80] reported the junction of PAMAM dendrimers with CDs and based on fluorescence quenching, the detection of chloroplatinate ions in solutions containing platinum nanoparticles was possible. Lastly, Ngu-Schwemlein and collaborators used CDs as a molecular scaffold for conjugating small dendritic structures (polyamidoamine) to act as carriers of small hydrophobic antibiotics and to enhance the uptake, increasing antibacterial action[81]**.**

As demonstrated by the small number of papers reported, the combination of PAMAM dendrimers and CDs is not extensively considered, and the lack of emphasis on gene delivery applications regarding these nanomaterials constitutes an opportunity to explore that relation.

1.6 Objectives

The aim of this master project was the synthesis of CDs (carboxylated and aminated terminal groups) based on the hydrothermal method, by using starting materials rich in carboxyl, hydroxyl, and amino groups. The second goal was the preparation of a PAMAM-CDs and DNA nanohybrid and lastly, biological studies comprising cytotoxicity, transfection efficiency, and intracellular imaging. A summary of the main goals and a schematic illustration are presented in figure 8. In the scheme of figure 8, the PAMAM-NH_2 dendrimer, carbon dots, and pDNA are not in scale. The structures were adjusted for visualization purposes only.

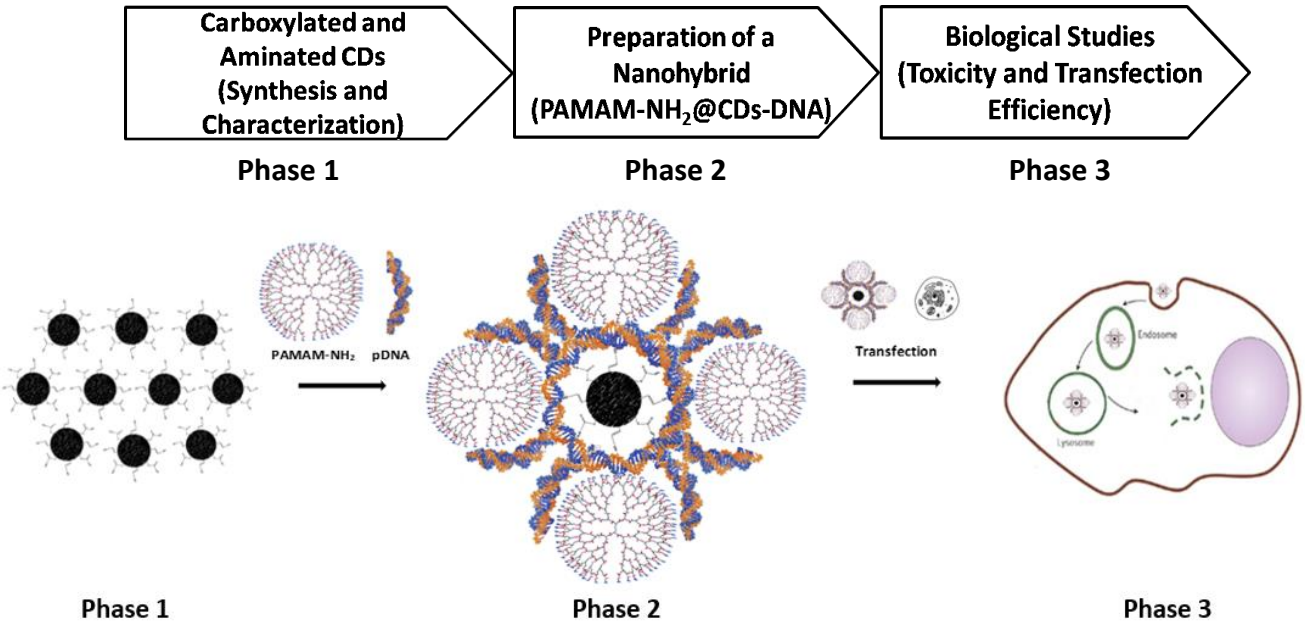

Figure 8. Schematic representation of the objectives of the work. **Phase 1**- Synthesis and characterization of carboxylated and aminated CDs; **Phase 2**- Preparation of a nanohybrid (PAMAM-NH_2@CDs-DNA) and **Phase 3**- Biological studies (Toxicity and transfection efficiency).

Chapter 2-Experimental

Chapter 2-Experimental

This chapter is dedicated to the experimental part of the work. The contents are divided by sub-chapter and comprise chemicals, instrumentation, protocols regarding synthesis, characterization, and different studies on CDs, CDs-DNA and CDs-PAMAM interactions.

2.1 Chemicals and Material

The chemicals and reagents used were Pyrene (99 %), Folic and Oxaloacetic acid (97% and 98% purity, respectively) from Sigma-Aldrich; Cyclohexane purchased from VWR Normapur; L-Ascorbic acid from TCI Chemicals; 1,6-Hexanediamine (99,5%) from Merck; and deuterated Dimethylsulfoxide-D6 (99,80%) bought from Acros Organics; Sodium and Potassium chloride from Fisher; Disodium and monopotassium phosphate purchased, and Potassium iodide from PanreacApplichem and Sodium hydroxide from Fisher. Dialysis membrane (cut off: 500-1000 Da) was obtained from Spectra Labs; double-strain DNA from salmon origin was acquired in Sigma-Aldrich; PicoGreen for DNA assay obtained in Intrivogen, and G5 PAMAM-NH_2 bought in Dendritech Inc. The plasmid DNA used in the DNA condensation studies was extracted from bacteria. The ultrapure(UP)-water used throughout the work was filtrated by a Milli-Q direct water purification system from Merck.

2.2 Instrumentation

The instrumentation used in the characterization was the Zetasizer Nano ZS equipped with a He-Ne laser (633 nm) from Malvern Instruments; Attenuated Total Reflectance FT-Infra Red Spectrometer from Perkin-Elmer; Fluorescence Spectrometer (LS55) from Perkin-Elmer; UV-Vis Spectrophotometer (Lambda 25) from Perkin-Elmer; UV-chamber from CAMAG (366 nm λexc); 400 MHz NMR (UltraShield™ 400 Plus ULTRA LONG HOLD) from Bruker; TEM equipment (Hitachi H-8100), equipped with thermionic emission LaB_6 and 200 kV acceleration voltage; Ultra-freezer (-86 ^{o}C) from Sanyo MDF; Freeze-Dryer (RVT400, -55 ^{o}C) and Microplate Reader (Victor^3) from Perkin-Elmer.

2.3 Synthesis and Purification of Carbon Dots

The CDs synthesis was performed using the hydrothermal method with folic acid, ascorbic acid, and oxaloacetic acid as the main starting materials (table 2). CDs based on folic acid (CDs-FA) were synthesized by mixing 0.2 g of folic acid with a 10 ml phosphoric acid solution (4.25 ml of H_3PO_4 and 5.75 ml of H_2O), the mixture had a mole ratio FA/H_3PO_4 of 0.005 and was heated for 2 hours at 100 ^{o}C. The CDs based on ascorbic acid (CDs-AA) were synthesized by heating 1 g (5.7 mmol) of ascorbic acid in water (20 ml) for 5 hours at 200 ^{o}C, in another approach 1 g of ascorbic acid was mixed with 0.5 g of 1,6-hexanediamine in 20 ml of water with a mole ratio between AA/HXDA of 1.3, and the reaction occurred (CDs-AA +1,6-HXDA) at 200 ^{o}C for 5 and 8 hours. A room temperature approach lasting for 15 days was also attempted combining 1 g of ascorbic acid with 0.5 g of 1,6-hexanediamine (CDs-AA + 1,6-HXDA, RT), the mole ratio of AA/HXDA was 1.3. The CDs based on oxaloacetic acid (CDs-OA) were attempted by preparing an oxaloacetic acid solution, 1 g (7.5 mmol) of oxaloacetic acid in water (20 ml) followed by a reaction time of 5 hours at 200 ^{o}C. The CDs based on oxaloacetic acid and 1,6-hexanediamine (CDs-OA + 1,6-HXDA) were performed by mixing 1 g of oxaloacetic acid with 0.5 g of 1,6-hexanediamine and using 5 and 8 hours of reaction time and 200 ^{o}C temperature, the mole ratio of OA/HXDA was 1.75. All reactions, excepting the room temperature reaction, took place inside an oil bath using a polytetrafluoroethylene container in a stainless-steel autoclave reactor (100 ml).

All the products were subjected to purification processes, namely centrifugation, and dialysis. Centrifugation was performed for 20 minutes at 10000 rpm, to separate the insoluble particles and, the dialysis of the black solutions (after synthesis) was made against water lasting between 24-48 hours (MWCO, 500-1000 Da). The reminiscent solutions were stored at room temperature and sheltered from light, and part was freeze-dried (lyophilization) for further tests and characterization.

Table 2. Starting materials and conditions used/employed in the synthesis of carboxylated and aminated carbon dots.

Short Identification	Starting Materials and synthesis	Reaction Parameters
CDs-FA	Folic Acid (0.2 g) + Phosphoric acid (5 ml) 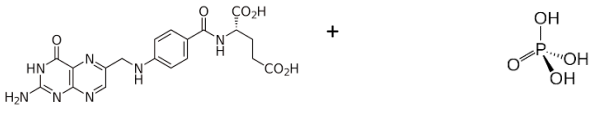	2 h, 100 °C  5.75 ml in H_2O -Mole ratio (FA/H_3PO_4) = 0.005
CDs-AA	Ascorbic Acid (1 g) 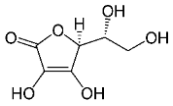	5 h, 200 °C  20 ml in H_2O 5.7 mmol of AA
CDs-AA +1,6-HXDA	Ascorbic Acid (1 g) + 1,6-hexanedimiane (0.5 g) 	5 h and 8 h, 200 °C  20 ml in H_2O Mole ratio (AA/HXDA) = 1.3
CDs-AA+1,6-HXDA (room temperature)	Ascorbic Acid (1 g) + 1,6-hexanedimiane (0.5 g) 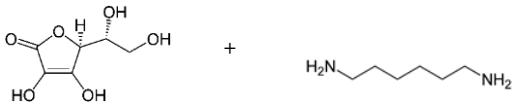	15 days, room temperature 20 ml in H_2O Mole ratio (AA/HXDA) = 1.3
CDs-OA	Oxaloacetic acid (1 g) 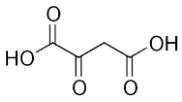	5 h, 200 °C  20 ml in H_2O 7.5 mmol of OA
CDs-OA+1,6-HXDA	Oxaloacetic acid (1 g) + 1,6-hexanedimiane (0.5 g) 	5 h and 8 h, 200 °C  20 ml in H_2O Mole ratio(OA/HXDA) = 1.75

2.4 CDs characterization

The UV-Vis spectra of carbon dots were collected using a UV-Vis spectrophotometer, and quartz cuvettes were employed in the measurements, the concentrations used to obtain all UV-Vis spectra were 0.03 mg/ml. The fluorescence and excitation spectra were obtained using a Fluorescence Spectrometer having the following experiment conditions: -excitation slit of 12 nm, -emission slit of 5 nm and a -scan speed of 500 nm/min. The fluorescence spectra were collected from excitation wavelengths of 260-500 nm with a 20 nm increment, these measurements were performed using a quartz cuvette, and a fixed mass concentration was used for all CDs samples namely, 0.2 mg/ml. Attenuated Total Reflectance FT-IR was used to detect the functional groups present on the CDs surface, the raw material was in solid state and the measurements made in ATR, respecting a 14% of light detected. The ^{1}H-NMR was used to observe the differences before and after synthesis and DMSO-D6 was used as the solvent, with an acquisition of 8 scans. The hydrodynamic size and ξ-potential of the CDs was retrieved from the dynamic light scattering technique using one independent measurement, and the size experiment conditions were: 10 runs-10 seconds while the ξ-potential collection conditions were: 20 runs (one independent measurement). The size measurement was made using a plastic cuvette whereas the zeta-potential required the use of a plastic capillary cell. The morphology and particle´s size was obtained using Transmission Electron Microscopy from Hitachi Center-Marked Grids, 50 mesh, 3.0mm O.D., Copper grid using a 200kV acceleration voltage.

2.5 Carbon Dots Studies

To study the effect of quenching, pH, fluorescence stability over time, and DNA condensation, the CDs were selected based on their results, namely TEM images that proved the existence of CDs, and so the CDs based on folic acid (CDs-FA), CDs based on ascorbic acid (CDs-AA), and CDs based on ascorbic acid and 1,6-hexanediamine room temperature (CDs-RT) were chosen.

2.5.1 Quenching Tests

The quencher effect on CDs-FA, CDs-AA, and CDs-RT was studied using potassium iodide as the quenching agent (KI). One individual solution with a mass concentration of 0.2 mg/ml for each CDs-FA, CDs-AA, and CDs-RT was prepared, along with a KI 500 mM solution. The KI concentrations used were between 20-200 mM (table S1, Appendix section 1.1). From each of the final solutions, 100 µl (duplicates) was placed inside a white 96-well plate, and the fluorescence intensity was recorded using a Microplate Reader and with the adequate fluorescence filters.

2.5.2 pH Tests

The pH effect on CDs-FA, CDs-AA, and CDs-RT was evaluated using a pH range between 3-10. One individual solution of 0.2 mg/ml was prepared for each CDs-FA, CDs-AA, and CDs-RT. 100 µL of each Carbon-based dot was placed in 4.9 ml of buffer solutions between 3-10 (table S2, Appendix section 1.1). Lastly, inside a white 96-well plate was placed 0.1 ml of the final solutions prepared (duplicates), and the fluorescence intensity was measured using the adequate fluorescence filter in the microplate reader.

2.5.3 Fluorescence stability over time

The fluorescence stability of CDs throughout time was evaluated by fluorescence spectroscopy. An individual solution of each CDs (CDs-FA, CDs-AA, and CDs-RT) with a fixed mass concentration of 0.2 mg/ml was prepared. These three stock solutions were kept away from light and new aliquots on a weekly basis were retrieved to measure its fluorescence intensity by using two different excitation wavelengths, 360 and 380 nm. The measurements were made over the course of 8 weeks.

2.5.4 DNA condensation

To study the capacity of CDs to condense pDNA, an individual solution of 0.2 mg/ml of each carbon-based dot (CDs-FA, CDs-AA and CDs-RT) was prepared. Plasmid DNA with a concentration of 0.5 μg/μl was used, and the CDs-pDNA ratios were 1:1, 10:1, 20:1, 40:1, and 100:1. Further information on the volumes used for pDNA, CDs, and TE solution are displayed in table S3, appendix section 1.1. The final solutions were then mixed using a vortex and incubated between 15-20 minutes. Inside a white 96-well plate was placed 100 μL of the final solutions (triplicates) following addition of 100 μL of Picogreen and incubation for 5 minutes. The fluorescence intensity was read using the adequate fluorescence filters in the microplate reader.

2.6 CDs-DNA Interaction

The interaction between dsDNA and different charged carbon dots was studied, and one individual solution of 0.2 mg/ml was prepared for each CDs-FA, CDs-AA, and CDs-RT. A 100 μg/ml solution of dsDNA was also prepared. In a 1:1 CDs-dsDNA ratio 100 μL of each was added in a 1.8 ml PBS solution and mixed using a vortex and allowed to interact between 15-30 minutes. The solutions were then analysed by UV-Vis, Fluorescence Spectroscopy, and Dynamic Light Scattering (ξ-potential).

2.7 CDs-PAMAM-NH_2 Interaction

To study the impact of the PAMAM-NH_2 conjugation on the fluorescence properties of CDs, a CDs-PAMAM-NH_2 junction was prepared. CDs-AA were selected for the purpose due to its negative ξ-potential. One individual solution of G5 PAMAM-NH_2 and CDs-AA were prepared with a 1.33 mg/ml concentration. Three different CDs-PAMAM ratios were tested (2:1, 1:1 and 1:2), and these interacted for a total of 24 hours under stirring conditions. UV-Vis, Fluorescence spectroscopy, and dynamic light scattering (hydrodynamic size and ξ-potential) were employed in the characterization of the conjugates.

Chapter 3-Results and Discussion

Chapter 3-Results and Discussion

This chapter contains the results obtained from CDs synthesis, using folic, ascorbic, and oxaloacetic acid as the main starting materials. Results from the CDs studies comprising quenching, pH, fluorescence stability over time, and DNA condensation are also presented and discussed. Two final sections are devoted to CDs-DNA and CDs-PAMAM interactions, with results from UV-Vis absorption, fluorescence, and ξ-potential.

3.1 Carbon Dots based on Folic acid

The carbon dots based on folic acid were initially obtained by Campos *et al*.[80] by mixing FA with phosphoric acid at 100 °C for 1 hour using reflux as the hydrothermal method. Our CDs-FA preparation is an adaption from the previous work, with differences in the reaction time (2 hours) and hydrothermal method (autoclave reactor). The synthesis of CDs based on folic acid was performed using the hydrothermal process at 100 °C for 2 hours in an oil bath, which employed folic acid and phosphoric acid as the starting materials. Folic acid is an interesting precursor for CDs synthesis due to the variety of functional groups composed by different elements, *e.g.,* carbon, nitrogen, and oxygen. The role of folic acid was to act as a carbon source, but also for other elements (N and O), while phosphoric acid acted as a fluorescence enhancer and oxidant agent. Moreover, phosphoric acid helped in the solubilization of folic acid, which was very hard to achieve in water.

The morphology and size of the CDs-FA was investigated by TEM (figure 9), and the results show a considerable number of carbon dots in both spots. The particles are spherical and present a certain degree of aggregation. The average size of the particles from spot A and B is 5.063 and 6.938 nm, respectively. Campos *et al.*[80] reported a total of 70 nanoparticles in contrast with our value of 420.

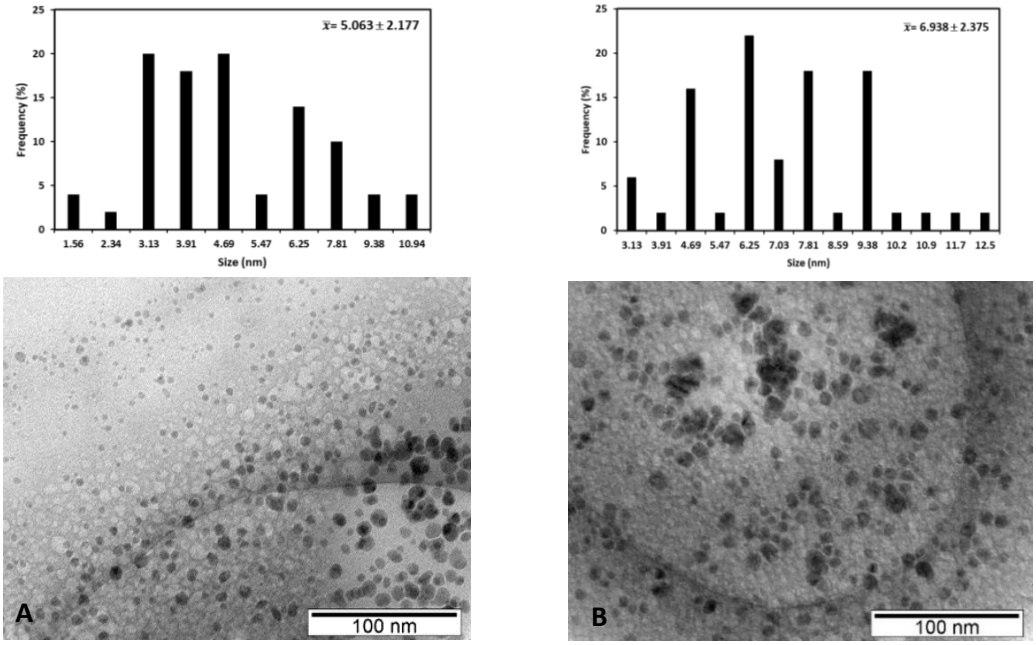

Figure 9. TEM image of CDs-FA and its respective size distributions. Two different spots: Image A- average of 5.063 nm ± 2.177 nm and Image B- average of 6.936 nm ± 2.375 nm. Both spots have a combined number of 420 NPs.

The functional groups of CDs-FA and its respective main starting material were determined by FT-IR (figure 10). Regarding folic acid, the vibration at 3543 cm^{-1} corresponds to the stretching vibration of -OH, and two bands at 3416/3316 cm^{-1} are from the presence of primary amines in the molecule. At 1680 cm^{-1} is the band assigned to ν-C=O and lastly at 1605 cm^{-1} is ascribed to the N-H bending. Concerning CDs-FA, a broad band centered at 3349 cm^{-1} is attributed to -OH and -NH stretching; a band at 1632 cm^{-1} is suggestive of the presence of a carbonyl group as well as a double bond between carbon, once it´s characteristic of the stretching of -C=O and C=C bonds. Also, at 1134 cm^{-1} is the resulting band of C-O stretching and at 980 cm^{-1}

the band of $H_2C=CH_2$ bending. Based on the surface functionality of the dots, we assume their surface is of hydrophilic nature. The ξ-potential of CDs-FA was positive (23.7 mV), correspondingly, Campos *et al.*[80] reported a positive value of 14.7 mV. Based on the ZP value the particles are relatively instable and can agglomerate, as the TEM image (figure 9) shows. The zeta-potential is a parameter used to measure the stability of the particles in solution, and it´s also possible to correlate either the positive or negative value with the type of surface groups of the particles. Based on the zeta-potential, we suggest the presence of N-type groups contributing to the positivity of the surface.

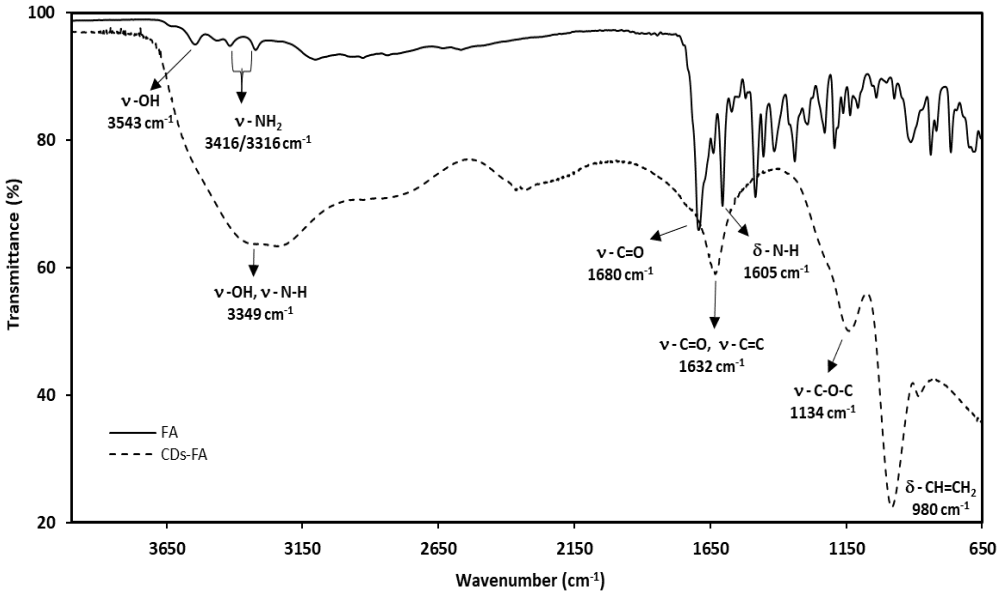

Figure 10. ATR FT-IR spectra of CDs-FA and its main starting material, folic acid.

NMR spectroscopy was used to identify the differences before and after synthesis, in that sense, the ^{1}H-NMR of folic acid and CDs-FA were obtained (figure 11) using as solvent DMSO-D6. The attribution of each signal to the CDs obtained is quite challenging to accomplish, although some assignments were made. The ^{1}H-NMR of folic acid (spectrum a) was made using DMSO-D6 has a solvent (peak at 2.5 ppm), the major peaks of FA were assigned, two signals detected at 1.9 and 2 ppm, and one at 2.3 ppm are ascribed to H_2C-CH_2 (alkane), peaks at 6.5 and 6.9 ppm are from the aromatic ring structure of folic acid (H-C=C-H), signals at 8 and 8.5 ppm are assigned to protons close to C-N and C=N (ring structure) bonds. After synthesis, it´s expected a different product (CDs-FA), with new bonds formed and different chemical environments; the ^{1}H-NMR of CDs-FA (spectrum b) presents significant chances, peaks at 2.3 and 3.3 ppm, and between 6-7 ppm suffered alterations after synthesis (table 3). Specifically, the signal attributed to HC-CH bonds (alkanes) centered at 2.3 ppm disappears, another peak at 3.3 ppm vanishes, and a slight shift from 6.9 to 6.7 ppm occurs in the peak attributed to the aromatic ring structure. Other peaks appear *e.g.* 2.6, 7.6, 9, and 9.9 ppm, but they are of difficult interpretation. To have a better structure estimation, it would be important the ^{13}C-NMR, 2D-NMR, and even X-ray photoelectron spectroscopy.

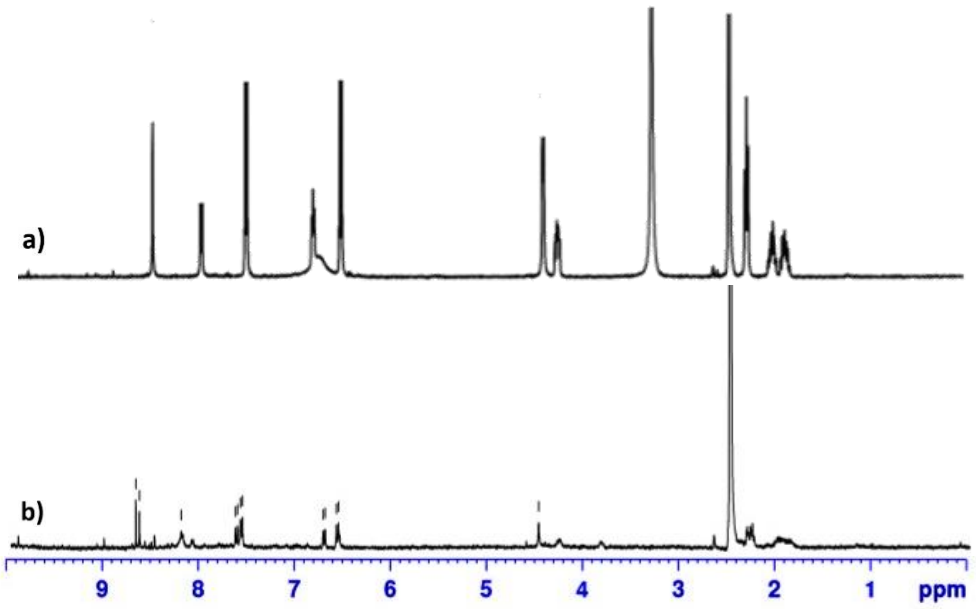

Figure 11. ^{1}H-NMR spectra of folic acid (a) and CDs-FA (b) using as solvent DMSO-D6.

Table 3. ^{1}H NMR signals before and after synthesis. Spectrum a) Folic Acid and spectrum b) CDs-FA.

Spectrum a) Folic Acid	**Spectrum b) CDs-FA**
Peak at 2.3 ppm, C-C-H (alkane)	Vanishes after synthesis
Peak at 3.3 ppm	Disappears after synthesis
Peaks at 6.9 ppm, C=C-H (aromatic ring structure)	Shift after synthesis to 6.7 ppm

Regarding the UV-Vis spectra (figure 12), the main starting material (folic acid) and reaction mixture before synthesis present a peak centred at 278 nm and 296 nm, respectively. Folic acid has a characteristic maximum at 278 nm[82], the addition of phosphoric acid allows a bathochromic shift to 296 nm due to a pH decrease. The CDs-FA also absorb in the UV-region, the absorption maximum is centralized at 286 nm. The absorption change allows to assume the production of new material, but since the pH of the mixture before and after synthesis are different (Table S4, Appendix section 1.2) it might also influence absorption. The absorption band at 286 nm might be from the n-π* transitions (C=O groups). The excitation spectrum of the

CDs-FA (figure 13) was obtained using an emission wavelength of 466 nm because at this wavelength the CDs-FA show its brightest fluorescence and the results show different excitation centres.

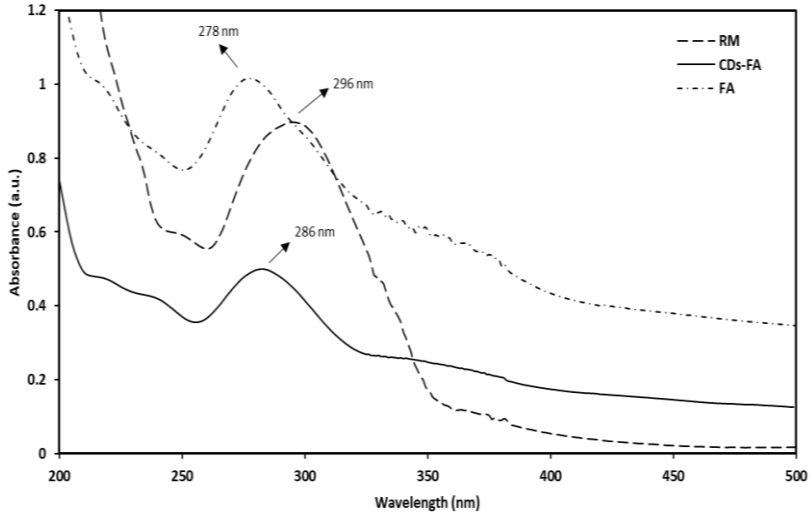

Figure 12. UV-Vis spectra of Carbon dots based on Folic acid (CDs-FA) and its respective reaction mixture before synthesis (RM), along with FA using water as a solvent.

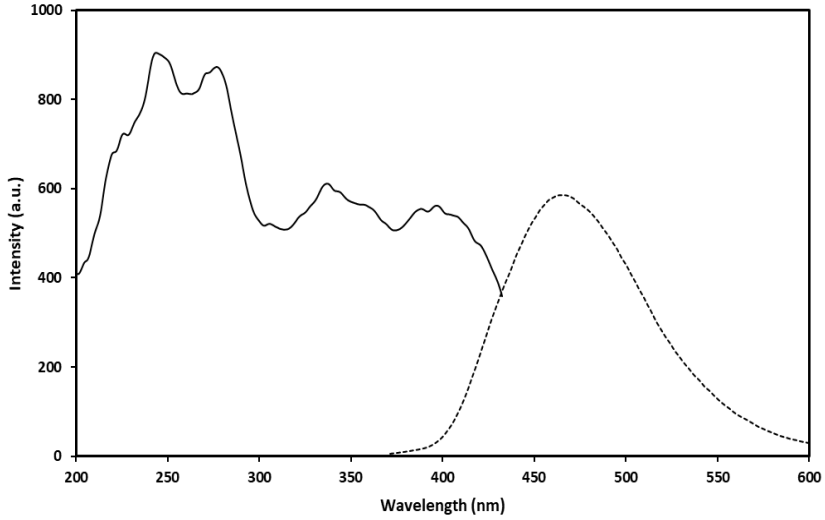

Figure 13. Excitation spectrum of CDs-FA using an emission wavelength of 466 nm and using water as a solvent.

The emission spectra of CDs-FA, emission/excitation dependency graph, and its RM before synthesis are summarized in figure 14, 15, and 16 respectively. The CDs-FA have an emission range between 477-491 nm, showing the strongest emission at 360 nm excitation. Comparing the fluorescence intensity of CDs-FA and RM before synthesis, the dots seem much more fluorescent. Before synthesis, the reaction mixture presents a pale-yellow colour, which later turns dark green (table S4, Appendix section 1.2). Moreover, a light blue colour emission is observed by UV-chamber (λ_{exc}= 366 nm). The QY of the CDs-FA was 19.7 %, in line with the values reported by Campos *et al.*[80](27%).

The emission/excitation dependency graph (figure 15) shows a blue shift between 300-380 nm excitations, after 400 nm excitation the emission reaches 490 nm, the color differences along the excitation interval go from blue to light blue. A possible explanation for the blue shift is, when dealing with organic nanoparticles, they have a lot of non-bonding electrons that can interact with hydrogen-bonding solvents mostly in the ground state and less in the excited state, as a result the n-π* transition will shift towards the shorter wavelength as the hydrogen bonding ability of the solvent increases. Generally, the red-shift occurs due to intermolecular charge transfer, but when the solute-solvent interactions are stronger than intermolecular interactions, then blue-shift occurs.

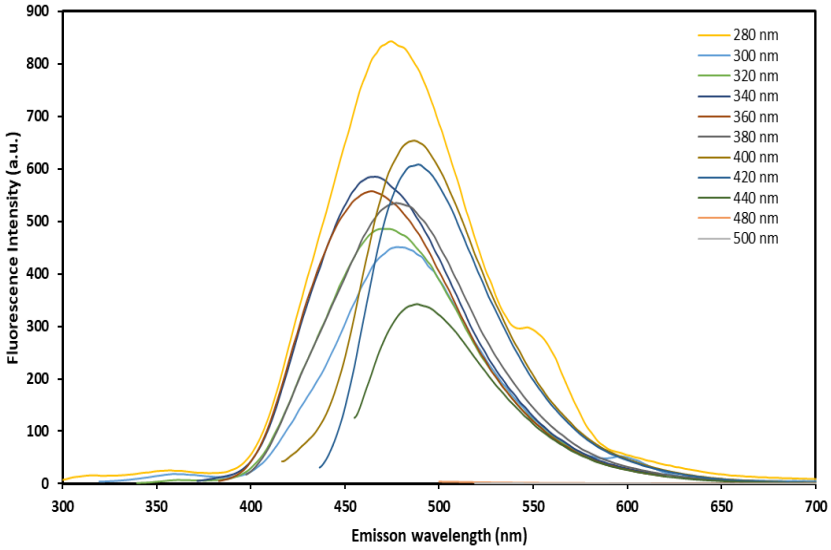

Figure 14. Emission spectra of CDs-FA obtained using an excitation wavelength between 280-500 nm, with an increment of 20 nm.

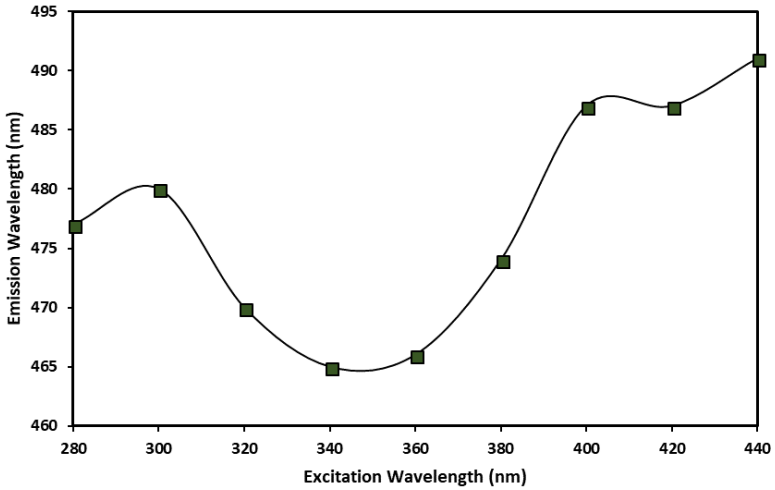

Figure 15. Emission wavelength obtained using 280-440 nm excitation, with 20 nm increments. From 280-440 nm excitation, the emission goes from 475-490 nm.

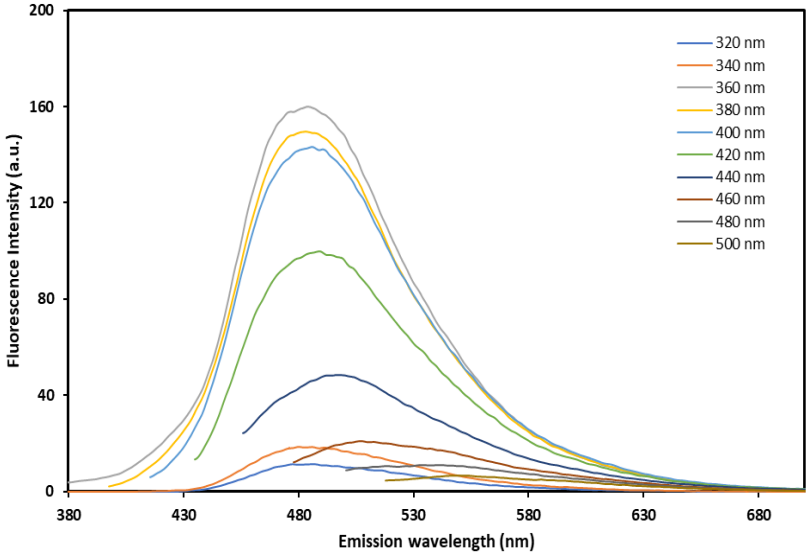

Figure 16. Emission spectra of the reaction mixture before synthesis obtained using an excitation wavelength between 320-500 nm (20 nm increment)

Based on the results obtained, we confirm the success of the approach, carbon dots based on folic acid were possible to be synthesized adapting the procedure of Campos *et al*.[80]. Some dissimilarities in the results obtained by Campos[80] and us, such as size, particles number, ξ-potential, and QY are certainly related with the adapted experimental conditions used, in summary, we were more efficient regarding particles number. The peculiar feature of CDs is their surface heterogeneity and based on the characterization (FT-IR and ξ-potential) it was projected the different surface functional groups of CDs-FA (figure 17), it should be noted that further techniques *e.g.* XPS would be important for surface estimation. The proposed surface has a mixture of carboxyl and different N-type groups.

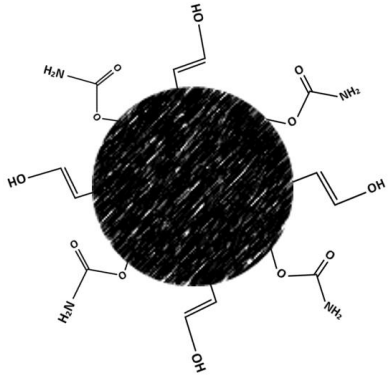

Figure 17. Representation of the CDs-FA obtained.

3.2 Carbon Dots based on Ascorbic acid

CDs synthesis based on ascorbic acid happened at 200 ^{o}C for 5 hours inside an autoclave reactor using an oil bath. The results obtained comprise TEM, ξ-potential, FT-IR, ^{1}H-NMR, UV-Vis, PL excitation, emission, and quantum yield.

Ascorbic acid is another interesting precursor for CDs synthesis, the different elements (C, O, and H) and functional groups (-COOH and -OH) composing the molecule are indeed attractive for the purpose. A few research groups considered the use of ascorbic acid, combining with other precursors and using natural extracts, as a green source of ascorbic acid[83-85]. Ascorbic acid itself inside an autoclave reactor with the conditions proposed constitutes a novelty. Nonetheless, Zhang and co-workers[86] already synthesized CDs based on this material, using 4 hours and 180 ^{o}C in an autoclave reactor, and the results will be used for comparison[86].

TEM was used to reveal the existence of dots (figure 18), and the results confirm the presence of carbon dots with a spherical shape and a considerable level of aggregation. Two arbitrary regions were analysed, spot A and B. Region A and B display the black dots with an average size of 4.236 and 4.146 nm, in contrast with Zhang *et al*.[86] (carbon dots with 2-2.5 nm). The ZP of the particles was -9.99 mV, the low value indicates a rapid agglomeration and flocculation, which is observed in the TEM image (figure 18). Moreover, the particles have a size range between 3-6.10 nm with a total number of 120 particles.

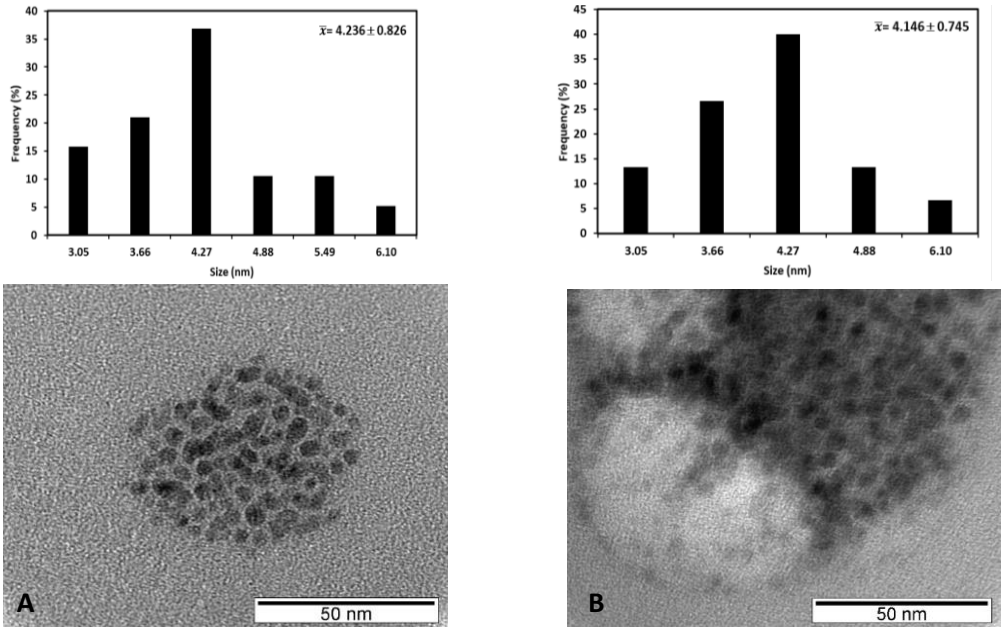

Figure 18. TEM image of CDs-AA and its respective size distribution. A-Average of 4.236 nm ± 0.826 nm and image B- average 4.146 nm ± 0.745. Both spots have a combined number of 120 NPs.

FT-IR revealed the surface functionality of the CDs-AA (figure 19) and the main differences between neat ascorbic acid and the new product. Ascorbic acid presents a sharp band at 3524 cm^{-1}, corresponding to the stretching of free -OH, while two bands at 3346/3308 cm^{-1} are ascribed to intramolecular hydrogen bonding. At 1750 and 1654 cm^{-1} are the bands assigned to ν-C=O and ν-C=C, respectively. C-O stretching was detected at 1024 cm^{-1}. As for the CDs-AA, the broadband at 3360 cm^{-1} is attributed to -OH stretching and 2934 cm^{-1} to C-H stretching. Vibration bands at 1707 cm^{-1} correspond to ν-C=O, and 1396 cm^{-1} to C-H bending mode, which is according to the reported by Zhang *et al*.[86]. Two other vibrations, namely at 1188 and 1016 cm^{-1} are assigned to C-O-C and C-O stretching. Based on the functional groups detected, the CDs-AA have mostly carboxyl and hydroxyl groups at the surface, which is also in concordance with the negative ξ-potential (-9.99 mV).

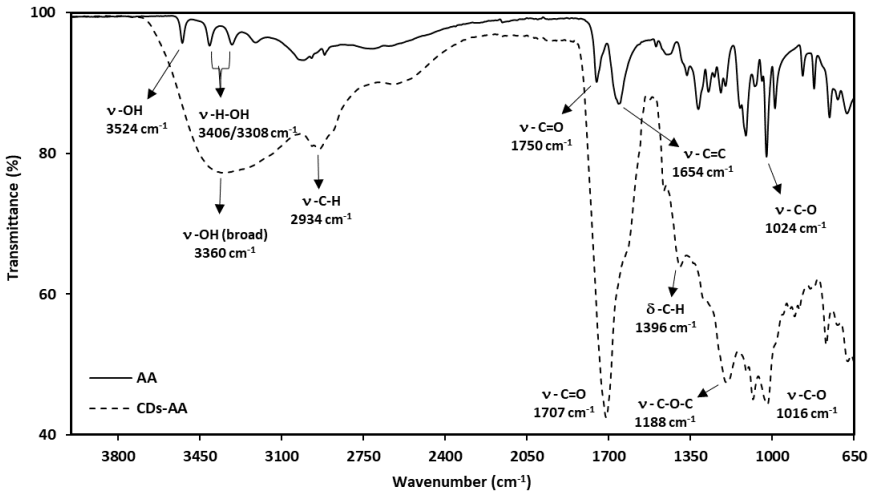

Figure 19. ATR FT-IR spectra of CDs-AA and its respective starting material, ascorbic acid.

NMR was used to establish the differences before and after synthesis. The ^{1}H-NMR of ascorbic acid (spectrum a) was obtained using DMSO-D6 has a solvent (peak at 2.5 ppm), AA presents its characteristic peaks; at 3.4 and 3.7 ppm is ascribed to H-C-O-C and H-C-OH, respectively, at 4.8 and 5 ppm are assigned to the H_2C-OH, and the peak at 8.4 ppm is attributed to C-O-H. After synthesis, and by observing the proton NMR of CDs-AA (spectrum b), ascorbic acid was completely decomposed, the two spectra exhibit a quite extensive number of differences. Peaks that are typical in ascorbic acid no longer remain, an extensive number of novel peaks appear (1.87, 2.2, 2.4, 5.5, 5.9, 6.4, 6.7 ppm and others) in the alkane/alkene and aromatic ring regions. The previously mentioned differences indicate the formation of a new product, but the exact attribution of each signal to form a representative structure of CDs-AA is difficult to accomplish. Further techniques such as XPS, or simply using ^{13}C-NMR and 2D-NMR would be crucial to have a better structure representation.

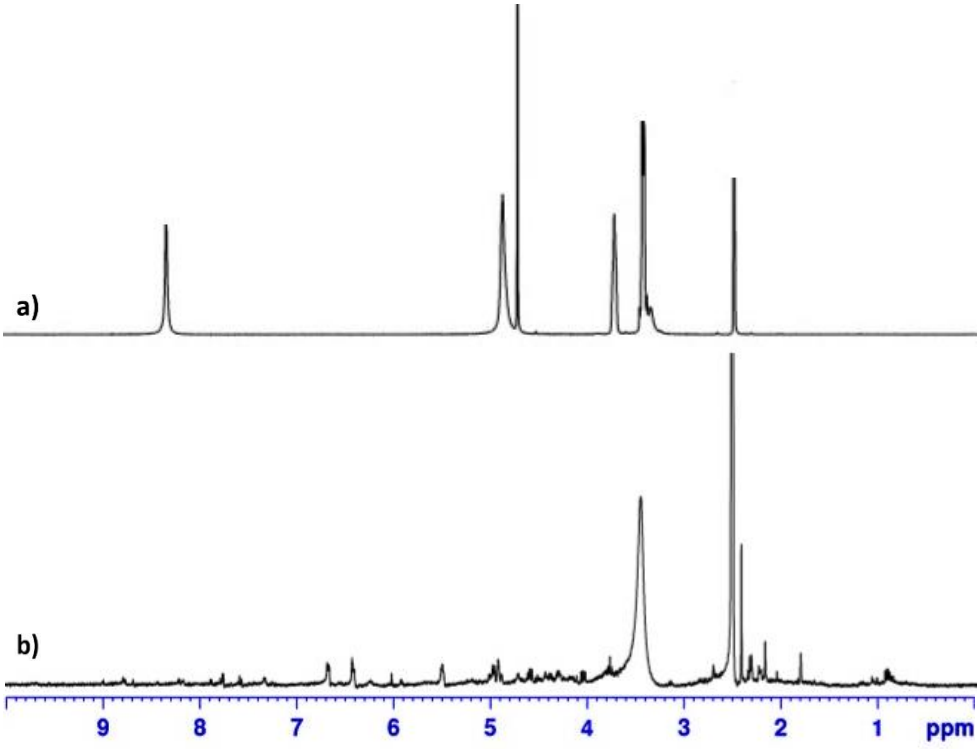

Figure 20. ^{1}H-NMR spectra of CDs-AA (spectrum b) and ascorbic acid (spectrum a), using as solvent DMSO-D6.

Table 4. ^{1}H-NMR peaks before and after synthesis. Spectrum a) ascorbic acid and spectrum b) CDs-AA.

Spectrum a) Ascorbic Acid	***Spectrum b) CDs-AA***
No peaks between 1.8-2.2 ppm	Two peaks appear at 1.87 and 2.2 ppm
No peak at 2.4 ppm	Appears a peak at 2.4 ppm
Peak at 3.7 ppm (H-C-OH)	Vanishes after synthesis
Peak at 4.8 ppm (H_2C-OH)	Disappears after synthesis
No peak at 6.4 and 6.7 ppm	Two peaks appear at 6.4 and 6.7 ppm
Peak at 8.2 ppm (C-O-H)	Disappears after synthesis

The UV-Vis spectra of CDs-AA and ascorbic acid are exposed in figure 21, the acid presents an absorption maximum at 268 nm whereas the CDs present two distinct absorptions, 227 and 275 nm, which are ascribed to π-π* and n-π* transitions, respectively. The excitation spectrum of CDs-AA (figure 22) was obtained using an emission wavelength of 431 nm and an excitation peak at 340 nm was obtained.

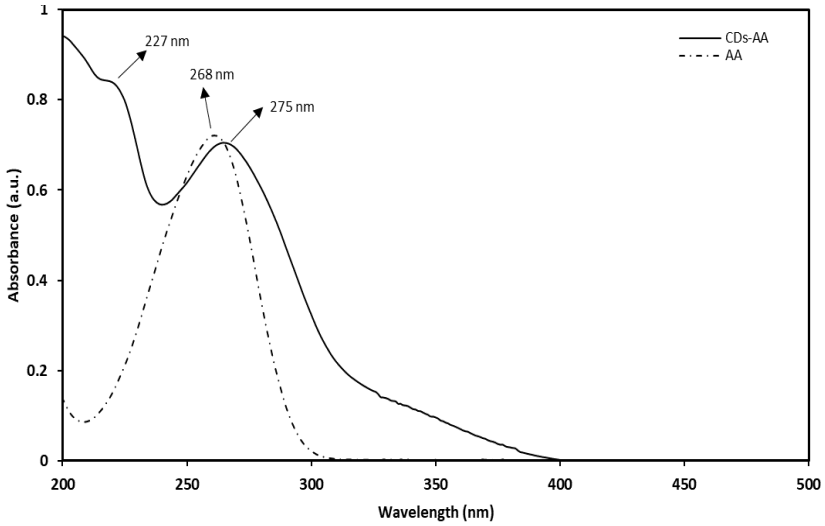

Figure 21. UV-Vis spectra of carbon dots based on ascorbic acid (CDs-AA) and its respective starting material, ascorbic acid, using water as solvent.

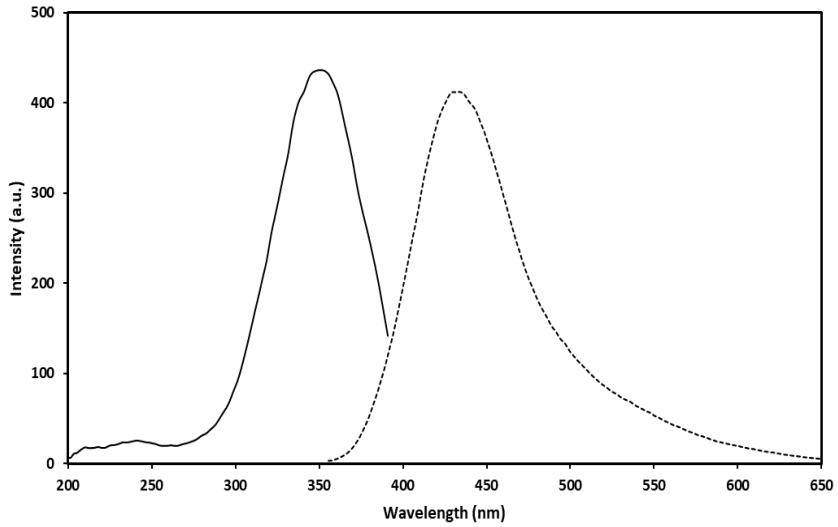

Figure 22. Excitation spectra of CDs-AA obtained using an emission wavelength of 431 nm, using water as solvent.

Regarding fluorescence, the fluorescence spectra of CDs-AA, emission/excitation dependency graph, and ascorbic acid are summarized in figures 23, 24, and 25 correspondingly. CDs-AA have an emission range from 419 to 520 nm, and the strongest fluorescence occurs at 340 nm excitation, while ascorbic acid has a maximum emission at 320 nm excitation. Furthermore, the CDs-AA are more fluorescent than its starting precursor and the QY obtained was 10.8 %, higher than the referred by Zhang *et al.*[86], 6.79% (4 hours synthesis). Another aspect is the emission-dependent excitation observed for CDs-AA, the reason might be the particles size distribution and the different emission trap sites of the dots. The fluorescent CDs present a blue emission colour when excited at 366 nm (Table S4, Appendix section 1.2).

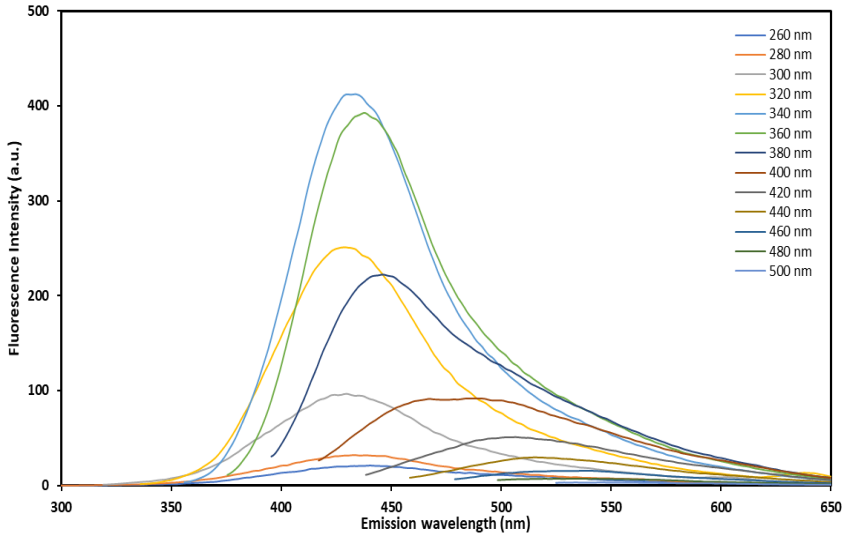

Figure 23. Emission spectra of CDs-AA with an excitation wavelength from 260-500 nm, using an increment of 20 nm.

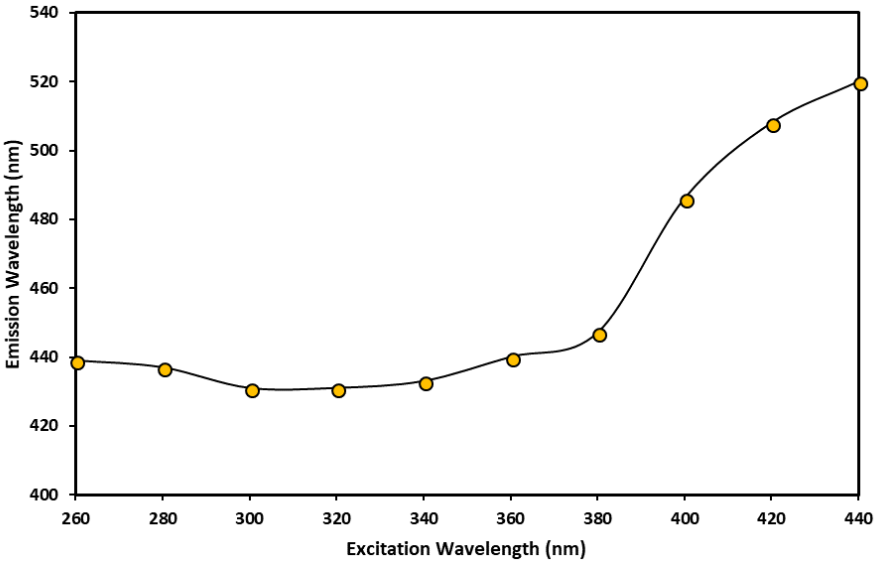

Figure 24. Emission wavelength obtained using 260-440 nm excitation, with 20 nm increments. From 260-440 nm excitation the emission goes from 440-520 nm.

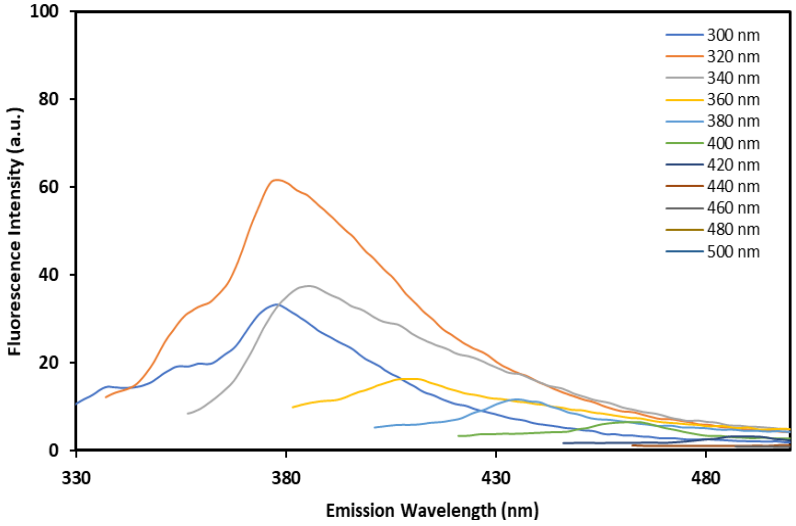

Figure 25. Emission spectra of ascorbic acid (starting material) using an excitation wavelength between 300-500 nm with a 20 nm increment.

Based on the results obtained, CDs based on ascorbic acid were possible to synthesized using novel experimental parameters. Using FT-IR and ξ-potential the determination of the surface functionality of the particles was tried, in that sense, the surface functionality was projected as a mixture of carboxylic and hydroxyl groups (figure 26).

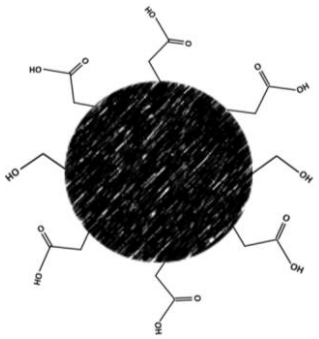

Figure 26. Representation of CDs-AA.

3.3 Carbon Dots based on Ascorbic acid-1,6-hexanediamine

The introduction of nitrogen elements on the surface of CDs improves the fluorescent properties, based on the knowledge and importance of that, 1,6-hexanediamine was added to ascorbic acid. Two reactions took place at 200 °C for 5 and 8 hours respectively, in addition to a third synthesis at room temperature lasting for 15 days. The combinations attempted with the conditions referred represents a novelty, and the subsequent are the results and discussion.

Transmission electron microscopy was used to confirm the presence of carbon dots, figures 27, 28, and 29 correspond to CDs-5h, CDs-8h, and CDs-RT, respectively. In respect to CDs-5h and 8 h, the 5 hours approach does not show the presence of carbon dots, and the average size of the small dots is 1.036 nm. The CDs-8h show 2-3 black dots with an average of 2 nm, other small black dots are also present in the image having an average size of 1.092 nm, not constituting enough sample to assume the success of the hydrothermal approach in this specific case, independent of the time length. Distinctively, the room temperature attempt had a considerable number of spherical carbon dots with an average size of 3.932 nm, and a total of 25 nanoparticles, a ZP of 35.2 mV was obtained meaning a moderate stability between the particles in solution.

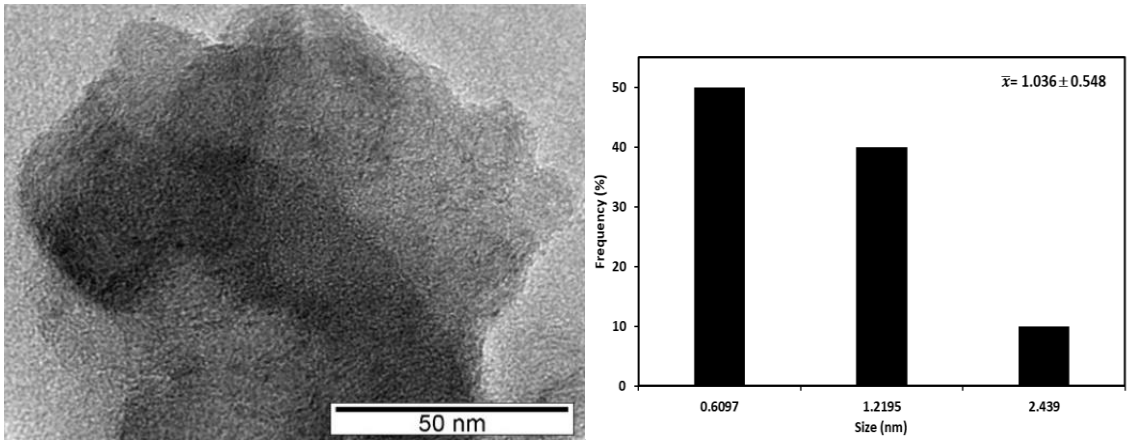

Figure 27. TEM image of CDs-AA+1,6-HXDA 5 h of synthesis with its respective size distribution. Average size of 1.036 nm ± 0.548 nm.

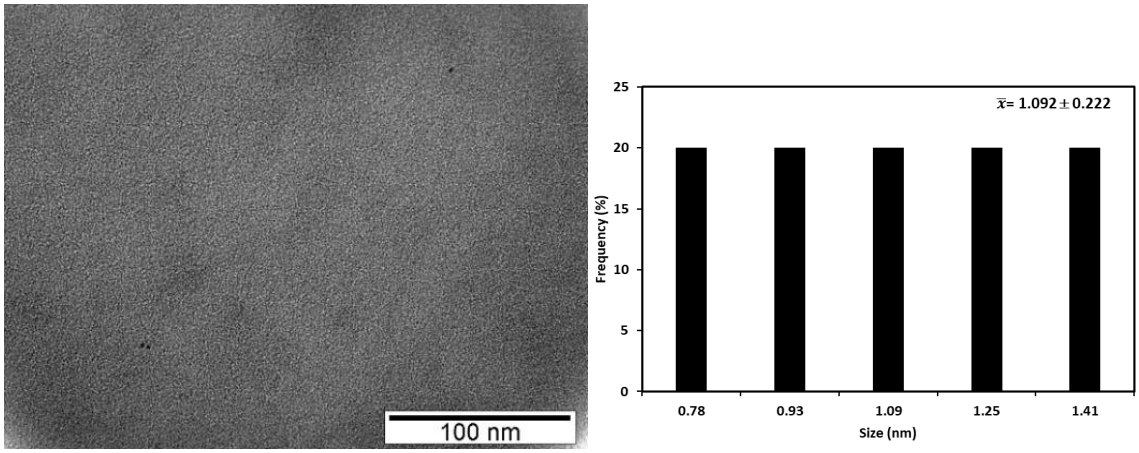

Figure 28. TEM image of CDs-AA+1,6-HXDA 8 h of synthesis with its respective size distribution. Average size of 1.092 nm ± 0.222 nm.

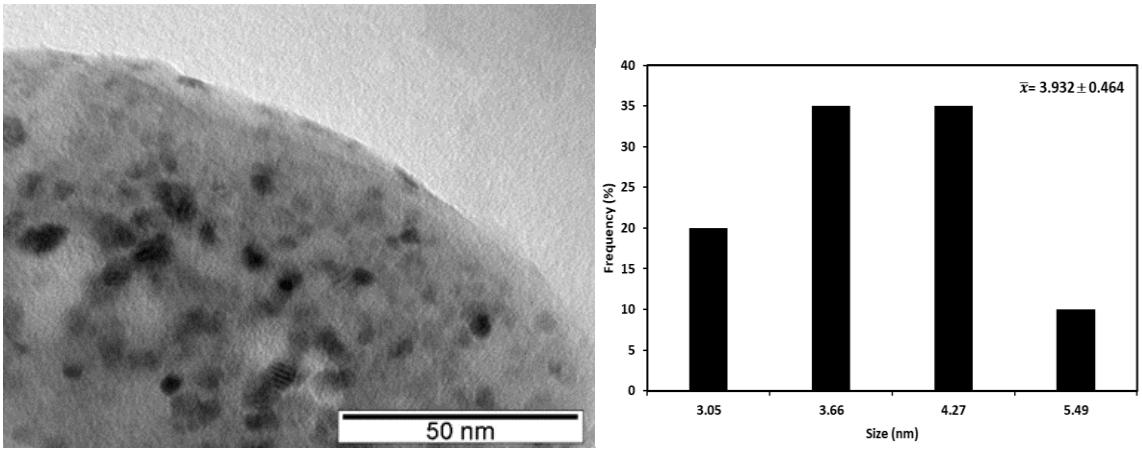

Figure 29. TEM image of CDs-AA+1,6-HXDA room temperature synthesis and its respective size distribution. Average size of 3.932 nm ± 0.464 nm. A total number of 25 NPs.

Infra-red spectroscopy detected the surface functional groups, figures 30 and 31 represent the spectra of CDs-AA+1,6-HXDA 5/8 hours and CDs-room temperature, respectively, along with their reaction mixture before synthesis. The reaction mixture presents symmetric and asymmetric stretching vibrations of C-H at 2931 cm^{-1} and 2861 cm^{-1}. Vibration at 1689 cm^{-1} is assigned to C=O, as 1562 cm^{-1} and 1358 cm^{-1} represent the bending modes of N-H and C-H, respectively. The hydrothermal approaches for 5 and 8 hours are quite similar regarding vibration bands, excepting the broadband at 3364 cm^{-1} which is more spacious for the 8 hours attempt. As for the remaining vibration bands, 2931 cm^{-1} and 2861 cm^{-1} correspond to symmetric/asymmetric vibration of C-H, 1567 cm^{-1} is assigned to the bending mode of N-H, and the absorptions at 1299 cm^{-1} and 1080 cm^{-1} are ascribed to C-N bending and C-O stretching.

Regarding the spectrum of CDs-room temperature (figure 31) the vibration band at around 3200 cm^{-1} corresponds to -OH stretching and at 1718 cm^{-1} to C=O groups. At 1374 cm^{-1} and 1299 cm^{-1} are the bands ascribed to C-H bending and C-N stretching, lastly, the band at 1036 cm^{-1} refers to C-O stretching vibration. The FT-IR spectrum of the reaction mixture before synthesis is slightly different compared to CDs-RT, the C=O band is positioned at 1709 cm^{-1} and after synthesis is shifted to 1718 cm^{-1}, the bending mode of N-H at 1551 cm^{-1} shifts to 1567 cm^{-1}, the vibration band appearing at 1358 cm^{-1} (C-H bending) is split into two new bands after synthesis (1374 cm^{-1} and 1299 cm^{-1}), which are assigned to the bending mode of C-H and stretching of C-N, respectively. Moreover, the ξ-potential obtained for 5 h, 8 h, and CDs-room temperature was 16.4, 22.5 and 35.2 mV, respectively.

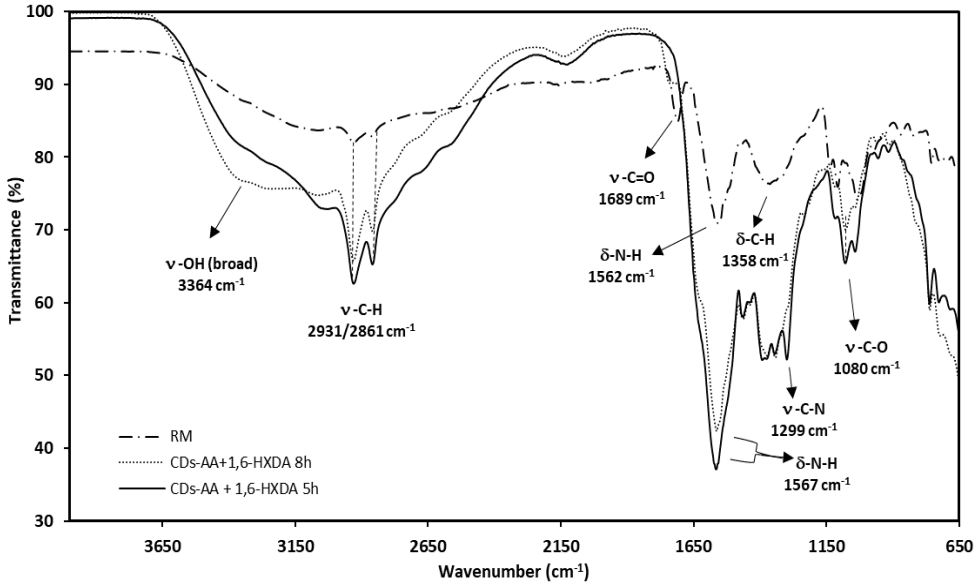

Figure 30. ATR FT-IR spectra of CDs-AA+1,6-HXDA 5h and 8h and its respective RM before synthesis.

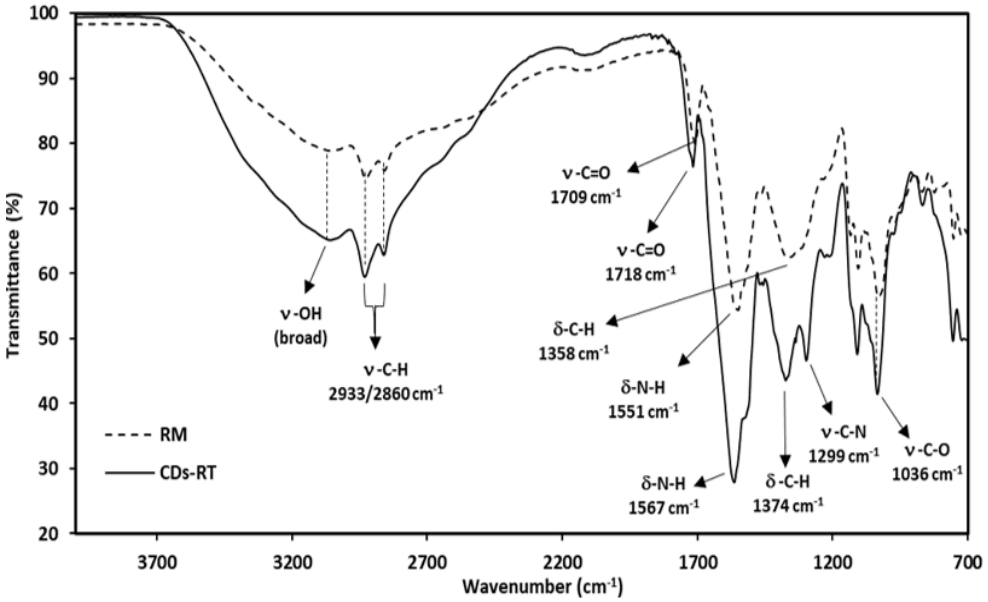

Figure 31. ATR FT-IR spectra of the reaction mixture at day 0 and CDs after 15 days of synthesis at room temperature.

NMR was used to detect the differences before and after synthesis. Table 5 and figure 32 represents the summary of peaks and the ^{1}H-NMR of the RM, CDs-5h, and 8h, respectively. The RM before synthesis is a mixture between ascorbic acid and 1,6-hexanediamine that can form condensed structures between the ascorbate ion and the NH_3^+ species of 1,6-HXDA. The ^{1}H-NMR of the reaction mixture (spectrum a) was obtained using DMSO-D6 has a solvent (peak at 2.5 ppm) and presents two peaks at 1.4 and 1.5 ppm in the alkane region, and others centered at 3.3, 3.5 ppm, and 3.9 ppm. Comparing the reaction mixture after 5 and 8 hours of synthesis, several new peaks appear, two major signals arise after synthesis (1.7 ppm and 8.5 ppm), specifically for CDs-8h, additional peaks appear at 2.7, 5.9, 6.7, 8, and 8.2 ppm. After synthesis, the exact attribution of the peaks is of great difficulty, the main conclusion is that a new product was synthesized after 5 hours, and after 8 hours the same product may remain, as the two spectra show similarities in terms of peaks.

A room-temperature synthesis was performed for 15 days, using ascorbic acid and 1,6-hexanediamine. The CDs-room temperature spectrum and signals are summarized in figure 33 and table 6,

respectively. The ^{1}H-NMR of CDs-RT (b) presents significant differences when compared to the reaction mixture before synthesis (a). After synthesis, new signals appear at 3 ppm and 4.1 ppm, along with a new group of signals centered at 8.2, 8.4, and 8.7 ppm. These differences mean that a new product was synthesized during the period of 15 days, precisely carbon dots (figure 29). The exact attribution of the signals obtained, predicting a structure for the carbon dots is hard to achieve, further techniques *e.g.* XPS or even a ^{13}C-NMR would help to predict more accurately the structure.

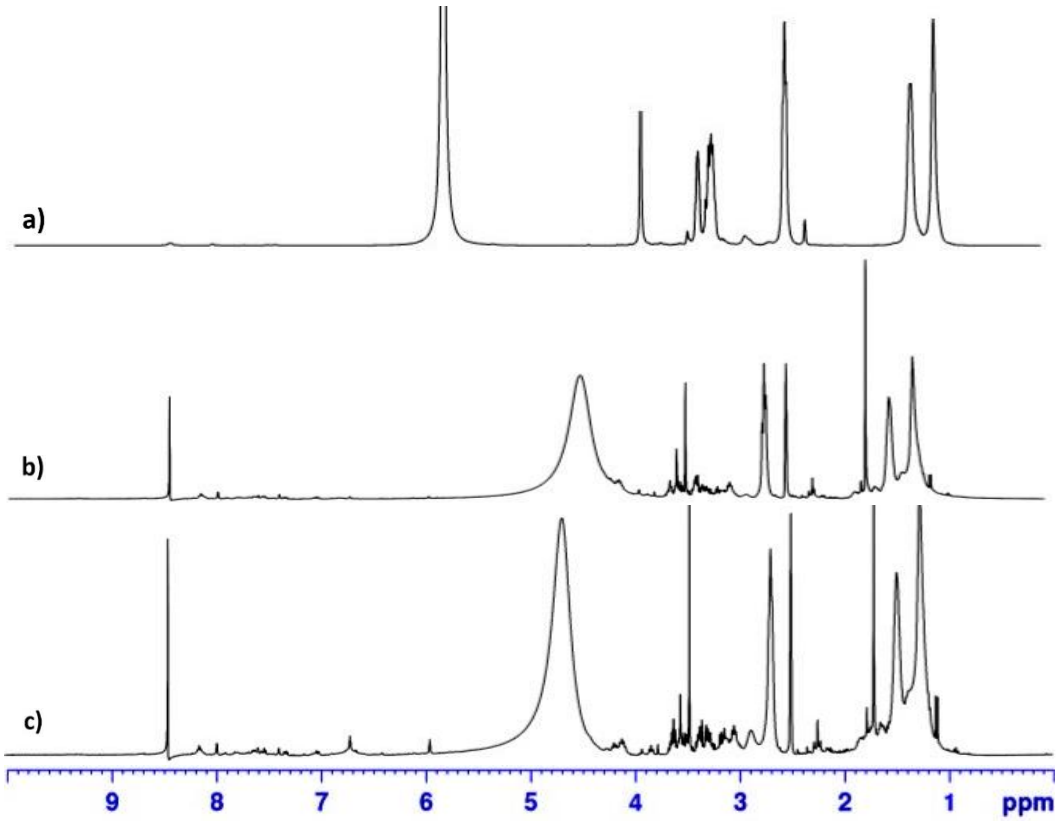

Figure 32. ^{1}H-NMR spectra of the reaction mixture before synthesis (a), CDs-5h of synthesis (b) and 8 h (c), using as solvent DMSO-D6.

Table 5. ^{1}H-NMR peaks before and after synthesis.
Spectrum a) reaction mixture, spectrum b) CDs-5h and spectrum c) CDs-8h.

Spectrum a) Reaction mixture	***Spectrum b) CDs-5h***	***Spectrum c) CDs-8h***
No peak	Peak at 1.7 ppm	Peak at 1.7 ppm
Peak at 3.2 ppm	No peak	No peak
Peak at 3.9 ppm	No peak	No peak
No peak	No peak	Peaks at 5.9 ppm and 6.7 ppm
No peak	Peak at 8.445 ppm	Peak at 8.445 ppm

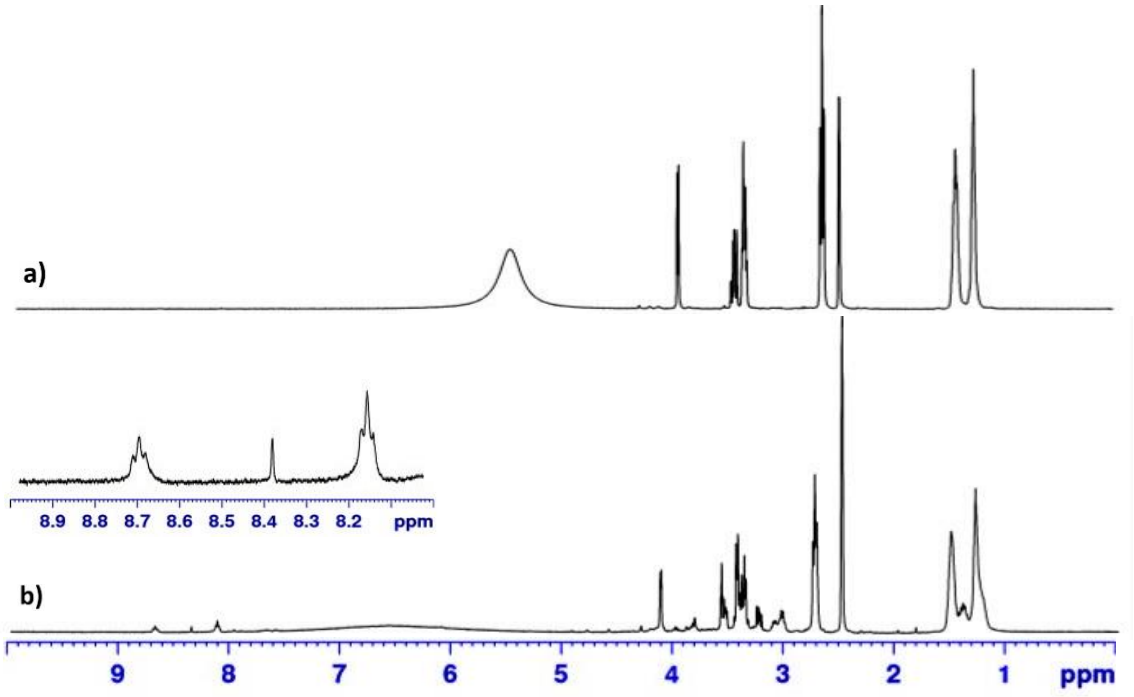

Figure 33. ^{1}H-NMR spectra of the reaction mixture before synthesis (a) and CDs after synthesis (b), using as solvent DMSO-D6.

Table 6. ^{1}H-NMR peaks before and after synthesis. Spectrum a) reaction mixture and spectrum b) CDs-RT.

Symbol	***Spectrum a) Reaction mixture***	***Spectrum b) CDs-RT***
1*	No peak	Peak at 3 ppm
2*	No peak	Peak at 4.1 ppm
3*	No peak	Peaks at 8.7 ppm, 8.4 ppm and 8.2 ppm

Regarding UV-Vis, figure 34 represents the UV-Visible spectra of the reaction mixture exposed to 200 °C for 5 and 8 hours as figure 35 corresponds to the room temperature approach. The reaction mixture before synthesis exhibits absorption at 266 nm, and after 5 hours of synthesis, the absorption band disappears. The synthesis was also performed for 8 hours and two new bands at 210 and 251 nm appeared; these are assigned to π-π* and n-π* transitions. The room temperature approach after 15 days of synthesis did not reveal any absorption. The excitation spectrum of CDs formed at room temperature (figure 36) was traced; emission at 419 nm resulted from excitation at 220 and 340 nm.

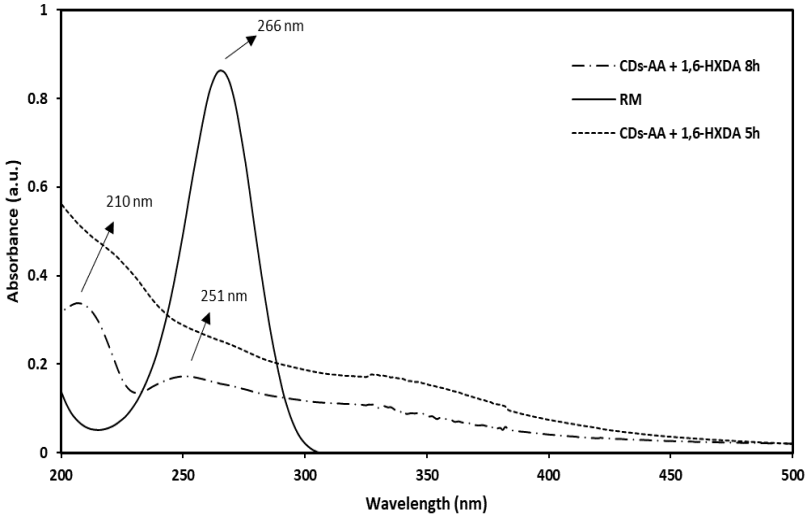

Figure 34. UV-Vis spectra of carbon dots based on ascorbic acid with 1,6-hexanediamine 5 h and 8h synthesis (CDs-AA + 1,6-HXDA 5h and 8h) with its respective RM before synthesis, using water as solvent.

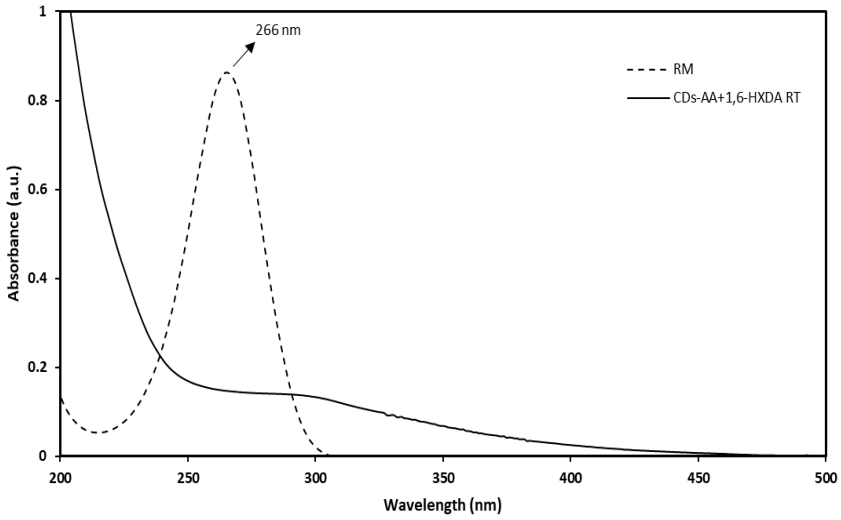

Figure 35. UV-Vis spectra of carbon dots based on ascorbic acid mixed with 1,6-hexanediamine (room temperature reaction) and its respective reaction mixture before synthesis, using water as solvent.

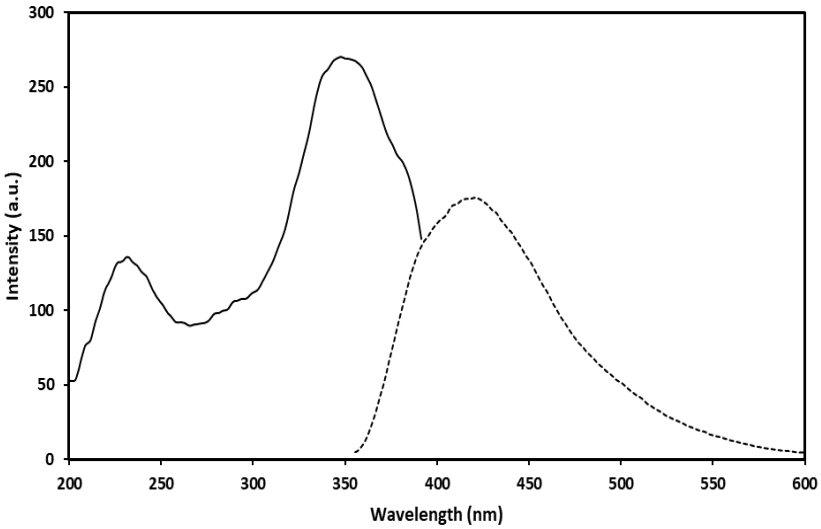

Figure 36. Excitation spectra of CDs-AA+1,6-HXDA RT obtained using an emission wavelength of 419 nm, using water as solvent.

The emission spectra of all the attempts, emission/excitation dependency graph, including the reaction mixture before synthesis are summarized in figures 37, 38, 39, 40, and 41 respectively. The 5 and 8 hours approach presents two equal emission ranges, 450-550 nm, the highest fluorescence value happens at 340 nm excitation. Concerning the CDs-room temperature, the emission range is between 420-500 nm and the strongest emission occurs at 340 nm excitation. These three attempts are significantly different compared with the reaction mixture before synthesis, concretely, regarding the emission position and fluorescence intensity. In addition, the QY of CDs-5h, CDs-8h, and CDs-RT is 25.1 %, 24.2 %, and 10.3 %, respectively.

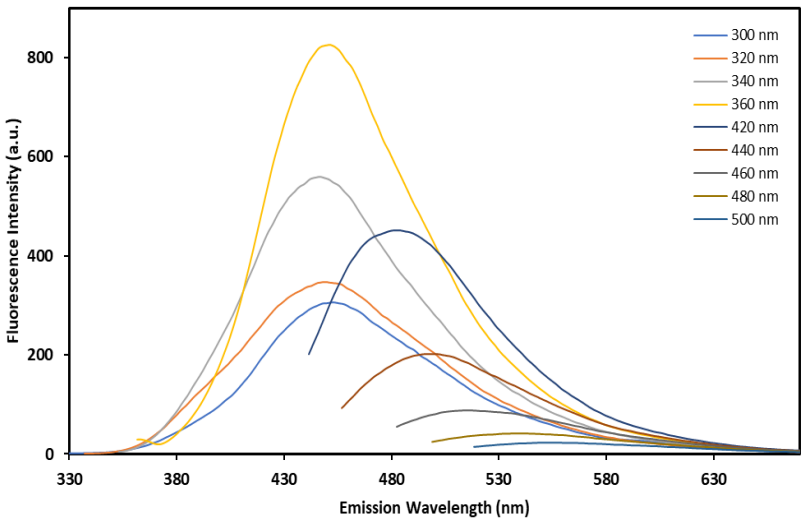

Figure 37. Emission spectra of CDs-AA+1,6-HXDA 5 h of synthesis, with an excitation wavelength between 300-500 nm using a 20 nm increment.

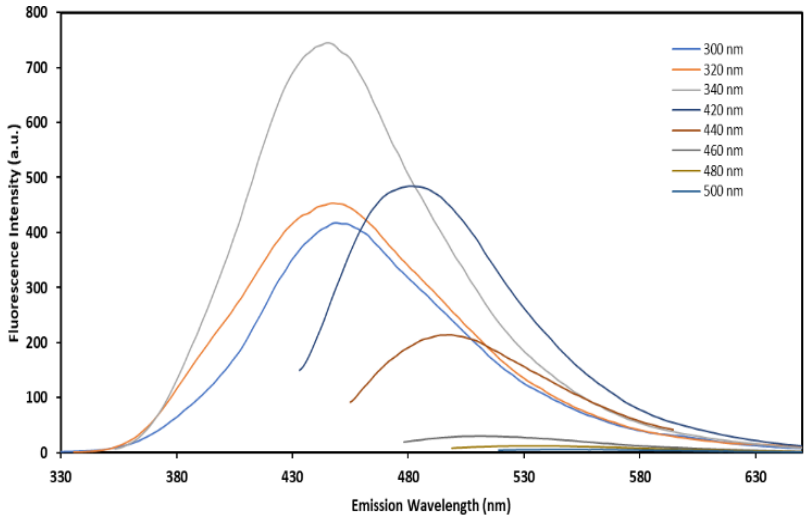

Figure 38. Emission spectra of CDs-AA+1,6-HXDA 8 h of synthesis, with an excitation wavelength between 300-500 nm using a 20 nm increment.

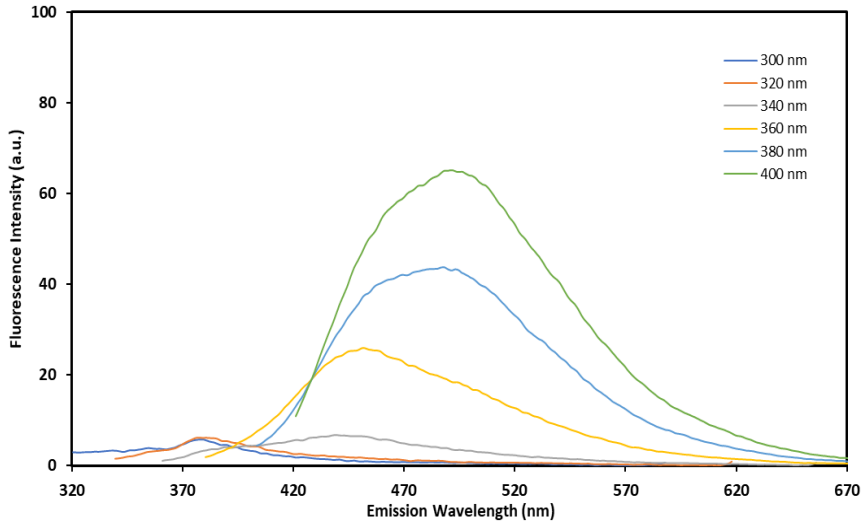

Figure 39. Emission spectra of the reaction mixture before synthesis, with an excitation wavelength between 300-400 nm using a 20 nm increment.

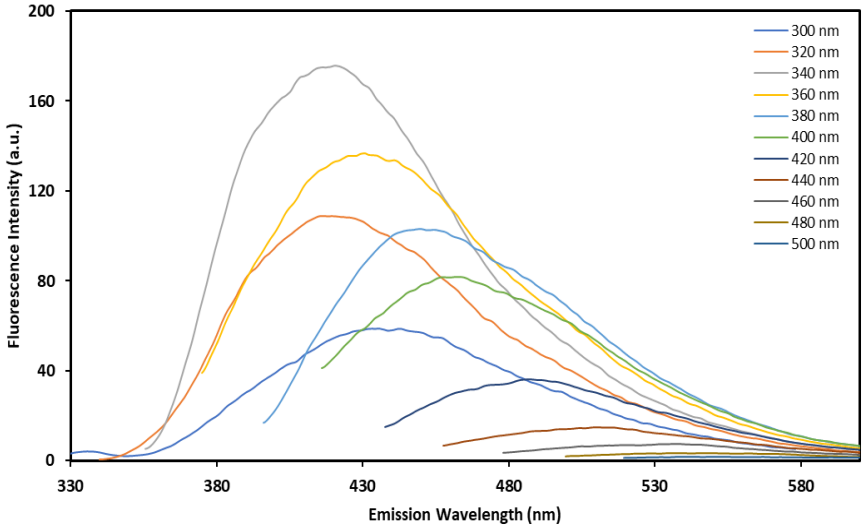

Figure 40. Emission spectra of CDs-AA+1,6-HXDA RT, room temperature synthesis with an excitation wavelength between 300-500 nm using a 20 nm increment.

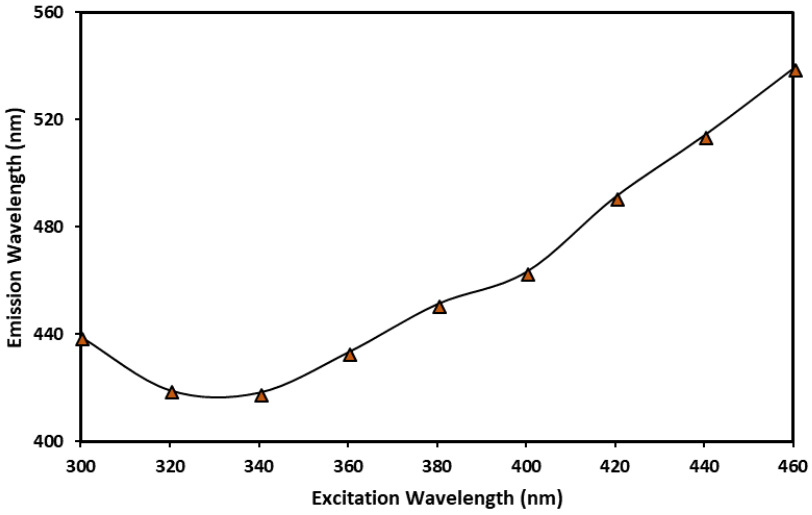

Figure 41. Emission wavelength obtained using 300-460 nm excitation of CDs-RT, with 20 nm increments. From 300-460 nm excitation, the emission goes from 440-530 nm.

Based on these results, we assume the generation of a new fluorescent product by employing ascorbic acid and 1,6-hexanediamine. A considerable number of black dots was verified only for the room temperature reaction, confirming the success of the approach. The hydrothermal approach (5h and 8h) wasn´t successful, even so, it might be possible the production of carbon dots, the problem is the synthesis length, meaning optimization of the experimental conditions. Concretely, in the beginning, the reaction conditions were 5 hours at 200^{o}C, and no black dots were observed by TEM. Then, the reaction time was increased to 8 hours, due to the need to generate a significant amount of carbon cores, but perhaps 8 hours in those harsh conditions was too much, and the CDs were possibly destroyed resulting in small fragments observable in the TEM images. Another aspect when dealing with amine precursors is the synthesis of small fluorescent molecules, *e.g.,* IPCA (imidazo[1,2-α]pyridic-7-carboxylic acid 1,2,3,5 tetrahydro-5-oxo), these appear after a certain time and are highly responsible for the fluorescent properties[87]. Although IPCA was only detected in citric acid-based approaches, there is a possibility of being present in the 5 and 8 hours approach.

The CDs-RT were possible to be synthesized at room temperature, although its reaction type and mechanism are of difficult clarification, we speculate on a kind of interaction between the ascorbate ion and NH_3^+ species of 1,6-hexanediamine, resulting in a condensation reaction with further polymerization along those 15 days, thus producing a specific carbon-based dot, the polymer dots. Also, the characterization by FT-IR and DLS (ξ-potential) helped to project the surface of the CDs-RT, figure 42. The surface functional groups of the particles are a mixture of carboxyl and different N-type structures; further techniques such as XPS would be important to have a better estimation.

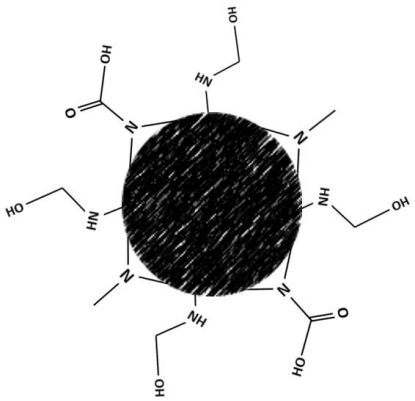

Figure 42. CDs-room temperature representation.

3.4 Carbon Dots based on Oxaloacetic acid

The synthesis of CDs was tried using oxaloacetic acid as the starting precursor and was placed inside an autoclave reactor for 5 hours at 200 ^{o}C. The following are the results from UV-Vis, emission, quantum yield, and TEM.

Oxaloacetic acid is another stimulating material to produce carbon dots due to its composition (C, O, and H) and functional groups such as carbonyl and carboxyl groups. Even though the material is not used for CDs synthesis, and knowing the potential of the precursor, we prepared a solution of oxaloacetic acid and placed inside an autoclave reactor and heated at 200 ^{o}C for 5 hours towards the synthesis of CDs.

TEM was used to observe the CDs morphology and size. According to figure 43, the CDs were not obtained. The densest black dots had an average size of 0.8 nm, too small to consider as carbon dots. The registered ξ-potential was 12 mV.

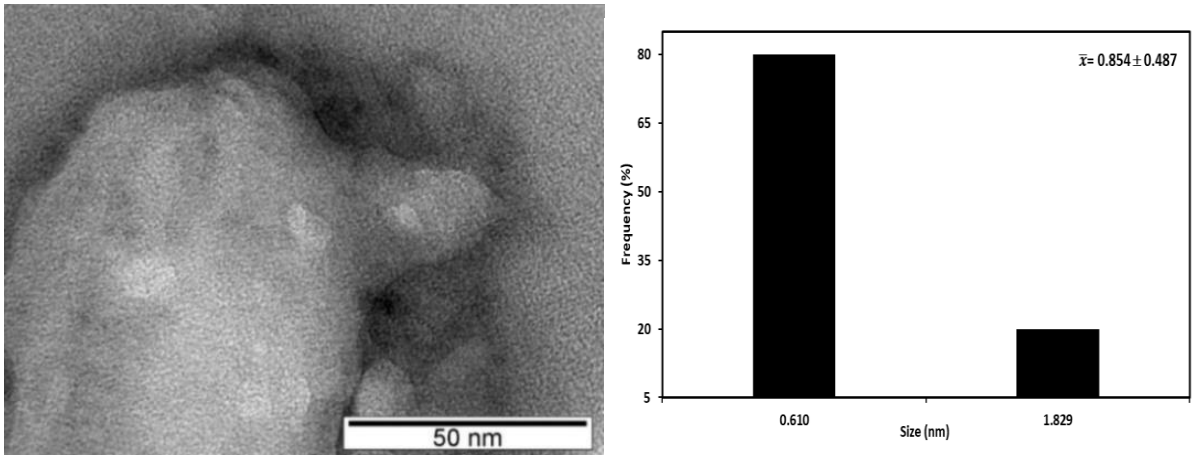

Figure 43. TEM image of CDs-OA and its respective size distribution.

Regarding the UV-Vis spectra of CDs-OA and its reaction mixture (figure 44), the reaction mixture before synthesis presents a shoulder at 256 nm which is shifted to 279 nm after synthesis.

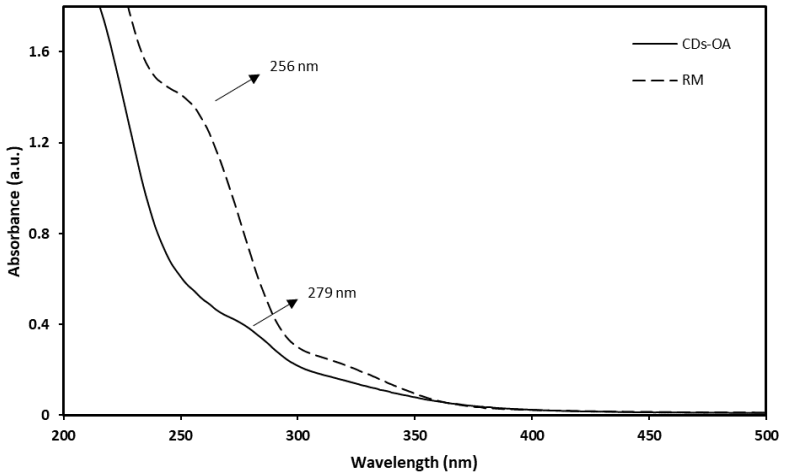

Figure 44. UV-Vis spectra of the carbon dots based on oxaloacetic acid (CDs-OA) with its respective reaction mixture before synthesis.

The emission spectra of CDs-OA and its reaction mixture are presented in figures 45 and 46, respectively. The CDs-OA have a maximum emission centred at 440 nm using a 340 nm excitation, while the reaction mixture has a maximum emission at 480 nm achieved by using an excitation wavelength of 400 nm. Additionally, the fluorescence intensity of the reaction mixture is smaller than the CDs-OA, and the QY was 18.6 %.

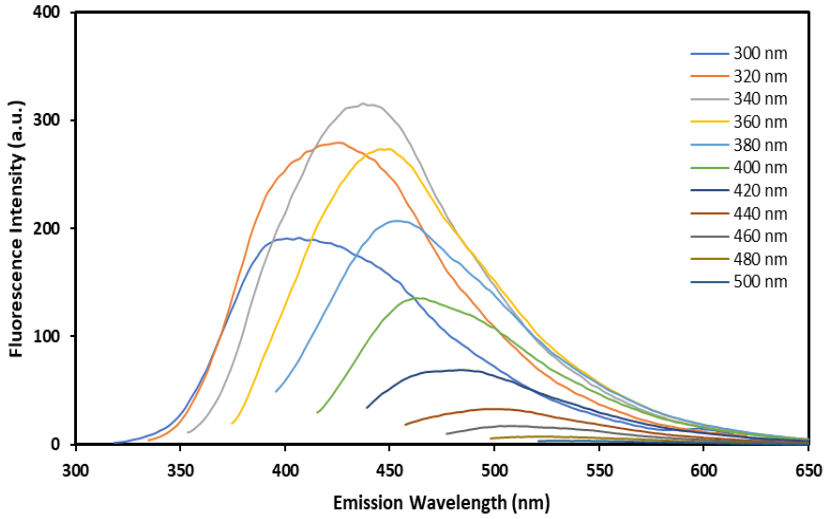

Figure 45. Emission spectra of CDs-OA with an excitation wavelength between 300-500 nm using an increment of 20 nm.

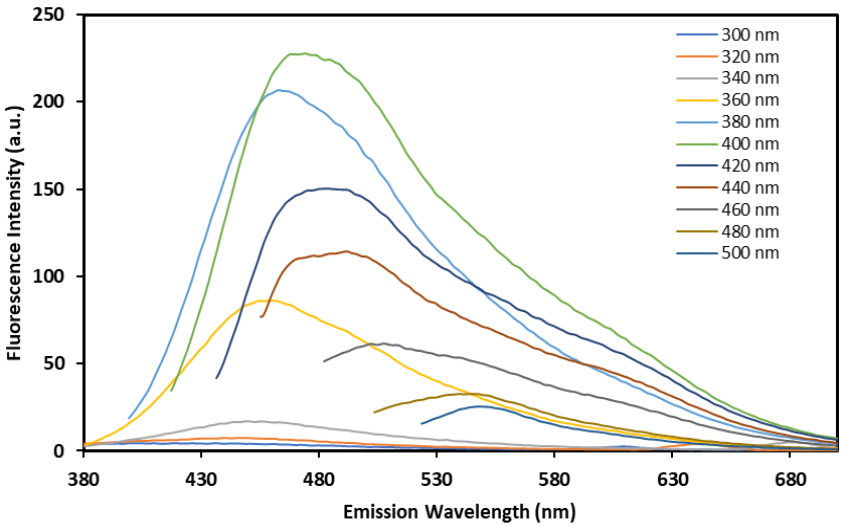

Figure 46. Emission spectra of the reaction mixture before synthesis, with an excitation between 300-500 nm and an increment of 20 nm.

Based on the results obtained, particularly the TEM images, no carbon dots were observed, confirming the failure of the attempt. Again, further optimization should be made to select the exact conditions for carbon dots synthesis.

3.5 Carbon Dots based on Oxaloacetic acid and 1,6-hexanediamine

As mentioned in section 3.3, amine precursors and carbon-based compounds are interesting for CDs synthesis. Exploring the potential of oxaloacetic acid as starting precursor and amine materials as emission enhancers, oxaloacetic acid was mixed with 1,6-hexanediamine at 200^{o}C for 5 and 8 hours inside an autoclave reactor and using an oil bath. This approach constitutes a novel approach since it is not mentioned in the literature. Thus, no term of comparison is available.

The TEM images obtained from CDs-5h (A) and CDs-8h (B) are summarized in figure 47. Only two particles were obtained for the 5 hours approach, and 8 hours reaction did not present any. Also, the ξ-potential of both 5 and 8 hours approach were -12.7 and -16.0 mV, respectively.

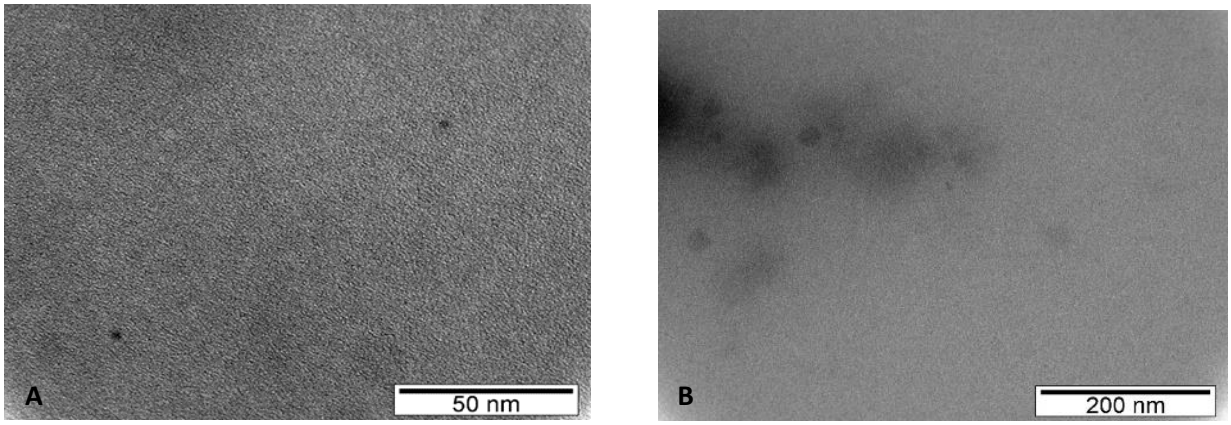

Figure 47. TEM image of CDs-5h of synthesis (A) and CDs-8h (B).

The surface functionality of the new products (figure 48) was detected using FT-IR. The reaction mixture before synthesis revealed the presence of C-H stretching vibration at 2920 cm^{-1} and 2851 cm^{-1}. The carbonyl group is centred at 1753 cm^{-1} and the bending mode of N-H at 1563 cm^{-1}. The 5h approach presents at 3348 cm^{-1} and 3262 cm^{-1} a broadband ascribed to -OH and primary amines, the C-H stretching vibration is at 2920 cm^{-1} and 2851 cm^{-1}, the bending mode of N-H is at 1548 cm^{-1}. The vibration at 1380 cm^{-1} is attributed to the bending mode of C-H. After 8 hours of synthesis, there are some significant differences comparing to the reaction mixture and CDs-5h, such as a small broadband at 3316 cm^{-1} corresponding to -OH and a stretching vibration at 1303 cm^{-1} ascribed to C-N stretching; the remaining vibration bands are quite like CDs-5h.

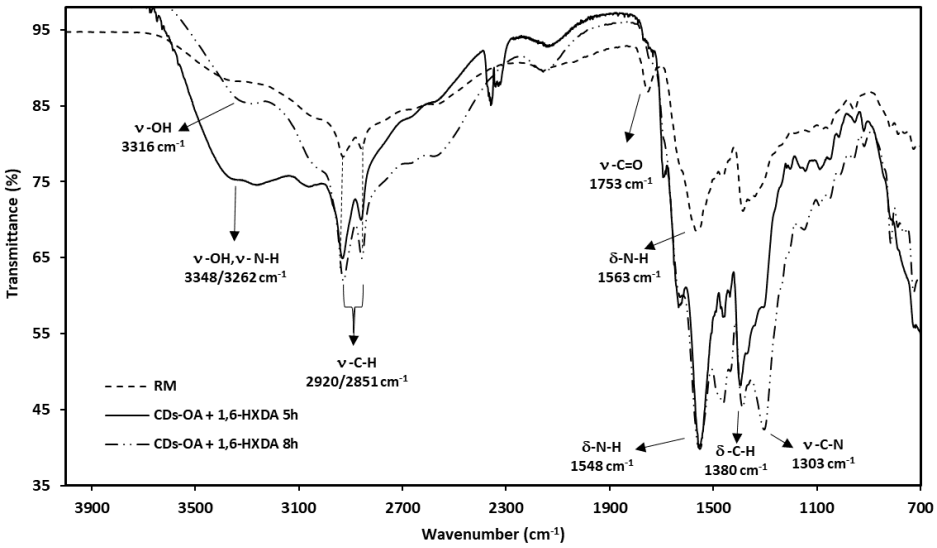

Figure 48. ATR FT-IR spectra of the reaction mixture before synthesis (RM), CDs 5 h and 8 h of synthesis.

Using ^{1}H-NMR (figure 49), it was possible to detect the differences before and after synthesis. The ^{1}H-NMR spectrum of the reaction mixture composed by oxaloacetic acid and 1,6-hexanediamine was obtained using DMSO-D6 has a solvent (peak at 2.5 ppm), the peaks detected for the mixture are centered at 1.2, 1.5, 2.5, 2.6, and 2.9 ppm, characteristic of the alkane/alkene region, the exact attribution of each one is of great difficulty since the two starting materials are interacting and thus creating a new chemical environment. After 5 and 8 hours of synthesis (spectrum b and c), peaks at 1 ppm, 8, 8.2 ppm and 8.9 ppm appear, meaning the synthesis of a new product. CDs by this approach were not produced has observed in the TEM images (figure 47), we assume the possibility of producing small and different fluorescent molecules, and so the attribution of the new peaks after synthesis is hard to assign, also the use of ^{13}C-NMR, 2D-NMR, and even XPS would help to assume the structures of the products synthesized.

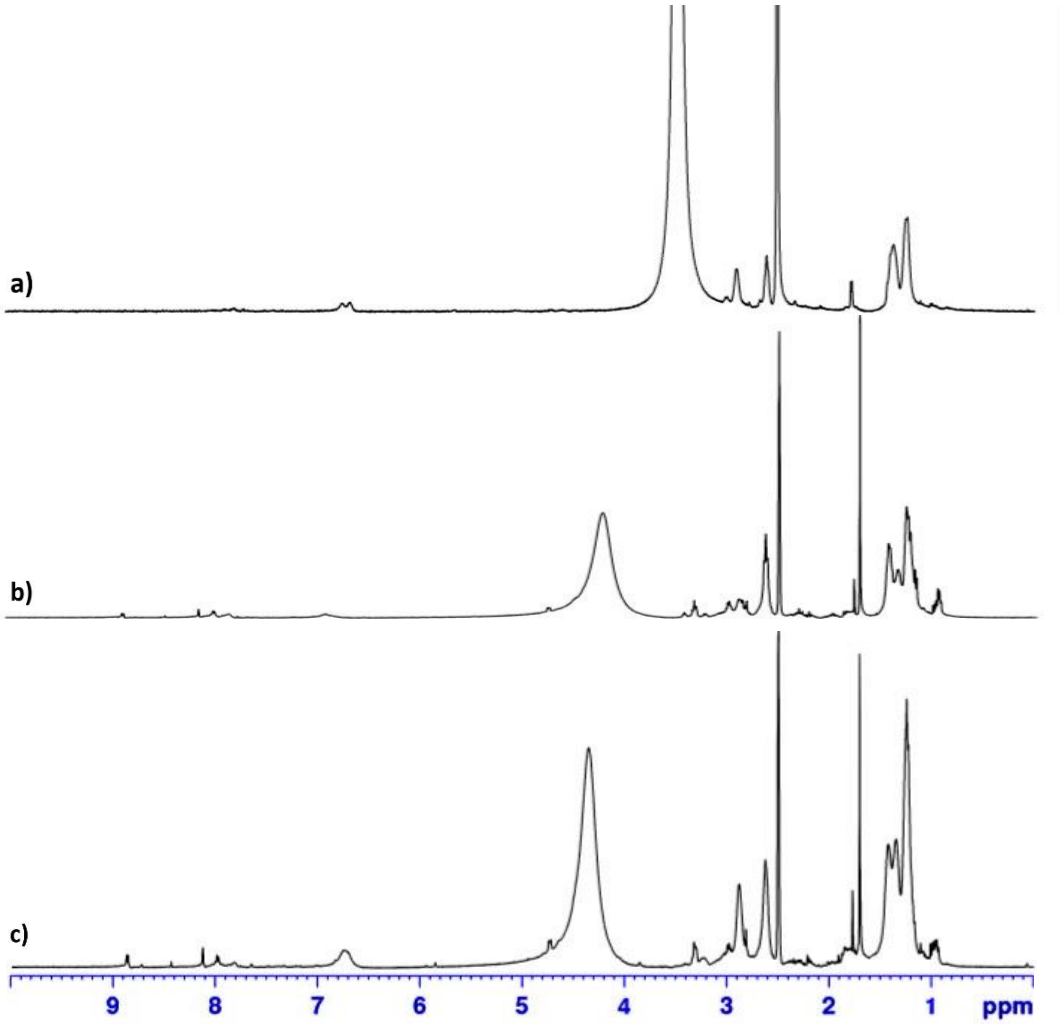

Figure 49. ^{1}H-NMR spectra of a) reaction mixture before synthesis b) CDs 5 h and c) CDs 8 h of synthesis, using as solvent DMSO-D6.

Table 7. ^{1}H-NMR peaks before and after synthesis.
Spectrum a) reaction mixture, spectrum b) CDs-5h and spectrum c) CDs-8h.

Spectrum a) Reaction mixture	Spectrum b) CDs 5 h	Spectrum c) CDs 8 h
No peak	Peak at 1ppm	Peak at 1 ppm
No peak	Two peaks at 8 ppm and 8.2 ppm	Two peaks at 8 ppm and 8.2 ppm
No peak	Peak at 8.9 ppm	Peak at 8.9 ppm

Regarding the UV-Vis spectra of the reaction mixture before synthesis, CDs-OA + 1,6-HXDA 5 h and 8 h are summarized in figure 50. The reaction mixture before synthesis presents an absorption maximum centred at 323 nm, while the CDs-5h present a maximum at 282 nm, after 8 hours of synthesis two absorption maximums appear at 241 nm and 282 nm, the latter are ascribed to π-π* and n-π* transitions.

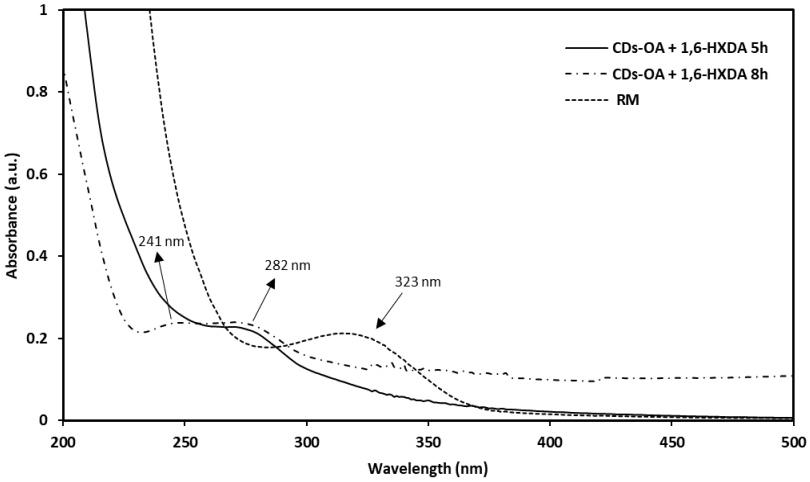

Figure 50. UV-Vis spectra of the Carbon dots based on oxaloacetic acid mixed with 1,6-hexanediamine 5 h and 8 h synthesis (CDs-OA + 1,6-HXDA 5 h and 8 h) with its respective reaction mixture before synthesis (RM), using water as solvent.

The emission spectra of CDs-5 h, 8 h, and RM before synthesis are summarized in figures 51, 52, and 53. The CDs-5h and 8h present emission dependent upon excitation. Specifically, CDs-5h present their maximum emission at 340 nm excitation, like CDs-8h; in contrast, the reaction mixture before synthesis presents a maximum emission at 380 nm of excitation. Moreover, the fluorescence intensity of CDs-5h and 8h is higher when compared to the reaction mixture. The QY of the CDs-5h and 8h was 39.58 and 30.81%, respectively.

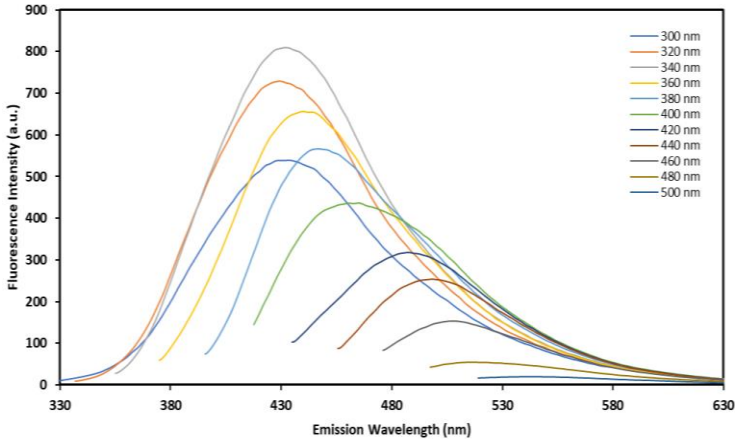

Figure 51. Emission spectra of CDs-OA + 1,6-HXDA 5 h with an excitation wavelength from 300-500 nm and an increment of 20 nm.

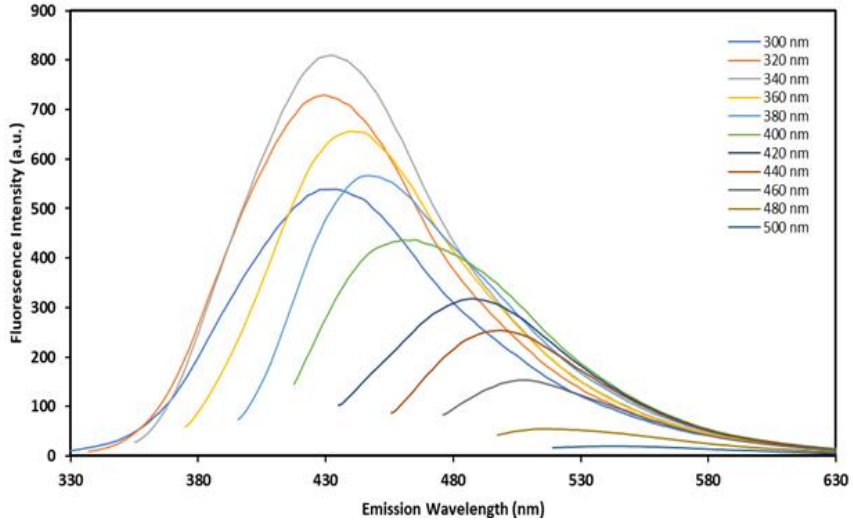

Figure 52. Emission spectra of CDs-OA + 1,6-HXDA 8 h with an excitation wavelength from 300-500 nm and an increment of 20 nm.

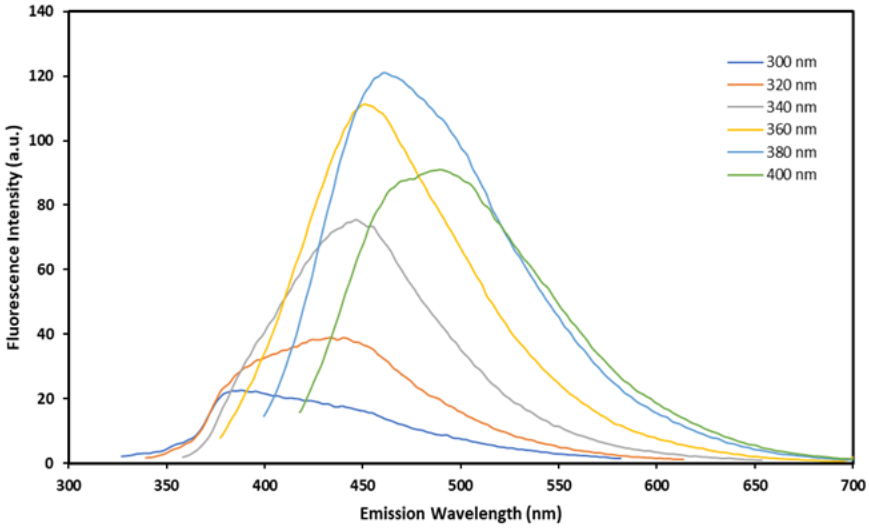

Figure 53. Emission spectra of the reaction mixture before synthesis from 300-400 with an excitation increment of 20 nm.

Based on the results obtained, especially TEM images, we were not able to produce CDs; we do not discard the possibility of having generated fluorescent molecules like the ones discussed in the previous approach, section 3.3. We started with 5 hours of synthesis, and only two black dots were seen, we felt the need to increase the reaction time for 8 hours, which didn't mostly improve. All the aminated approaches performed in this work present the need of optimization.

3.6 Carbon Dots Studies

The carbon dots used for further studies comprising quenching, pH, fluorescence stability, and DNA condensation were the dots based on folic acid (CDs-FA), ascorbic acid (CDs-AA), and based on ascorbic acid-1,6-hexanediamine room temperature (CDs-RT). The selection process was based on the confirmation of the carbon dots by TEM.

3.6.1 Quencher Effect

The effect of quenching on the CDs based on folic acid, ascorbic acid, and room temperature approach was studied using KI as the ionic agent. The KI concentrations were between 20-200 mM, and the results are summarized in figures 54, 55, and 56 respectively for CDs-FA, CDs-AA, and CDs-RT. The CDs-FA show a total 95 % fluorescence intensity decrease at 200 mM, the CDs-AA and CDs-RT also suffer an intensity reduction that reaches a total of 50% and 70% at 200 mM, respectively. Moreover, the initial addition of 20 mM potassium iodide decreases the intensity of the fluorophores to 50%, 17%, and 35% when compared to the control, respectively for the CDs-FA, CDs-AA, and CDs-RT.

Quenching refers to a process where the fluorescence intensity of a given substance decreases. Iodide is known for their quenching capabilities; therefore, it can decrease the fluorescence intensity of a given fluorophore. The collisional quenching is the quenching type for iodide, and in contact with an atom or molecule facilitates non-radiative transitions to the ground-state. The results obtained show that the increase of KI concentration lead to a larger amount of quencher in solution, colliding more frequently with the carbon dots, consequently decreasing their fluorescence intensity. The CDs-AA (figure 55) were the most photostable out of the three tested, and this might be related with the charge of the dots, which is of negative nature (confirmed by ξ-potential), meaning some repulsive effect between the quencher and the negative-CDs occurred.

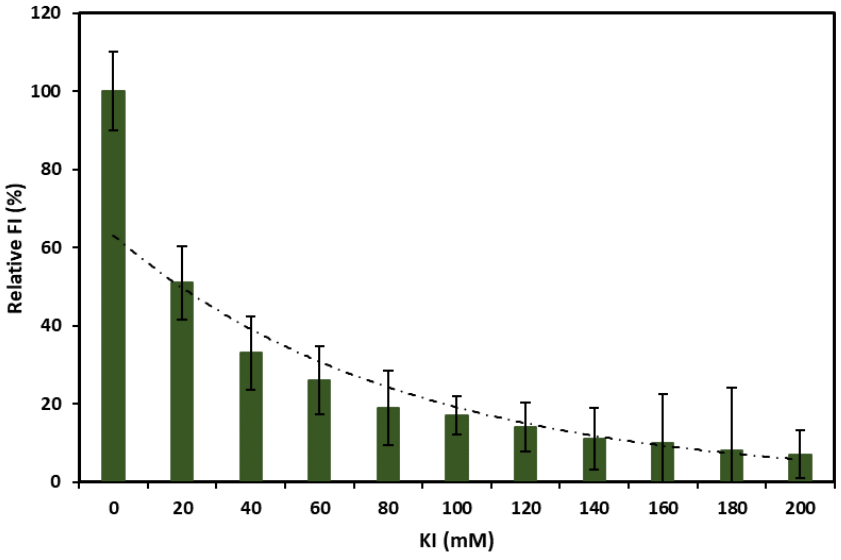

Figure 54. Quenching effect on CDs-FA, using water as solvent.

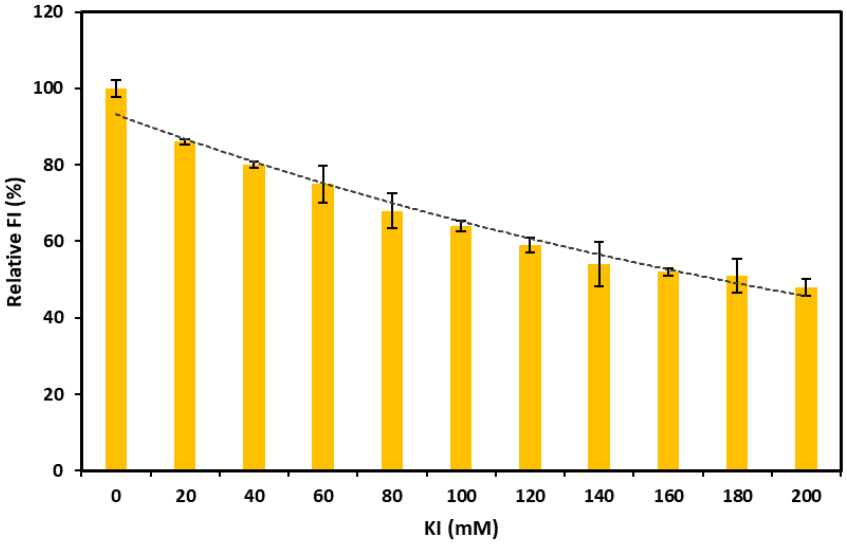

Figure 55. Quenching effect on CDs-AA, using water as solvent.

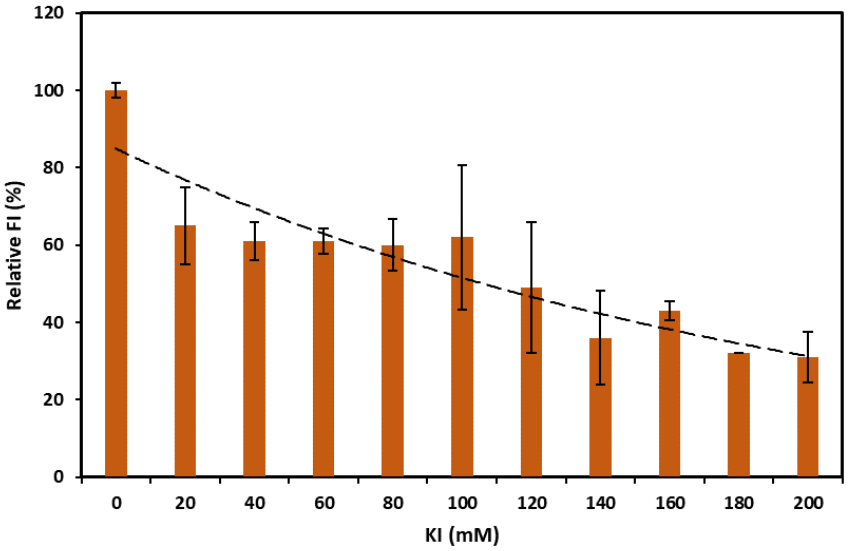

Figure 56. Quenching effect on CDs-RT, using water as solvent.

3.6.2. pH

The pH effect was tested in CDs-FA, CDs-AA, and CDs-RT and results are presented in figures 57, 58 and 59, respectively. The pH of the raw CDs-FA is 2.56, and present at pH 9 its maximum fluorescence intensity. At acidic pH, the particles are considerably stable, and between pH 7-9 the fluorescence intensity increases. Regarding CDs-AA, they have a pH of 3.16, the fluorescence intensity increases from acidic to almost neutral pH, reaching its maximum at pH 6, following a decrease in alkaline environments. Lastly, the raw CDs-RT have a pH of 8.16 and increase gradually their fluorescence intensity from acidic to alkaline environments, reaching its maximum at pH 9.

In the literature, it has been found that the maximum fluorescence intensity of carbon dots occurs at neutral conditions whereas in others a gradual increase from acidic to basic conditions happens[88,89]. Our results present the same trend, the CDs-FA, and CDs-RT gradually increases their intensity from acidic to basic conditions, while the CDs-AA show higher fluorescence intensities at neutral pH. The CDs-FA and CDs-RT share a positive ξ-potential which is in part due to the different N-type groups on their surfaces. The possible explanation for the stability of the fluorescence intensity in CDs-FA is their capacity to act as a buffer, specifically between pH 3-7, the carboxyl and amino groups present on the surface can neutralize the effect of H^+ species, maintaining the fluorescence integrity of the dots. When the pH reaches basic environments (pH 8-10), the fluorescence intensity increases, the OH^- species can enhance and promote the CDs-FA surface to emit more fluorescence. The same explanations can be used for the case of CDs-AA and CDs-RT, which have a surface composed by a mixture of carboxyl, hydroxyl groups and different N-type moieties, respectively. Additionally, the results from absorption and emission of CDs-FA, CDs-AA, and CDs-RT (figures S28-S33, Appendix section 1.5) show clearly the pH effect on the fluorescence intensities of the particles and showing the same trend obtained in figures 57, 58, and 59. Based on the results obtained, different pH environments can enhance and improve the fluorescence intensity of all three carbon-based dots.

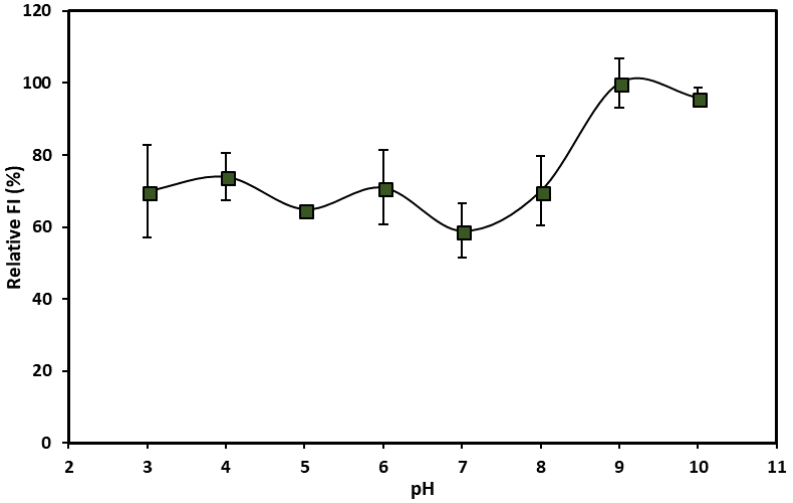

Figure 57. pH effect in CDs-FA.

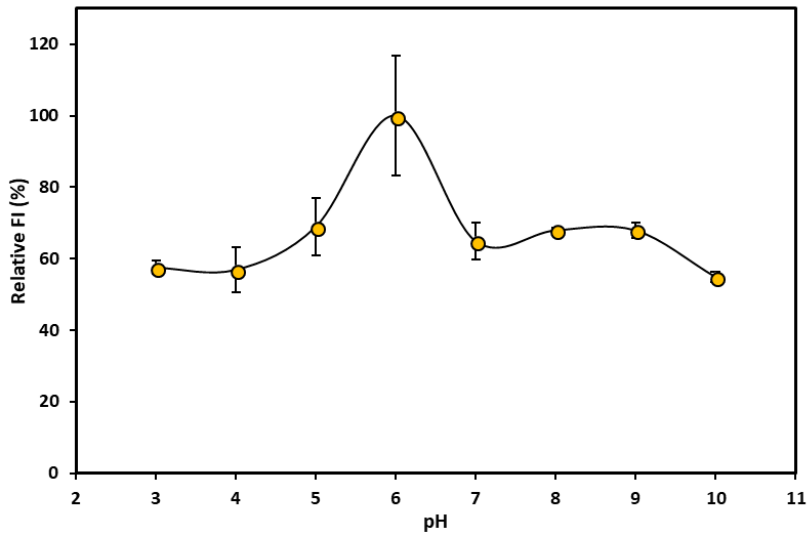

Figure 58. pH effect in CDs-AA.

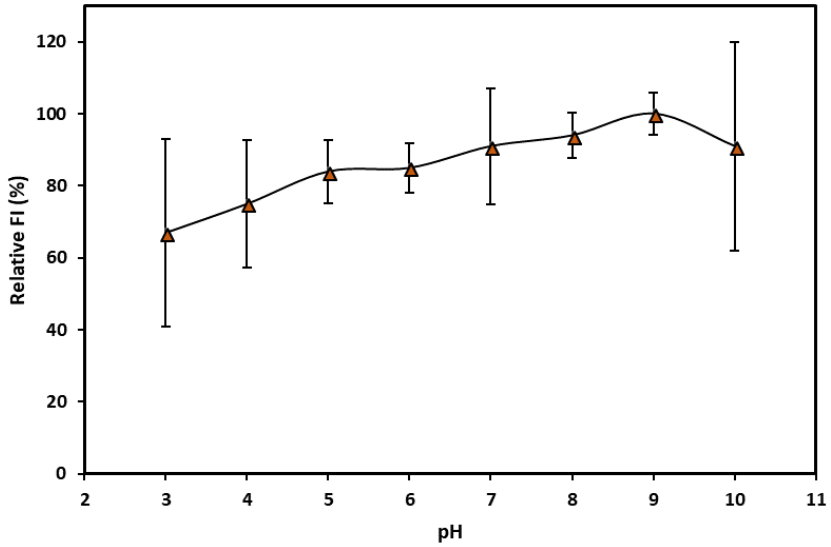

Figure 59. pH effect in CDs-RT.

3.6.3 Fluorescence stability

The fluorescence stability of CDs-FA, CDs-AA, and CDs-RT was evaluated using weekly fluorescence intensity readings in a fluorimeter. Over the course of 8 weeks, the CDs were subjected to measurements by using 360 and 380 nm excitation wavelengths. The results are presented in figures 60 and 61, respectively for 360 nm and 380 nm excitation. The CDs-FA are stable regarding fluorescence intensity until the first 21 days, after which, the fluorescence increases between 28 and 42 days, suffering a decrease after 49 days. The CDs-AA are relatively photostable over the course of 49 days with a considerable decrease after 56 days of study. The CDs-RT increase gradually their fluorescence intensity over the course of 49 days and suffer a decrease in day 56. Using the 380 nm excitation, all three samples present the same graphical behaviour as the ones from 360 nm excitation. The three solutions share a considerable intensity decrease after 56 days of study.

The results obtained show relative fluorescence stability between day 0 and day 49 for all three carbon-based dots, and it would be interesting to study the fluorescence stability after 56 days.

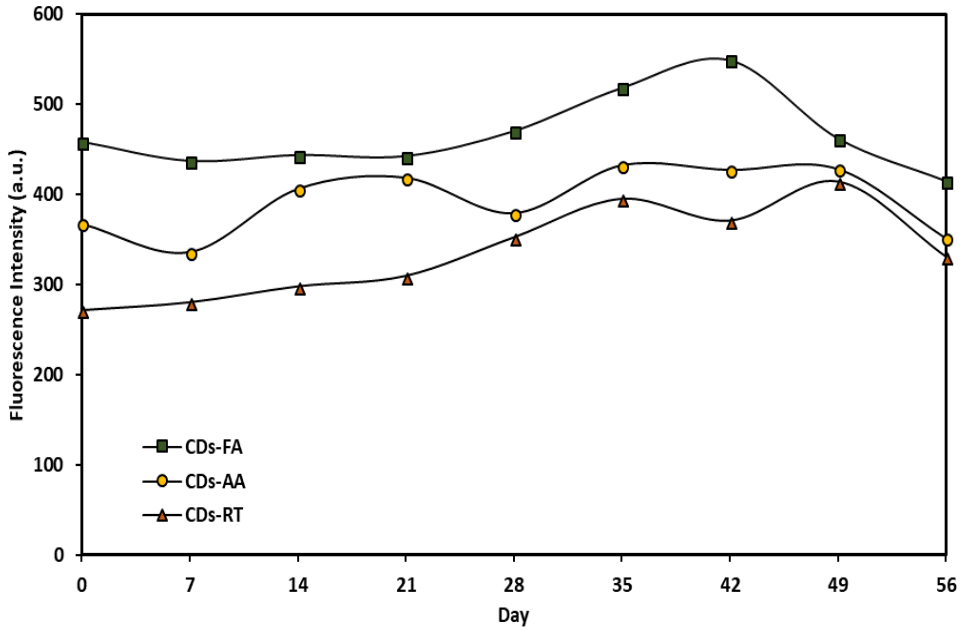

Figure 60. Fluorescence stability over time of CDs-FA, CDs-AA and CDs-RT, using 360 nm excitation.

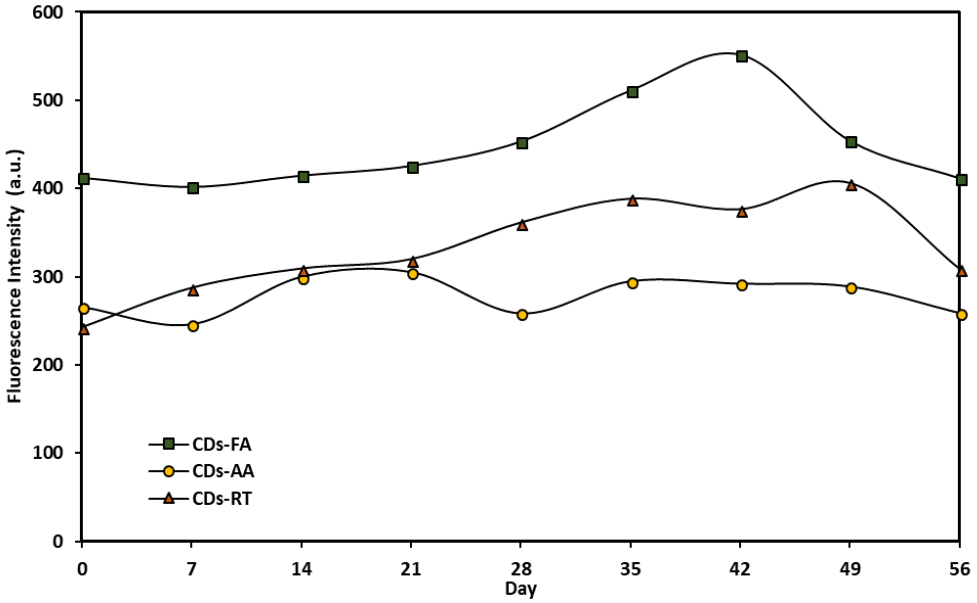

Figure 61. Fluorescence stability over time of CDs-FA, CDs-AA, and CDs-RT, using 380 nm excitation.

3.6.4 DNA condensation

CDs condensation properties were studied using pDNA. Different CDs-pDNA ratios were used, explicitly 1:1, 10:1, 20:1, 40:1 and 100:1. The results obtained are presented in figures 62 (PicoGreen assay), figures 63, 64, and 65 are from the number distribution of CDs-FA, CDs-AA, and CDs-RT respectively at different pDNA ratios. In respect to CDs-FA, the PicoGreen assay results show an almost complete DNA condensation at 100:1 ratio, whereas the CDs-AA show a total of 20% condensation at 100:1 proportion. The CDs-RT shows the least interesting results, the percentage of total DNA condensation at 100:1 ratio was only 70 %.

Dynamic light scattering was used to obtain the hydrodynamic size and ξ-potential of the different CDs-pDNA ratios. The number distribution shows that pDNA possesses a hydrodynamic size around 100 nm. The results from CDsFA-DNA condensation, show a decrease in the size distribution after CDsFA-DNA ratio increase. The CDs-AA and CDs-RT also have a decrease in the size distribution after CDs-DNA proportions increase. In table 8, the values of ξ-potential are shown, and pDNA shows a negative ξ-potential (-15.3 mv) which is characteristic, due to the phosphorous groups composing them, upon CDs-DNA ratio increase the ξ-potential suffers minor changes. Distinctively at 40:1 ratio of CDsFA-DNA, a meaningful change was obtained (-15.3 to -4.83 mV).

The PicoGreen assay is used to investigate the capacity of a material to condense DNA. The PicoGreen is a molecule that when bound to dsDNA gives a fluorescent signal. If the fluorescent signal decreases it means that the material (*e.g.* CDs) used is condensing DNA and PG will no longer bond to dsDNA and emit fluorescence. The PicoGreen assay results along with DLS measurements show an almost complete pDNA condensation by CDs-FA and CDs-AA, but this result is only possible using big CDs-pDNA ratios, concretely 100:1. The concentration of the dots at this ratio is around 0.18 mg/ml and still is not enough for complete condensation, and that might be dangerous regarding cytotoxicity. Furthermore, all CDs used in the study have the same mass concentration, but that does not mean that they present the same number of carbon nanoparticles. Meaningfully, the TEM images of both CDs-FA, CDs-AA, and CDs-RT present a total of 420, 120, and 25 NPs, respectively, and it might be possible that the CDs-RT show the least interesting result because of their small number of carbon dots.

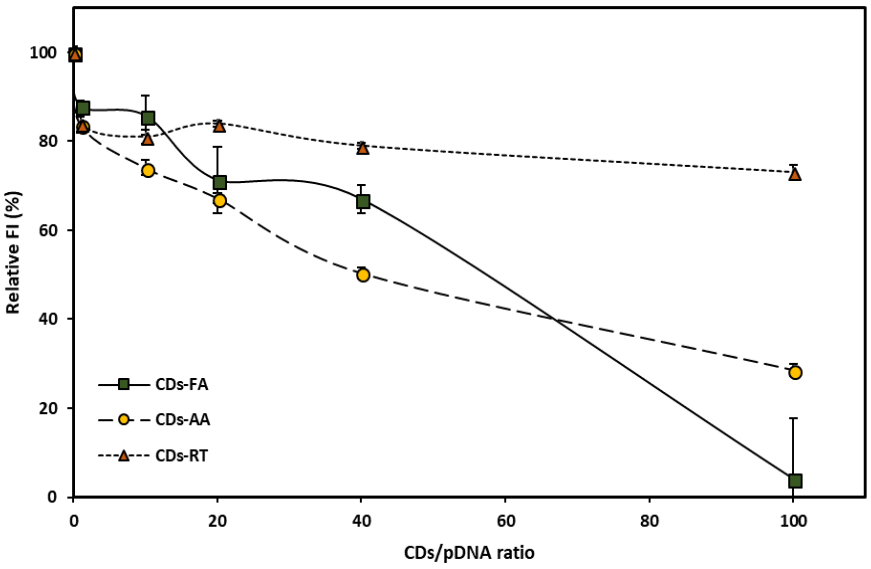

Figure 62. PicoGreen assay of CDs-FA, CDs-AA, and CDs-RT.

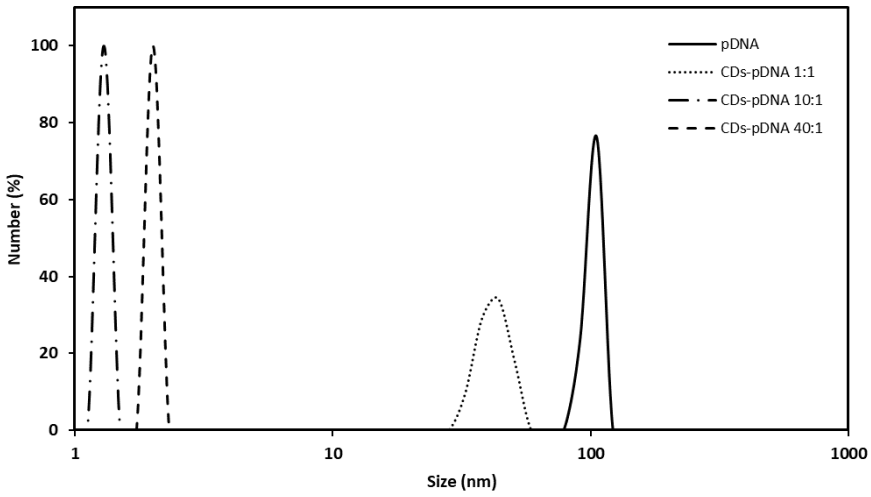

Figure 63. Hydrodynamic size distribution of CDs-FA interacting with pDNA. Number size distribution.

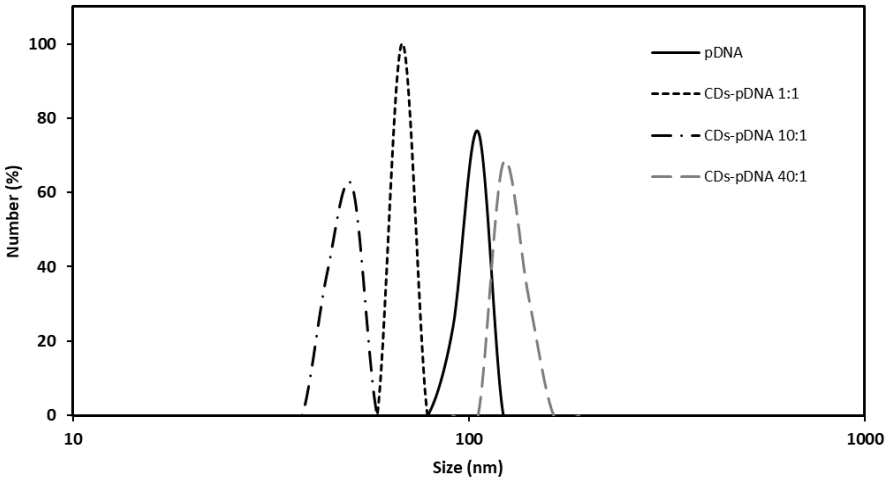

Figure 64. Hydrodynamic size distribution of CDs-AA interacting with pDNA. Number size distribution.

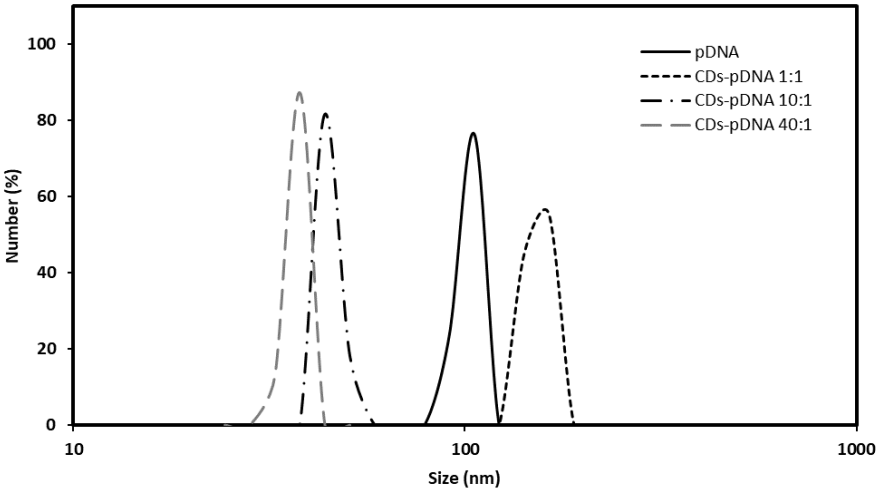

Figure 65. Hydrodynamic size distribution of CDs-RT interacting with pDNA. Number size distribution.

Table 8. ξ-potential values of pDNA and CDsFA-DNA, CDsAA-DNA, and CDsRT-DNA at different ratios.

Sample	ξ-potential (mV)
pDNA	-15.3
CDsFA-DNA 1:1	-10.6
CDsFA-DNA 10:1	-16.3
CDsFA-DNA 40:1	-4.83
CDsAA-DNA 1:1	-16.2
CDsAA-DNA 10:1	-18.1
CDsAA-DNA 40:1	-14.3
CDsRT-DNA 1:1	-11.0
CDsRT-DNA 10:1	-15.7
CDsRT-DNA 40:1	-13.2

3.7 CDs-DNA Interaction

With the aim of studying the impact of DNA in the fluorescence properties of CDs, a CDs-DNA interaction was tested. CDs-FA, CDs-AA, and CDs-RT interacted individually with dsDNA between 15-30 minutes. The results are summarized in figures 66, 67, 68, 69, 70, and 71 are from the absorption/emission of CDsFA-dsDNA, CDsAA-dsDNA, and CDsRT-dsDNA. Regarding CDsFA and CDsFA-dsDNA absorption, at low concentrations, CDs-FA show two absorption maximum at 217 and 280 nm, and dsDNA its characteristic peak centred at 260 nm. After the interaction, a broad band between 240-320 nm appears, with a maximum absorption around 275 nm (figure 66). The emission spectra show the conjugate decreasing significantly it's fluorescence intensity when compared with CDs-FA itself. (figure 67). The ξ-potential of dsDNA is -47.8 mV, after interaction with CDs-FA increases to -18.4 mV (table 9).

Regarding CDs-AA interaction with dsDNA, the UV-Vis spectra of CDs-AA show its characteristic absorption maximum centred at 220 and 270 nm, respectively. After reaction with dsDNA, the complex formed presents a maximum absorption at 260 nm; curiously, the absorption trend is quite like dsDNA itself (figure 68). The emission spectra (figure 69) show after complexation with dsDNA minor changes in the fluorescence intensity and the emission position suffers a slight blue-shift when compared to CDs-AA. The ξ-potential after interaction is different when compared to dsDNA, -36.5 mV. Lastly, the CDs-RT show after complexation with dsDNA an absorption spectrum quite like dsDNA (figure 70). The emission spectra show a decrease in the amount of fluorescence (figure 71), and the ξ-potential increases to -12.4 mV after interaction with dsDNA (table 9).

Based on the results obtained, dsDNA quenched the fluorescence of CDs-FA and CDs-RT, meaning the formation of a complex. CDs-FA and CDs-RT have a positive ξ-potential possibly due to the different N-type structures present on their surface, and since dsDNA has negative charge the interaction occurred electrostatically. Since the dots synthesized are spherical the type of surface functional groups plays a key role for interacting with dsDNA, the least negative values of ξ-potential obtained for the two types of carbon-based dots, also indicate the interaction with DNA. Concerning the results obtained for CDs-AA, these were expected, as discussed in the introduction (section 1.5), the interaction between dsDNA and a spherical particle would depend a lot on the type of surface functional groups unlike the GQDs structure, which depends mostly on the honeycomb network (π-π conjugation), therefore the negative surface of CDs-AA which is mostly composed of carboxyl/hydroxyl groups suffered a repulsive effect when contacting with dsDNA, and no complexation occurred.

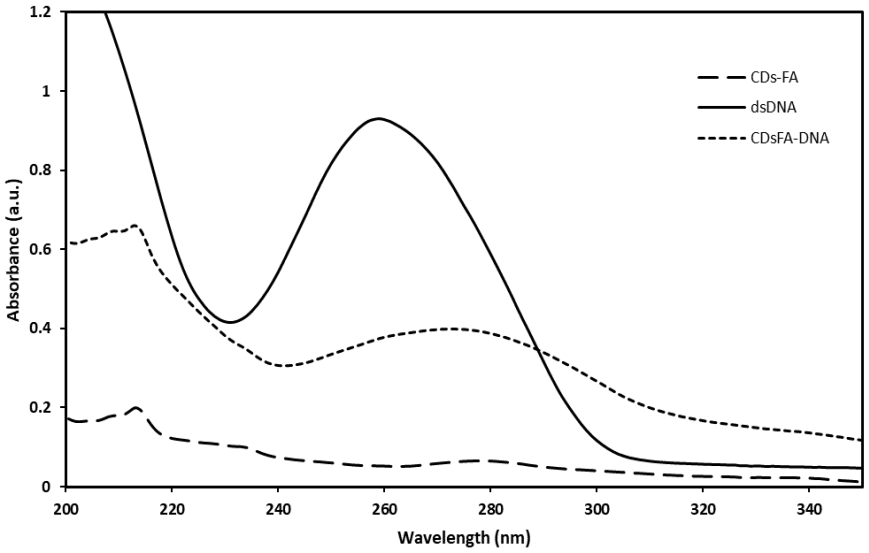

Figure 66. UV-Vis spectra of CDs-FA, double-strain DNA, and CDsFA-DNA interaction.

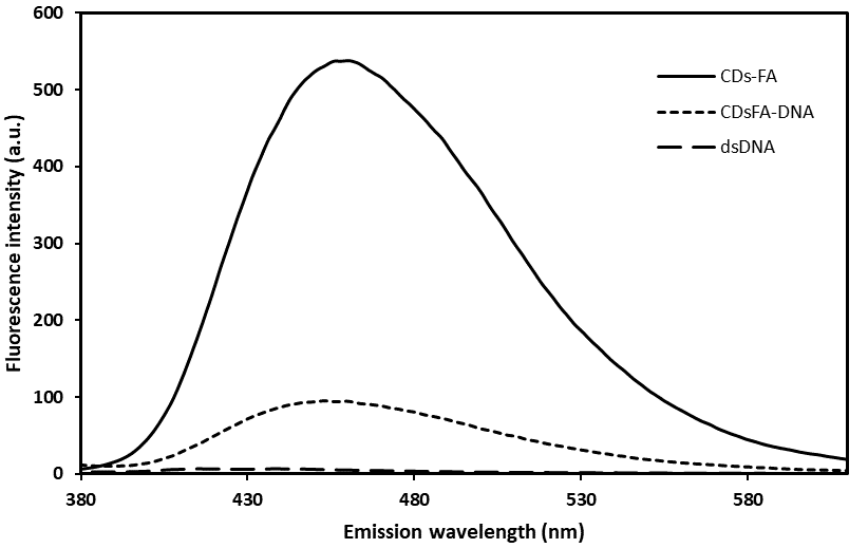

Figure 67. Emission spectra of CDs-FA, double-strain DNA, and CDsFA-DNA interaction.

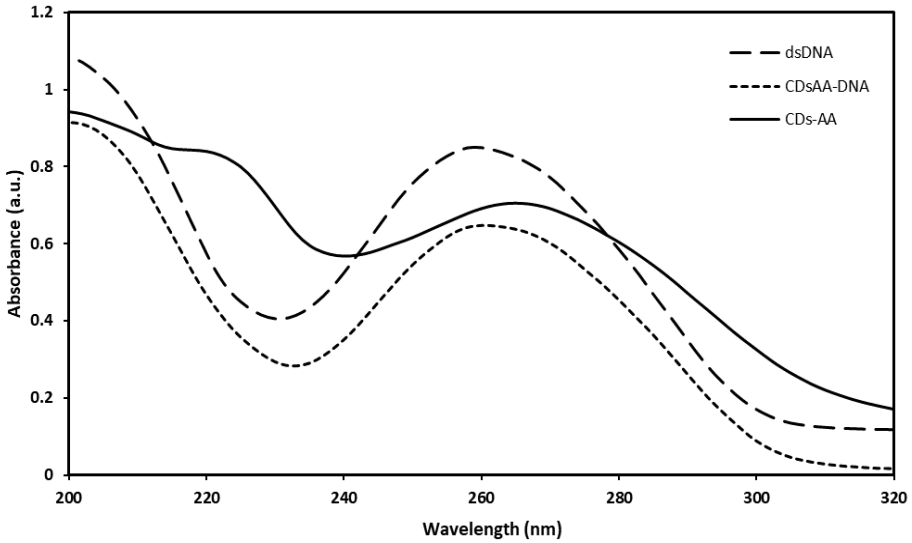

Figure 68. UV-Vis spectra of CDs-AA, double-strain DNA, and CDsAA-DNA interaction.

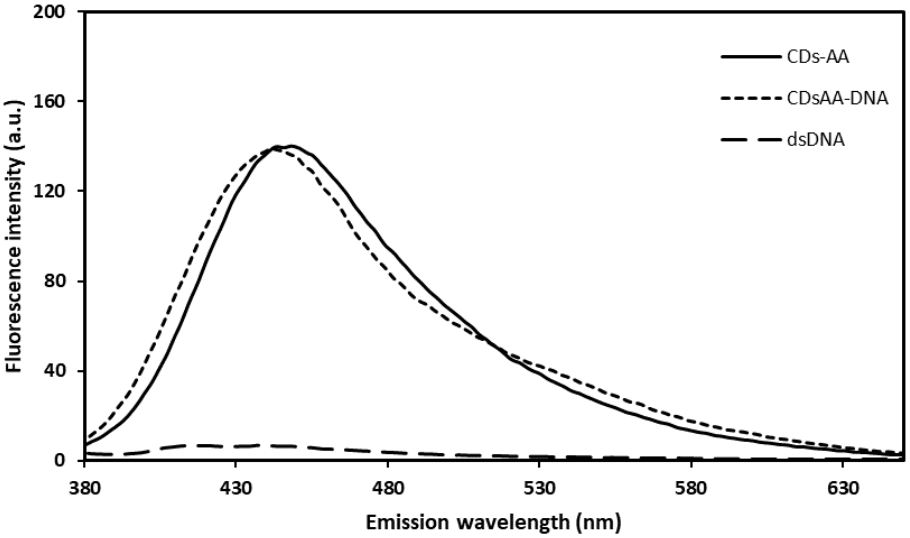

Figure 69. Emission spectra of CDs-AA, double-strain DNA, and CDsAA-DNA interaction.

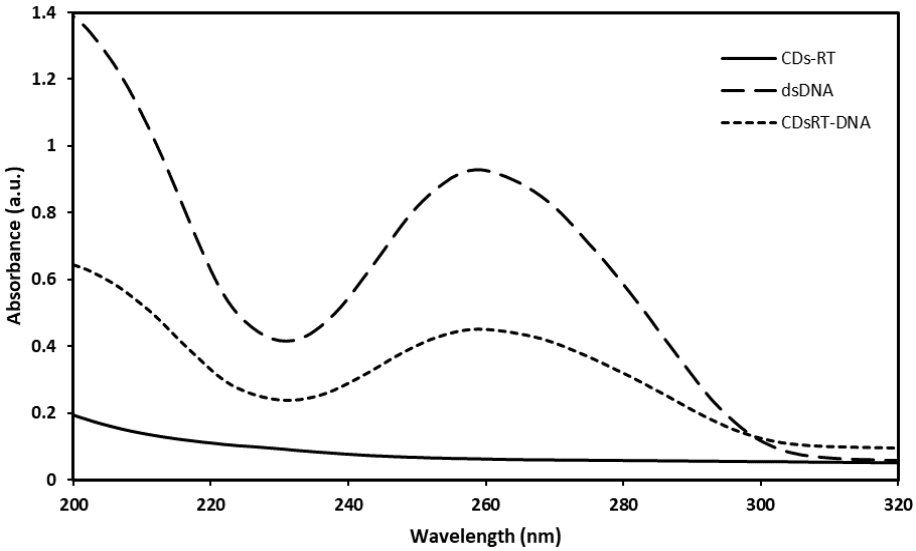

Figure 70. UV-Vis spectra of CDs-RT, double-strain DNA, and CDsRT-DNA interaction.

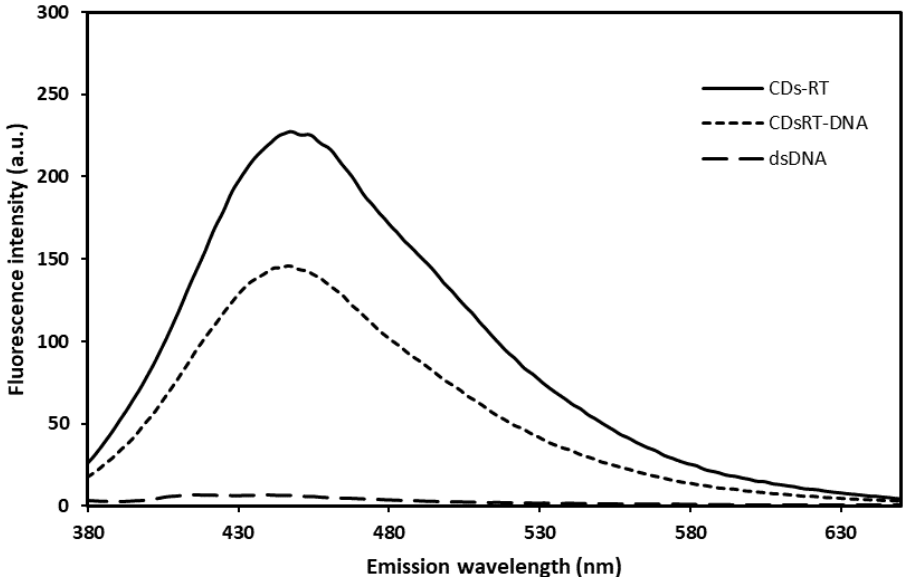

Figure 71. Emission spectra of CDs-RT, double-strain DNA, and CDsRT-DNA interaction.

Table 9. ξ-potential values of dsDNA and CDsFA-DNA, CDsAA-DNA, and CDsRT-DNA.

Sample	ξ-potential (mV)
dsDNA	-47.8
CDsFA-DNA	-18.4
CDsAA-DNA	-36.5
CDsRT-DNA	-12.4

3.8 CDs-PAMAM-NH_2 Interaction

The interaction between CDs and PAMAM was tested following a simple reaction occurring for 24 hours at room temperature. The results contain UV-Vis absorption, emission, and ξ-potential. The type of carbon-based dot used for the interaction was CDs-AA since it´s of negative ξ-potential. The results are presented in figures 72 and 73, respectively the absorption and emission spectra of the conjugates, and a representation of the CDs@PAMAM interaction in figure 74. Different ratios between CDs-PAMAM-NH_2 were tested, concretely 1:1, 2:1, and 1:2. The CDs-AA show its characteristic peaks at 220 and 270 nm, after reaction with PAMAM-NH_2 the absorption maximum at 260 nm prevails. Regarding emission, figure 73 represents the fluorescence intensity at different excitation wavelengths between the CDs-AA and CDs-PAMAM. The results obtained show a significant decrease in the fluorescence intensity after interaction with PAMAM. The 1:2 ratio between CDs-PAMAM outstands from the three tested. Another interesting aspect is that the fluorescence intensity increases after 400 nm excitation, in contrast with the fluorescence of CDs-AA. Regarding ξ-potential (table 9), CDs-AA present a negative value of -9.99 and G5 PAMAM-NH_2 30.4 mV. The different ratios studied show slight differences in the ξ-potential before and after synthesis, decreasing their positivity after 24 hours of interaction.

Based on the results obtained, particularly from figure 73, PAMAM dendrimers seem to quench CDs-AA, and by that we can assume the interaction, even knowing that techniques such as NMR and FT-IR would provide a complete characterization. The 1:2 ratio of CDsAA-PAMAM-NH_2 presented the best results out of the three tested, and it seems that increasing the quantity of PAMAM permits enhancement of the fluorescence intensity after 400 nm excitation. The interaction between CDs-AA (negative ξ-potential) occurs by electrostatic interaction with PAMAM-NH_2 dendrimers, generating a conjugate. Based on the fluorescence quenching of CDs-AA we confirm that the interaction has an impact on the fluorescence properties of the dots. Moreover, the enhancement of the fluorescence intensity after 400 nm excitation may be due to a variety of reasons, but the most plausible seems to be an approximation between the N-groups of the dendrimer onto CDs-AA surface allowing a charge-transfer process. Finally, the effect of the different PAMAM generations namely: 0,1,2,3, and 4 on the fluorescence of CDs would be interesting to explore in the future.

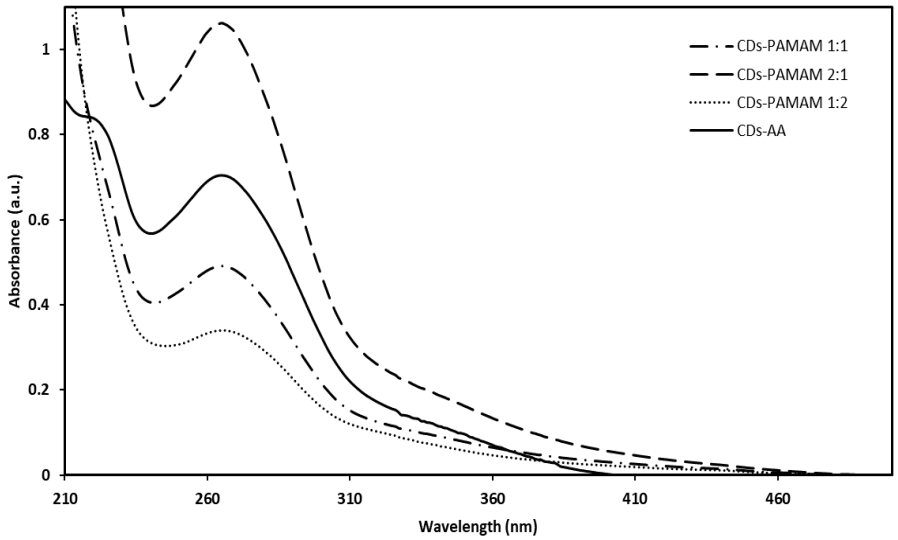

Figure 72. UV-Vis spectra of CDs-AA, CDs-PAMAM 1:1, CDs-PAMAM 2:1, and CDs-PAMAM 1:2.

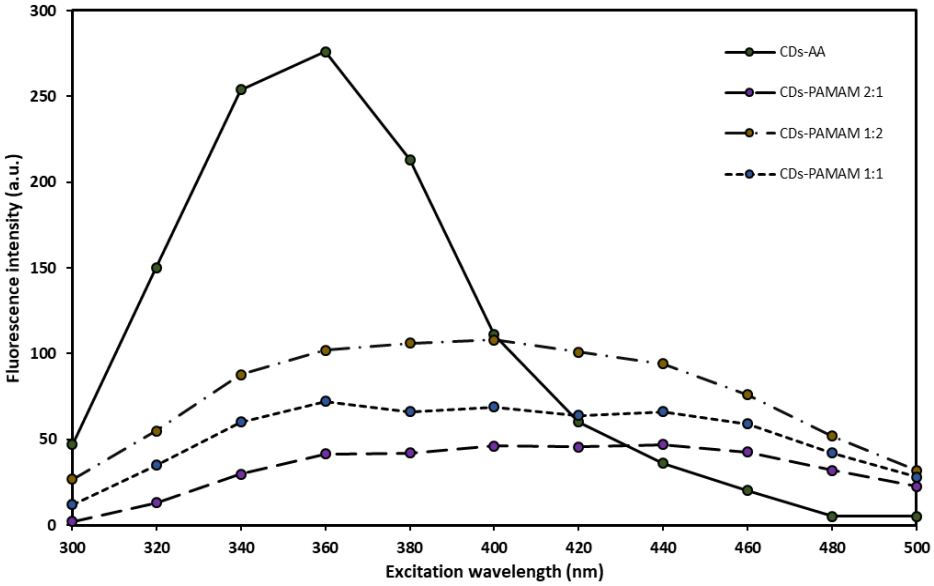

Figure 73. Fluorescence intensity of CDs-AA, CDs-PAMAM 1:1, CDs-PAMAM 2:1 and CDs-PAMAM 1:2 from 300-500 nm with 20 nm excitation.

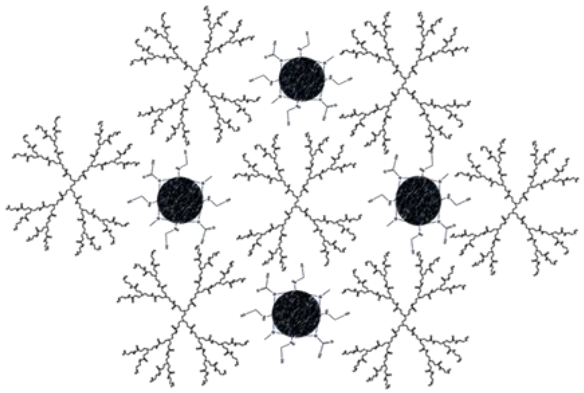

Figure 74. Representation of the CDs@PAMAM interaction.

Table 10. ξ-potential values of CDs-AA, G5 PAMAM-NH_2, and CDs-PAMAM-NH_2 at different ratios.

Sample	ξ-potential (mV)	
CD-AA	-9.99	
G5 PAMAM-NH_2	30.4	
Interaction CDs-PAMAM	Before synthesis	After synthesis
CDs-PAMAM 1:1	52.7	40.5
CDs-PAMAM 1:2	44.4	40.2
CDs-PAMAM 2:1	60.1	45.6

Chapter 4- Conclusions

4. Conclusions

The aim of this master thesis was the preparation of a nanohybrid between CDs-PAMAM and DNA for gene delivery applications. The work was divided into three main phases: Phase 1- synthesis and characterization of carboxylated and aminated carbon dots; Phase 2- preparation of a nanohybrid between CDs-PAMAM-NH_2@DNA and Phase 3- biological studies comprising cytotoxicity, transfection efficiency, and colocalization. Based on the work and results obtained, only phase 1 was realised entirely, and part of phase 2 was achieved. Concretely in phase one, three of the eight approaches attempted for CDs synthesis were successful. The CDs based on FA consisted on an adaption from a previous work, the results were interesting. The CDs based on AA with the conditions used constitutes a novelty, and the TEM images confirmed the success of the approach.

We were able to produce at room temperature, during a 15 days period, and by mixing ascorbic acid with 1,6-hexanediamine, carbon dots (CDs). This ‘‘accidental’’ result was never reported in the literature, constituting a new and innovative approach to the preparation of CDs. Also, this approach needs further investigation regarding reaction mechanism and likely future applications.

Regarding the CDs studies, namely, quenching, pH, fluorescence stability over time, and PicoGreen assay, the results showed that the CDs-AA are relatively photostable in contrast with CDs-FA and CDs-RT, and that the pH can influence the fluorescence intensity of all CDs tested. Regarding the fluorescence stability over time, all CDs have a good fluorescence stability over the period of 49 days. The PG assay confirmed the DNA condensation properties of CDs-FA, CDs-AA, and CDs-RT, with the best result belonging to CDs-FA.

Concerning phase 2 and phase 3, the preparation of a complex between CDs-PAMAM-NH_2@DNA for gene delivery applications was never reported in the literature, and the results obtained in phase 2, show that before attempting the preparation of a complex and performing its biological studies, we should have in mind the impact of those interactions on the maintenance and integrity of the properties of the materials constituting the complex. In the future, it would be interesting to investigate the effect of the different dendrimers generations on the CDs fluorescence and even the impact on the transfection efficiency of the complex.

Chapter 5- Bibliography

Chapter 5- Bibliography

5. References

1. Kroto, H.W.; Heath, J.R.; O´Brien, S.C.; Curl, R.F.; Smalley, R.E.; C60: Buckminsterfullerene. *Nature,* **1985**, *318*, 162-163 https://doi.org/10.1038/318162a0
2. Segawa, Y.; Ito, H.; Itami, K.; Structurally uniform and atomically precise carbon nanostructures. *Nat. Rev. Mat.* **2016**, *1*, 15002 https://doi.org/10.1038/natrevmats.2015.2
3. Martin, N.; Guldi, D.M.; Echegoyen, L.; Carbon nanostructures- Introducing the latest web themed issue. *Chem. Commun.* **2011**, *47*, 604-605 https://doi.org/10.1039/C0CC90122A
4. Wang, Y.; Hu, A.; Carbon Quantum Dots: synthesis, properties and applications. *J. Mat. Chem. C* **2014**, *2*, 6921-6939 https://doi.org/10.1039/C4TC00988F
5. Monthioux, M.; Kuznetsov, V.; Who should be given the credit for the discovery of carbon nanotubes? *Carbon*, **2006**, *44*, 1621-1623 https://doi.org/doi:10.1016/j.carbon.2006.03.019
6. Iijima, S.; Helical microtubules of graphitic carbon. *Nature*, **1991**, *354*, 56-58 https://doi.org/10.1038/354056a0
7. Boehm, H.P.; Clauss, A.; Fischer, G.O.; Hofman, U.; "Das Adsorptionsverhalten sehr dünner Kohlenstoff-Folien" Zeitschrift für anorganische und allgemeine Chemie*,* **1962**, *316*, 119-127 https://doi.org/10.1002/zaac.19623160303
8. Kroto, H.W.; C60: Buckminsterfullerene, The Celestial Sphere that Fell to Earth. *Angew. Chem.*, **1992**, *31*, 111-246 https://doi.org/10.1002/anie.199201113
9. Yadav, B.C.; Kumar, R.; Structure, properties and applications of fullerenes. *Int. J. of Nanotechnol. Appl.*, **2008**, *2*, 15-24
10. Janssen, R.; Hummelen, J.; Sariciftici, N.; Polymer-Fullerene Bulk Heterojunction Solar Cells. *MRS Bull.* **2005**, *30*, 33-36 https://doi.org/10.1557/mrs2005.6
11. GoldSchleger, N.F.; Fullerenes and Fullerene-based materials in Catalysis. *Fullerenes Sci. Technol*. **2001**, *9*, 255-280 https://doi.org/10.1081/FST-100104493
12. Galvan, Y.P.; Alperovich, I.; Zdotukhin, P.; Prazdnova, E.; Mazaenko, M.; Belanova, A.; Christyakov, V.; Fullerenes as anti-aging antioxidants. *Curr. Aging Sci.*, **2017**, *10*, 56-67
13. Savagatrup, S.; Makaram, A.S.; Burka, D.J.; Lipomi, D.J.; Mechanical properties of conjugated Polymers and Polymer-Fullerene composites as a function of Molecular Structure. *Adv. Funct. Mater*., **2014**, *24*, 1169-1181 https://doi.org/10.1002/adfm.201302646
14. Varshney, K.; Carbon Nanotubes: A review on synthesis, properties and applications. *Int. J. Eng. Res. Gen. Sci*. **2014**, *2*, 660-677
15. Chavan, R.; Desai, U.; Mhatre, P.; Chinchole, R.; A Review: Carbon Nanotubes. *Int. J. Pharm. Sci. Res*. **2012,** *13*, 125-134
16. Serp, P.; Corrias, M.; Kalck, P.; Carbon nanotubes and nanofibers in catalysis. *Appl. Catal., A*, **2003**, *253*, 337-358 https://doi.org/10.1016/S0926-860X(03)00549-0
17. Yang, N.; Chen, X.; Ren, T.; Zhang, P.; Yang, D.; Carbon nanotube based biosensors. *Sens. Actuators, B*., **2015**, *207*, 690-725 https://doi.org/10.1016/J.SNB.2014.10.040
18. He, H.; Pham-Huy, L.A.; Dramou, P.; Xiao, D.; Zuo, P.; Pham-Huy, C.; Carbon nanotubes: Applications in Pharmacy and Medicine. *BioMed. Res. Int.* **2013**, *2013*, 1-12 https://doi.org/10.1155/2013/578290
19. Allen, M.J.; Tung, V.C.; Kaner, R.B.; Honeycomb Carbon: A Review of Graphene. *Chem. Rev.* **2010**, *110*, 132-145 https://doi.org/10.1021/cr900070d
20. Chang, P.W.; Choi, H.-J.; Filer, A.; Baeek, J.-B.; Graphene in photovoltaic applications: organic photovoltaic cells (OPVs) and dye-sensitized solar cells (DSSCs) *J. Mater. Chem. A*, **2014**, *2*, 12136-12149 https://doi.org/10.1039/C4TA01047G
21. Raccichini, R.; Varzi, A.; Passerini, S.; Scrosati, B.; The role of graphene for electrochemical energy storage. *Nat. Mat.* **2015**, *14*, 271-279 https://doi.org/10.1038/nmat4170
22. Stankovich, S.; Dikin, D.A.; Dommett, G.B.; Ruoff, R.; Graphene-based composite materials. *Nature*, **2006**, *442*, 282-286 https://doi.org/10.1038/nature04969
23. Pastrana-Martinez, L.M.; Morales-Torres, S.; Figueiredo, J.L.; Faria, J.L.; Silva, A.M.; Graphene oxide-based ultrafiltration membranes for photocatalytic degradation of organic pollutants in salty water. *Water Res*. **2015**, *77*, 179-190 https://doi.org/10.1016/j.watres.2015.03.014
24. Xu, X.; Ray, R.; Gu, Y.; Ploehn, H.J.; Gearheart, L.; Raker, K.; Scrivens, W.A.; Eletrophoretic analysis and purification of fluorescent single-walled carbon nanotube fragments. *J. Am. Chem. Soc.* **2004**, *126*, 12736-12737 https://doi.org/10.1021/ja040082h
25. Sun, Y-P.; Zhou, B.; Lin, Y.; Wang, W.; Fernando, K.A.S.; Panthank, P.; Jaouad, M.; Harruf, B.A.; Wang, X.; Wang, H.; Luo, P.G.; Yang, H.; Kose, M.E.; Chen, B.; Veca, L.M.; Xie, S-Y.; Quantum-sized carbon dots for bright and colourful photoluminescence. *J. Am. Chem. Soc.* **2006**, *128*, 7756-7757 https://doi.org/10.1021/ja062677d
26. Cayuela, A.; Soriano, M.L.; Carrillo-Carrión, C.; Valcárcel, M.; Semiconductor and carbon-based dots: The need for consistency. *Chem. Commun*., **2016**, 52, 1311-1326 https://doi.org/10.1039/C5CC07754K
27. Liu, W.; Li, C.; Ren, Y.; Sun, X.; Pan, W.; Li, Y.; Wang, J.; Wang, W.; Carbon dots: surface engineering and applications. *J. Mater. Chem. B* **2016**, *4*, 5772-5788 https://doi.org/10.1039/C6TB00976J
28. Wang, S.; Cole, I.S.; Zhao, D.; Li, Q.; The dual roles of functional groups in the photoluminescence of graphene quantum dots. *Nanoscale*, **2016**, *8*, 7449-7458 https://doi.org/10.1039/C5NR07042B

29. Zhu, S.; Song, Y.; Zhao, X.; Shao, J.; Zhang, J.; Yang, B.; The photoluminescence mechanism in carbon dots (graphene quantum dots, carbon nanodots and polymer dots): current state and future perspective. *Nano Research*, **2015**, *8*, 355-381 https://doi.org/10.1007/s12274-014-0644-3
30. Sharma, A.; Gadly, T.; Gupta, A.; Ballal, A.; Ghosh, S.; Kumbhakar, M.; Origin of excitation dependent fluorescence in carbon nanodots. *J. Phys. Chem. Lett.*, **2016**, *7*, 3695-3702 https://doi.org/10.1021/acs.jpclett.6b01791
31. Wang, J.; Cao, S.; Ding, Y.; Ma, F.; Lu, W.; Sun, H.; Theoretical investigations of optical origins of fluorescent graphene quantum dots. *Sci. Rep.* **2016**, *6*, 1-5 https://doi.org/10.1038/srep24850
32. Reyes, D.; Camacho, H.; Camacho, M.; Mayorge, M.; Weathers, D.; Salano, G.; Wang, Z.; Neogi, A.; Laser ablated carbon nanodots for light emission. *Nanoscale Res. Lett.* **2016**, *11*, 424-435 https://doi.org/10.1186/s11671-016-1638-8
33. Li, X.; Zhao, Z.; Pan, C.; Electrochemical exfoliation of carbon dots with narrowest full width at half maximum in their fluorescence spectra in the ultraviolet region using only water as electrolyte. *Chem. Commun*., **2016**, *52,* 9406-9409 https://doi.org/10.1039/C6CC03080G
34. Huang, Z.; Li, Y.; Zhang, X.; Ridu, A.E.; Ostrikov, K.; Fast Microplasma synthesis of blue luminescent carbon quantum dots at ambient conditions. *Plasma Process Polym.* **2015**, *12*, 59-65 https://doi.org/10.1002/ppap.201400133
35. Stan, C.S.; Albu, C.; Coroala, A.; Popa, M.; Sutiman, D.; One step synthesis of fluorescent carbon dots through pyrolysis of N-hydroxysuccinimide. *J. Mater. Chem. C* 2015, *3*, 789-795 https://doi.org/10.1039/C4TC02382J
36. He, G.; Xu, M.; Shu, H.; Li, X.; Yang, Z.; Zhang, L.; Su, Y.; Hu, N.; Zhang, Y.; Rapid solid -phase microwave synthesis of highly photoluminescence nitrogen doped carbon dots for Fe^{3+} detection and cellular bioimaging. *Nanotechnology*, **2016**, *27*, 1-10
37. Ma, Z.; Ming, H.; Huang, H.; Liu, Y.; Kang, Z.; One step ultrasonic synthesis of fluorescent N-doped carbon dots from glucose and their visible-light sensitive photocatalytic ability. *New J. Chem.* **2012**, *36*, 861-864 https://doi.org/10.1039/C2NJ20942J
38. Rong, M.-C.; Zhang, K.-Z.; Wang, Y.-R.; Chen, X.; The synthesis of B, N-carbon dots by a combustion method and the applications of fluorescence detection for Cu^{2+}. *Chin. Chem. Lett.,* **2016**, *28*, 1119-1124 https://doi.org/10.1016/j.cclet.2016.12.009
39. Kwon, W.; Rhee, S.-W.; Facile synthesis of graphitic carbon quantum dots with size tunability and uniformity using reverse micelles. *Chem. Commun*. **2012**, *48*, 5256-5258 https://doi.org/10.1039/C2CC31687K
40. Huang, L.; Yang, S.; Chen, L.; Chen, S.; Hydrothermal synthesis of fluorescent carbon dots towards ion response and silk screen patterns. *Chem. Lett.* **2015**, *44*, 1251-1253 https://doi.org/10.1246/cl.150338
41. Qian, Z.; Ma, J.; Shan, X.; Feng, H.; Shao, L.; Chen, J.; Highly luminescent N-doped carbon quantum dots as an effective multifunctional fluorescence sensing platform. *Chem. Eur. J.* **2014**, *20*, 2254-2263 https://doi.org/10.1002/chem.201304374
42. Shen, J.; Li, Q.; Zhang, Y.; She, X.-J.; Wang, C.-F.; Chen, S.; Nitrogen-doped carbon dots derived polyamidoamine dendrimers. *RSC Advances*, **2016**, *6*, 59702-59707 https://doi.org/10.1039/C6RA12261B
43. Lu, S.; Guo, S.; Xu, D.; Li, X.; Zhao, Y.; Gu, W.; Xue, M.; Hydrothermal synthesis of nitrogen-doped carbon dots with real time live-cell imaging and BBB penetration capabilities. *Int. J. Nanomedicine*, **2016**, *11*, 6325-6336 https://doi.org/10.2147/IJN.S119252
44. Liu, X.; Pang, J.; Xu, F.; Zhang, X.; Simple approach to synthesize amino-functionalized carbon dots by carbonization of chitosan. *Sci. Rep*., **2016**, *6*, 31100 https://doi.org/10.1038/srep31100
45. Jiang, K.; Sun, S.; Zhang, L.; Lu, Y.; Wu, A.; Cai, C.; Lim, H.; Red, green, and blue luminescence by carbon dots full-color emission tuning and multicolour cellular imaging. *Angew. Chem. Int. Ed*. **2015**, *54*, 5360-5363 https://doi.org/10.1002/anie.201501193
46. Wang, N.; Wang, Y.; Guo, T.; Yang, T.; Chen, M.; Wang, J.; Green preparation of carbon dots with papaya as carbon source for effective fluorescent sensing of Iron (III) and Escherichia coli. *Biosens. and Bioelectron*., **2016***, 85*, 68-75 https://doi.org/10.1016/j.bios.2016.04.089
47. Das, B.; Dadhich, P.; Pal, P.; Srivas, P.; Bankoti, K.; Dhara, S.; Carbon nanodots from date molasses: new nanolights for the in vitro scavenging of reactive oxygen species. *J. Mater. Chem. B*., **2014**, *2*, 6839-6847 https://doi.org/10.1039/C4TB01020E
48. Essner, J.; Laber, C.; Ravula, S.; Polo-Parada, L.; Baker, G.; Pee-dots: biocompatible fluorescent carbon dots derived from the upcycling of urine. *Green Chem.,* **2016**, *18*, 243-250 https://doi.org/10.1039/C5GC02032H
49. Mehta, V.N.; Jha, S.; Singhal, R.; Kailasa, S.; Preparation of multicolour emitting carbon dots for HeLa cell imaging. *New. J. Chem*. **2014**, *38*, 6152-6160 https://doi.org/10.1039/C4NJ00840E
50. Sahu, S.; Behera, B.; Maiti, T.K.; Mohapatra, S.; Simple one-step synthesis of highly luminescent carbon dots from Orange juice: Application as excellent bio-imaging agents. *Chem. Commun*., **2012**, *48*, 8835-8837 https://doi.org/10.1039/C2CC33796G
51. Barbosa, C.; Correa, J.; Medeiros, G.; Rodrigues, H.O.; Neto, B.; Carbon dots (C-dots) from cow manure with impressive subcellular selectivity tuned by simple chemical modification. *Chem. Eur. J.,* **2015**, *21*, 5055-5060 https://doi.org/10.1002/chem.201406330
52. Kasibabu, B.; D´Souza, S.; Jha, S.; Synthesis of fluorescent carbon dots for bacteria and fungus cell imaging. *Anal. Methods.* **2015**, *7*, 2373-2378 https://doi.org/10.1039/C4AY02737J
53. Guo, Y.; Zhang, Z.; Cao, F.; Leng, Y.; Thermal treatment of hair for the synthesis of sustainable carbon quantum dots and the applications for sensing Hg^{2+}. *Sci. Rep*., **2016**, *6*, 3795-3802 https://doi.org/10.1038/srep35795
54. Zhu, S.; Meng, Q.; Wang, L.; Zhang, J.; Song, Y.; Jin, H.; Zhang, K.; Sun, H.; Wang, H.; Yang, B.; Highly Photoluminescent Carbon Dots for Multicolor Patterning, Sensors, and Bioimaging. *Angew. Chem. Int. Ed.* **2013**, *52*, 3953-3957 https://doi.org/10.1002/anie.201300519
55. Qu, D.; Zheng, M.; Zhang, L.; Zhao, H.; Xie, Z.; Jing, X.; Haddad, R.E.; Fan, H.; Sun, Z.; Formation mechanism and optimization of highly luminescent N-doped graphene quantum dots. *Sci. Rep*., **2014**, *4*, 5294 https://doi.org/10.1038/srep05294

56. Dai, B.; Wu, C.; Lu, Y.; Ding, D.; Xu, S.; Synthesis and formation mechanism of S-doped carbon dots from low-molecule-weight organics. *J. Lumin.,* **2017**, *190*, 108-114 https://doi.org/10.1016/j.jlumin.2017.04.054
57. Zhu, Y.; Ji, X.; Pan, C.; Sun, Q.; Song, W.; Fang, L.; Chena, Q.; Banks, C.E.; A carbon quantum dot decorated RuO_2 network: Out-standing supercapacitances under ultrafast charge and discharge. *Energy Environ. Sci.* **2013**, *6*, 3665-3675 https://doi.org/10.1039/C3EE41776J
58. Jaishanker, M.; Tseten, T.; Anbalagan, N.; Mathew, B.B.; Beeregowda, K.N.; Toxicity, mechanism and health effects of some heavy metals. *Interdiscip. Toxicol.*, **2014**, *7,* 60-72 https://doi.org/10.2478/intox-2014-0009
59. Guidelines for drinking-water quality. 4th Edition World Health Organization, Geneva, 2011
60. Ding, Y.; Ling, J.; Cai, J.; Wang, S.; Li, X.; Yang, M.; Zha, L.; Yan, J.; Carbon dots-based hybrid fluorescent sensor for detecting free chlorine in water media. *Anal. Methods*, **2016**, *8*, 1157-1161 https://doi.org/10.1039/C5AY03143E
61. Kong, D.; Yan, F.; Han, Z.; Xu, J.; Guo, X.; Chen, L.; Cobalt (II) ions detection using carbon dots as a sensitive and selective fluorescent probe. *RSC Adv.* **2016**, *6*, 67481-67487 https://doi.org/10.1039/C6RA12986B
62. Ma, Y.; Zhang, Z.; Xu, Y.; Ma, M.; Chen, B.; Wei, L.; Xiao, L.; A Bright carbon-dot-based fluorescent probe for selective and sensitive detection of Mercury ions. *Talanta,* **2016**, *161,* 476-481 https://doi.org/10.1016/j.talanta.2016.08.082.
63. Liu, C.; Zhang, P.; Zhai, X.; Tian, F.; Li, W.; Yang, J.; Liu, Y.; Wang, H.; Wang, W.; Liu, W.; Nano-carrier for gene delivery and bioimaging based on carbon dots with PEI-passivation enhanced fluorescence. *Biomaterials*, **2012**, *33*, 3604-3613 https://doi.org/10.1016/j.biomaterials.2012.01.052
64. Mewada, A.; Pandey, S.; Thakur, M.; Jadhav, D.; Sharon, M.; Swarming carbon dots for folic acid mediated delivery of doxorubicin and biological imaging. *J. Mater. Chem. B*, **2014**, *2*, 698-705 https://doi.org/10.1039/C3TB21436B
65. Li, H. L.; Zhang, Y. W.; Wang, L.; Tian, J. Q.; Sun, X. P.; Nucleic acid detection using carbon nanoparticles as a fluorescent sensing platform. *Chem. Commun.* **2011**, *47*, 961-963 https://doi.org/10.1039/C0CC04326E
66. Yu, C.M.; Wu, Y.L.; Zeng, F.; Wu, S.Z.; Yu, C.M.; Wu, Y.L.; Zeng, F.; Wu, S.Z.; A fluorescent ratiometric nanosensor for detecting NO in aqueous media and imaging exogenous and endogenous NO in live cells. *J. Mater. Chem. B*, **2013**, *1*, 4152-4159 https://doi.org/10.1039/C3TB20686F
67. Vögtle, F.; Richardt, G.; Werner, N.; Dendrimer Chemistry: Concepts, Syntheses, Properties, Applications. Wiley-VCH Verlag GmbH & Co. KGaA, Weinheim. 2009, 354 https://doi.org/10.1002/9783527626953
68. Newkome, G.R.; Moorefield, C.N.; Vögtle, F.; Dendrimers and Dendrons. Wiley-VCH Verlag GmbH & Co. KGaA, Weinheim. 2001 https://doi.org/10.1002/3527600612.fmatter
69. Svenson, S.; Tomalia, D.A.; Dendrimers in biomedical applications-reflections on the field. *Adv. Drug Del. Rev.* **2005**, *57*, 2106-2129 https://doi.org/10.1016/j.addr.2005.09.018
70. Liu, W.; Li, C.; Ren, Y.; Sun, X.; Pan, W.; Li, Y.; Wang, J.; Wang, W.; Carbon dots: surface engineering and applications. *J. Mater. Chem. B*, **2016**, *4*, 5772-5788 https://doi.org/10.1039/C6TB00976J
71. Ding, C.; Zhu, A.; Tian, Y.; Functional surface engineering of c-dots for fluorescent biosensing and in vivo bioimaging. *Acc. Chem. Res*. **2014**, *47*, 20-30 https://doi.org/10.1021/ar400023s
72. Ramalingan, K.; Castro, R.; Pires, P.; Shi, X.; Rodrigues, J.; Xiao, S.; Tomás, H.; Gene delivery using dendrimer/pDNA complexes immobilized in electrospun fibers using Layer-by-Layer technique. *RSC Adv.* **2016**, *6*, 97116-97128 https://doi.org/10.1039/C6RA22444J
73. Mignani, S.; Rodrigues, J.; Tomás, H.; Zablocka, H.; Shi, X.; Caminade, A.-M.; Majoral, J.-P.; Dendrimers in combination with natural products and analogues as anti-cancer agents. *Chem. Soc. Rev.* **2018**, *47*, 514-532 https://doi.org/10.1039/C7CS00550D
74. Chen, C.; Wang, H.; Biomedical Applications and Toxicology of Carbon Nanomaterials. Wiley-VCH Verlag GmbH & Co. KGaA, Weinheim. 2016 https://doi.org/10.1039/C7CS00550D
75. Feng, L.; Zhao, A.; Ren, J.; Qu, X.; Lighting up left-handed Z-DNA: photoluminescent carbon dots induce DNA B to Z transition and perform DNA logic operations. *Nucleic Acids Res.,* **2013**, *41*, 7987-7996 https://doi.org/10.1093/nar/gkt575.
76. Qian, Z.S.; Shan, X.Y.; Chai, L.J.; Ma, J.J.; Chen, J.R.; Feng, H.; DNA nanosensor based on biocompatible graphene quantum dots and carbon nanotubes. *Biosensors and Bioelectronics*., **2014**, *60*, 64-70 https://doi.org/10.1016/j.bios.2014.04.006.
77. Lu, L.; Guo, L.; Wang, X.; Kang, T.; Cheng, S.; Complexation and intercalation modes: a novel interaction of DNA and graphene quantum dots. *RSC Adv.* **2016***, 6*, 33072-33075 https://doi.org/10.1039/C6RA00930A
78. Zong, J.; Yang, X.; Trinchi, A.; Hardin, S.; Cole, I.; Zhu, Y.; Li, C.; Muster, T.; Wei, G.; Photoluminescence enhancement carbon dots by gold nanoparticles conjugated via PAMAM dendrimers. *Nanoscale*, **2013**, *5*, 11200-11206 https://doi.org/10.1039/C3NR02527F
79. Matai, I.; Sachdev, A.; Dackirisamy, G.; Self-assembled hybrids of fluorescent carbon dots and PAMAM dendrimers for Epirubicin Delivery and Intracellular imaging. *Appl. Mater. Interf.* **2015**, *7*, 11423-11435 https://doi.org/10.1021/acsami.5b02095
80. Campos, B.; Oliva, M.; Contreras-Cáceres, R.; Rodriguez-Castellón, E.; Jimenéz-Jimenéz, J.; Esteves da Silva, J.; Algarra, M.; Carbon dots on based folic acid coated with PAMAM dendrimers as platform for Pt (IV) detection. *J. Colloid Interface Sci.*, **2016**, *465*, 165–173 https://doi.org/10.1016/j.jcis.2015.11.059
81. Ngu-Schwemlein, M.; Chin, S.F.; Hileman, R.; Drozdovski, C.; Upchurch, C.; Hargrove, A.; Carbon nanodots as molecular scaffolds for development of antimicrobial agents. *Bioorg. Med. Chem. Lett*. **2016**, *26*, 1745-1749 https://doi.org/10.1016/j.bmcl.2016.02.047
82. Dartola, M.L.; Denofrio, M.P.; Zurbano, B.; Gimenez, C.S.; Ogilby, P.R.; Lorente, C.; Thomas, A.H.; Mechanism of photooxidation of folic acid sensitized by unconjugated pteris. *Photochem. Photobiol. Sci.* **2010**, *9*, 1604-1612 https://doi.org/10.1039/c0pp00210k

83. Zhao, Z.; Zhang, J.; Wang, Y.; Chen, L.; Zhang, Y.; Hydrothermal synthesis of fluorescent nitrogen-doped carbon quantum dots from ascorbic acid and valine selective determination of picric acid in water samples. Int. J. Environ. Anal. Chem. 2016, 96, 1402-1413 https://doi.org/10.1007/s10895-017-2189-9
84. Sugiarti, S.; Darmawan, N.; Synthesis of fluorescent carbon nanoparticles from Ascorbic acid. *Indones. J. Chem.* **2015**, *15*, 141-145 http://dx.doi.org/10.22146/ijc.964
85. Sajid, P.A.; Chetty, S.; Praneetha, S.; Murugan, A.; Kumar, Y.; Periyasamy, L. One-pot microwave-assisted in situ reduction of Ag^{+} and Au^{3+} ions by citrus limon extract and their carbon-dots nanohybrids: a potential nano-bioprobe for cancer cellular imaging. *RSC Adv.* **2016**, *6*, 103482-103490 https://doi.org/10.1039/C6RA24033J
86. Zhang, B.; Liu, C-Y.; Liu, Y.; A novel one-step approach to synthesize fluorescent carbon nanoparticles. *Eur. J. Inorg. Chem.* **2010**, *2010*, 4411-4414 https://doi.org/10.1002/ejic.201000622
87. Song, Y.; Zhu, S.; Zhang, S.; Fu, Y.; Wang, L.; Zhao, X.; Yang, B.; Investigation from chemical structure to photoluminescent mechanism: a type of carbon dots from the pyrolysis of citric acid and an amine. *J. Mater. Chem. C* **2015**, *3,* 5976-5984 https://doi.org/10.1039/C5TC00813A
88. Kong, W.; Wu, H.; Ye, Z.; Li, R.; Xu, T.; Zhang, B.; Optical properties of pH-sensitive carbon-dots with different modification. *J. Lumin.* **2014**, *148*, 238-242 https://doi.org/ https://doi.org/10.1016/j.jlumin.2013.12.007
89. Liu, H.; Ye, T.; Mao, C.; Fluorescent carbon nanoparticles derived from candle soot. *Angew. Chem. Int. Ed.* **2007**, *46*, 6473-6475 https://doi.org/10.1002/anie.200701271

Appendix

Appendix

1. Supporting Information

1.1 CDs studies supporting tables

The following are the tables containing the volumes used for quenching, pH, and DNA condensation studies (table S1, S2, and S3 respectively).

Table S1. Volumes used of KI, CDs, and pH 7 solution for the quenching studies.

M (KI)	0	20	40	60	80	100	120	140	160	180	200
V (KI)	0	40	80	120	160	200	240	280	320	360	400
V (CDs)	500	500	500	500	500	500	500	500	500	500	500
V (pH 7)	500	460	420	380	340	300	260	220	180	140	100
Total volume	1000	1000	1000	1000	1000	1000	1000	1000	1000	1000	1000

Note: All the volumes added are in μL.

Table S2. Volumes used of CDs and buffer solution for the pH studies.

pH	3	4	5	6	7	8	9	10
CDs (ml)	0.1	0.1	0.1	0.1	0.1	0.1	0.1	0.1
Buffer (ml)	4.9	4.9	4.9	4.9	4.9	4.9	4.9	4.9
Total volume	5	5	5	5	5	5	5	5

Table S3. Volumes added of pDNA, CDs, and TE solution for DNA condensation studies.

Eppendorf	1	2	3	4	5	6
CDs/pDNA	0	1:1	10:1	20:1	40:1	100:1
V of pDNA	10	10	10	10	10	10
V of CDs	0	10	90	180	360	900
TE 1x	990	980	900	810	630	90
Total volume	1000	1000	1000	1000	1000	1000

Note: All the volumes added are in μL

1.2 Photographs, pH, ξ-potential and QY of CDs

This section contains the photographs before and after synthesis, pH values, ξ-potential, PL maximum emission and quantum yield of all the approaches attempted towards the synthesis of CDs.

Table S4. Photographs, pH, ξ-potential and QY of all the approaches tried.

Reaction	Mixture before synthesis	Mixture after synthesis	CDs (Visible/UV light)	pH		ξ-potential (mV)	PL Max Em (nm)	QY (%)
				Before synthesis	After synthesis			
Folic Acid + H_3PO_4, 2 h at 120 °C				0.26	0.38	23.7	477	19.7
Ascorbic acid, 5 h at 200 °C				2.28	2.18	-9.99	433	10.8
Ascorbic acid + 1,6-HXDA, 5 h at 200 °C		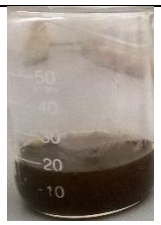		10.59	7.52	16.4	455	25.8
Ascorbic acid + 1,6-HXDA, 8 h at 200 °C			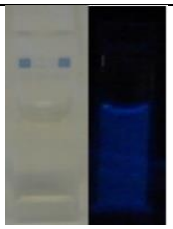	10.50	7.09	22.5	444	24.3
Ascorbic acid + 1,6-HXDA, 15 days at room temperature	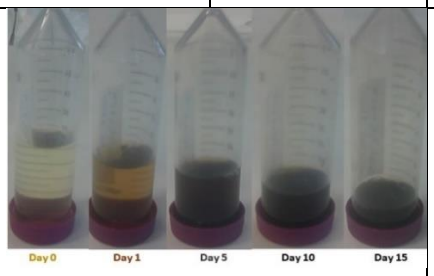			10.7	10.6	35.2	419	8.74

Oxaloacetic acid, 5 h at 200 °C	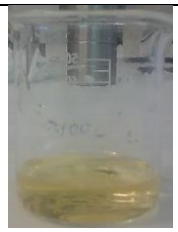			1.39	1.62	12.0	440	14.5
Oxaloacetic acid + 1,6-HXDA, 5 h at 200 °C				3.81	8.03	-12.7	430	39.6
Oxaloacetic acid + 1,6-HXDA, 8 h at 200 °C				3.86	8.35	-16.0	434	30.8

1.3 DLS measurements

The following results contain the hydrodynamic size distribution both intensity and number, of carbon dots and CDs-PAMAM-NH_2 interaction, respectively sections 1.3.1 and 1.3.2.

1.3.1 Carbon dots

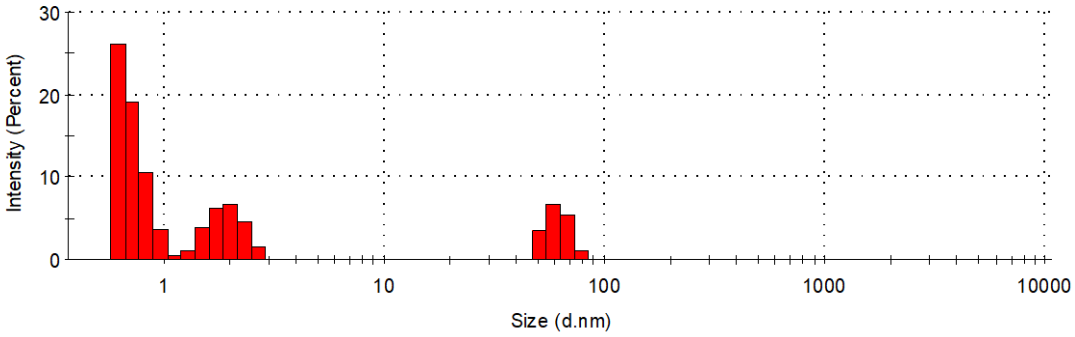

Figure S1. Hydrodynamic size distribution of the CDs-FA (Intensity %).

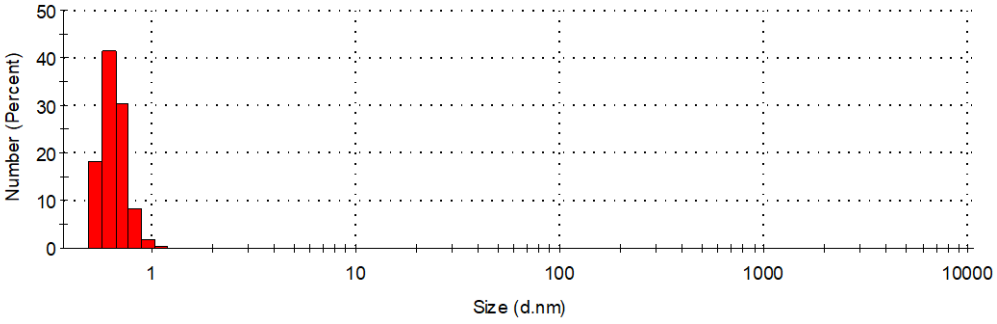

Figure S2. Hydrodynamic size distribution of the CDs-FA (Number %).

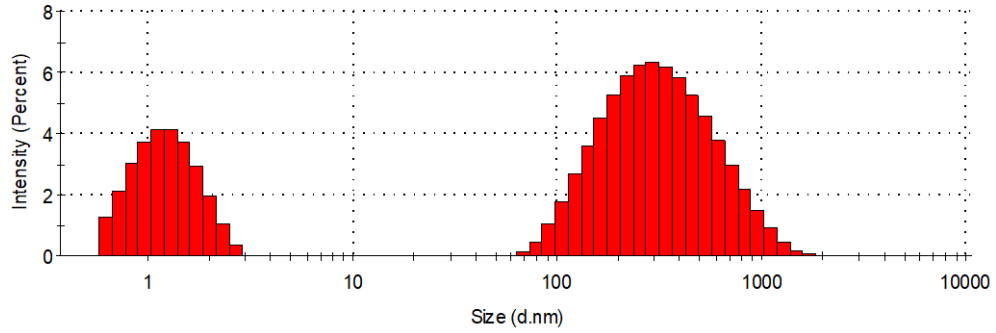

Figure S3. Hydrodynamic size distribution of the CDs-AA (Intensity %).

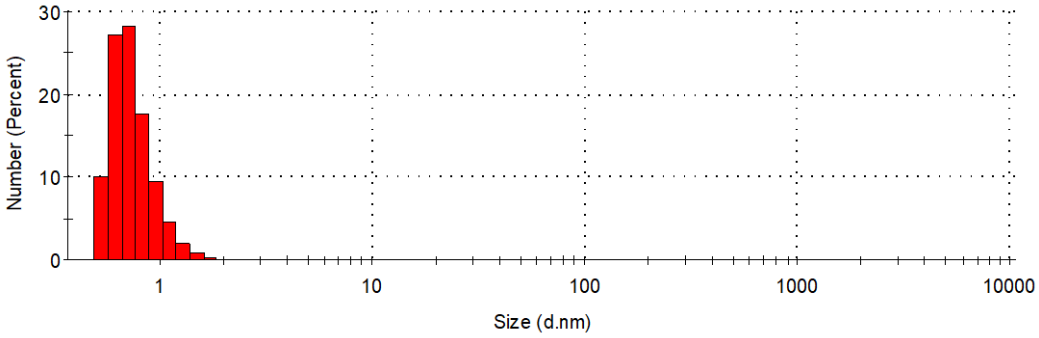

Figure S4. Hydrodynamic size distribution of the CDs-AA (Number %).

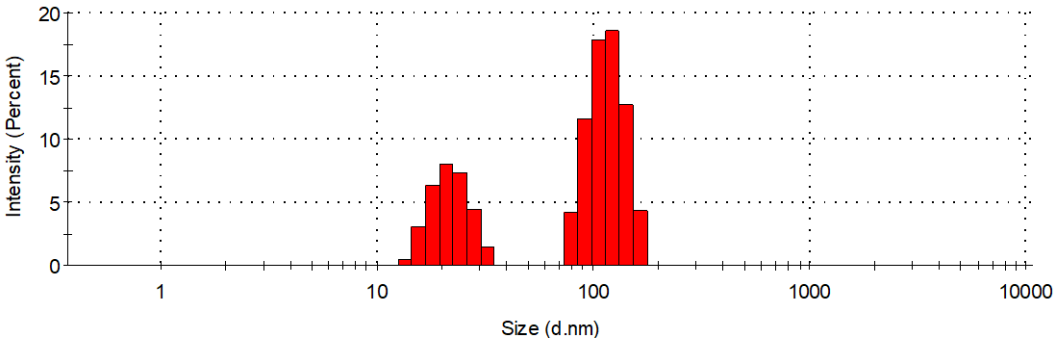

Figure S5. Hydrodynamic size distribution of CDs-AA+1,6-HXDA 5 h. (Intensity %)

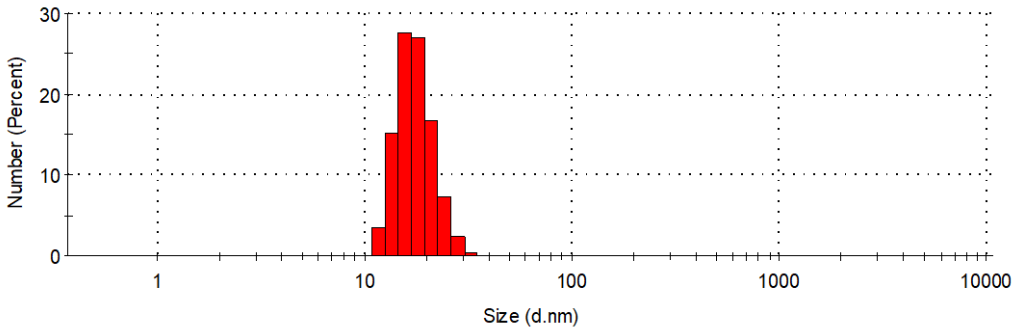

Figure S6. Hydrodynamic size distribution of CDs-AA+1,6-HXDA 5 h. (Number %)

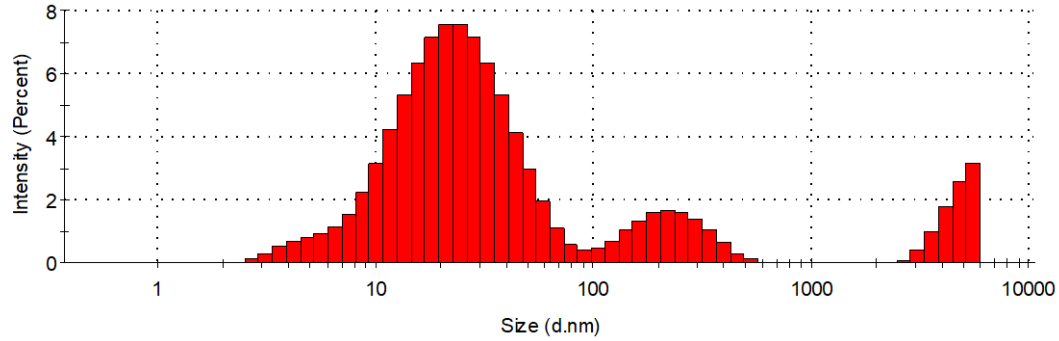

Figure S7. Hydrodynamic size distribution of CDs-AA+1,6-HXDA 8 h. (Intensity %)

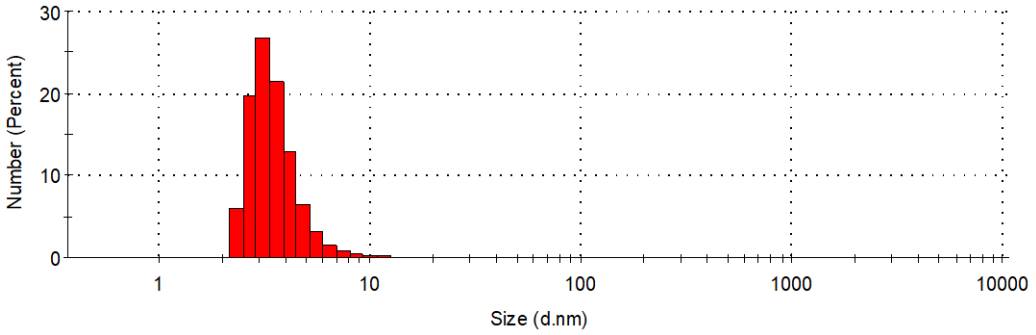

Figure S8. Hydrodynamic size distribution of CDs-AA+1,6-HXDA 8 h. (Number %)

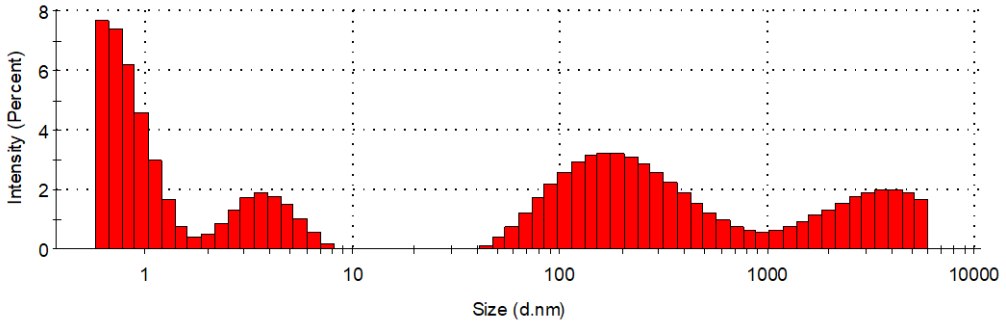

Figure S9. Hydrodynamic size distribution of CDs-AA+1,6-HXDA RT. (Intensity %)

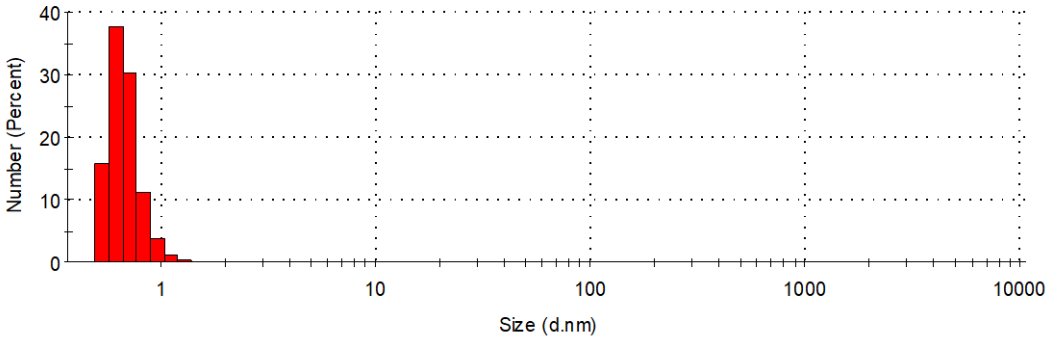

Figure S10. Hydrodynamic size distribution of CDs-AA+1,6-HXDA RT. (Number %)

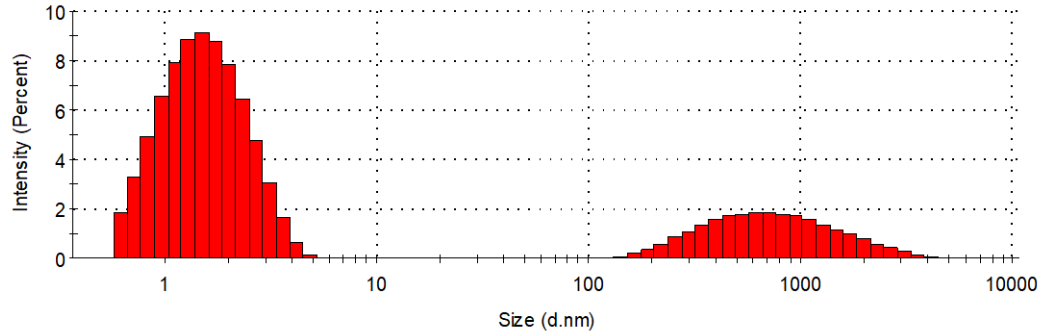

Figure S11. Hydrodynamic size distribution of the CDs-OA. (Intensity %)

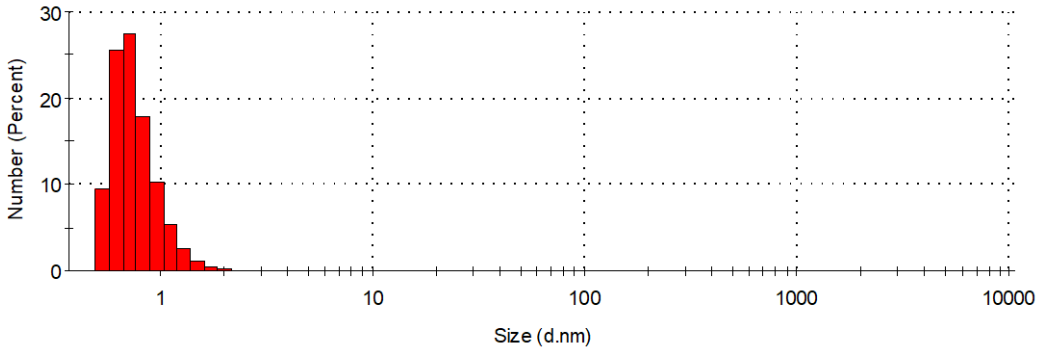

Figure S12. Hydrodynamic size distribution of the CDs-OA. (Number %)

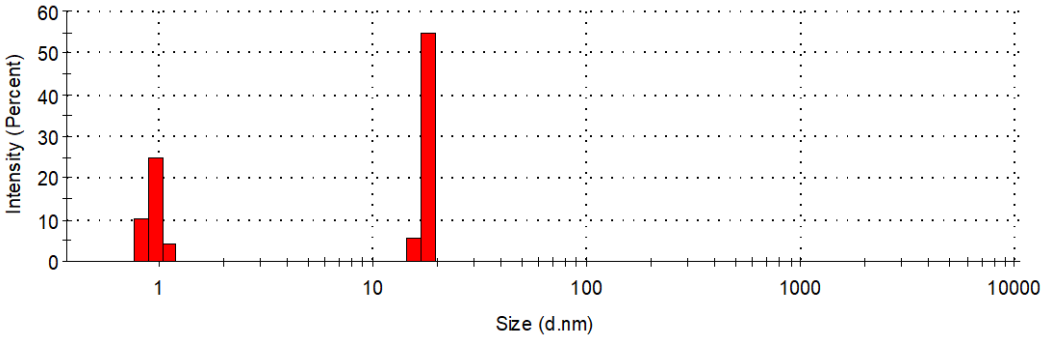

Figure S13. Hydrodynamic size distribution of CDs-OA + 1,6-HXDA 5 h. (Intensity %)

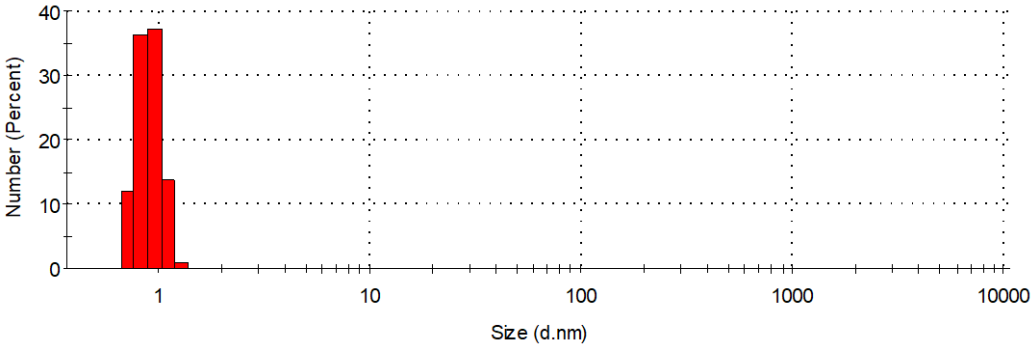

Figure S14. Hydrodynamic size distribution of CDs-OA + 1,6-HXDA 5 h. (Number %)

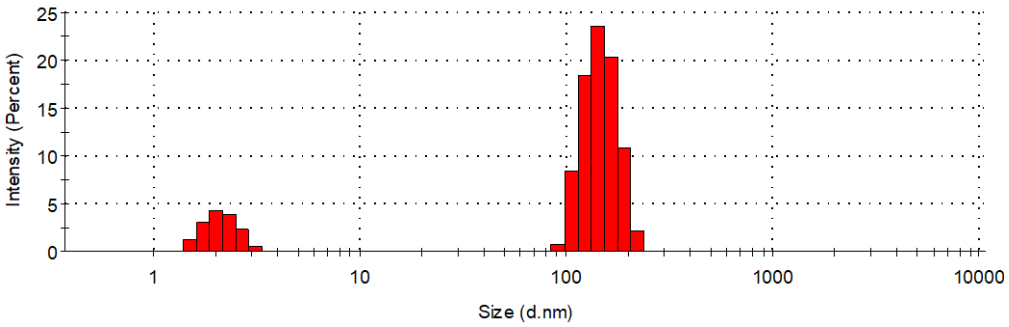

Figure S15. Hydrodynamic size distribution of CDs-OA + 1,6-HXDA 8 h. (Intensity %)

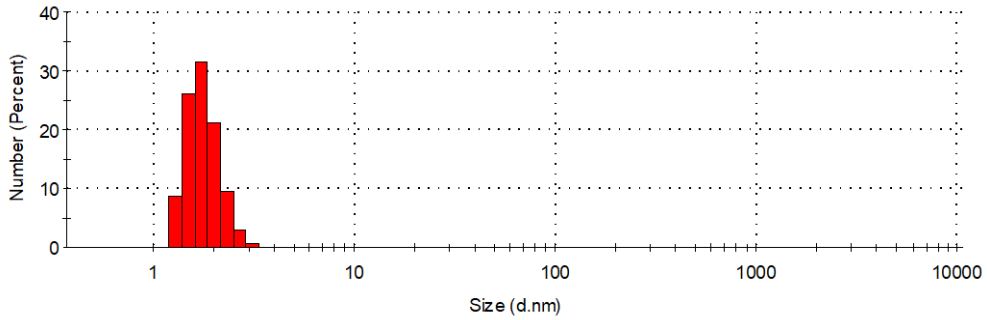

Figure S16. Hydrodynamic size distribution of CDs-OA + 1,6-HXDA 8 h. (Number %)

1.3.2 Carbon dots-PAMAM-NH_2 Interaction

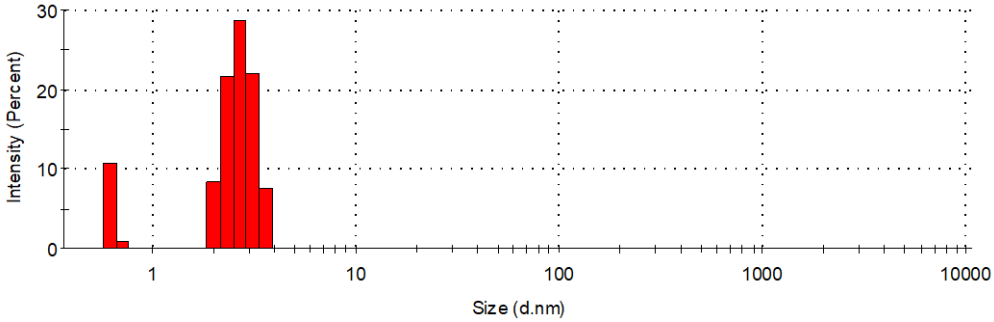

Figure S17. Hydrodynamic size distribution of G5 PAMAM-NH_2 (Intensity %).

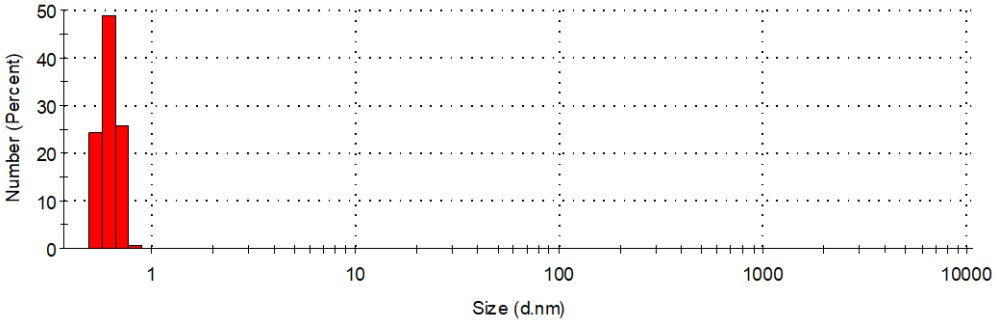

Figure S18. Hydrodynamic size distribution of G5 PAMAM-NH_2 (Number %).

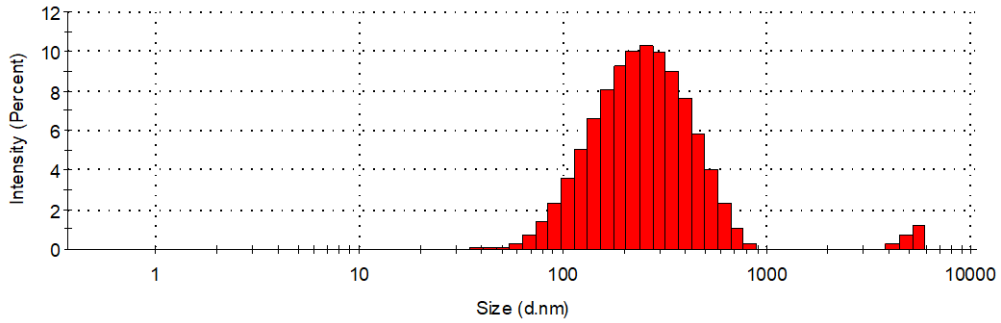

Figure S19. Hydrodynamic size distribution of CDs-AA (Intensity %).

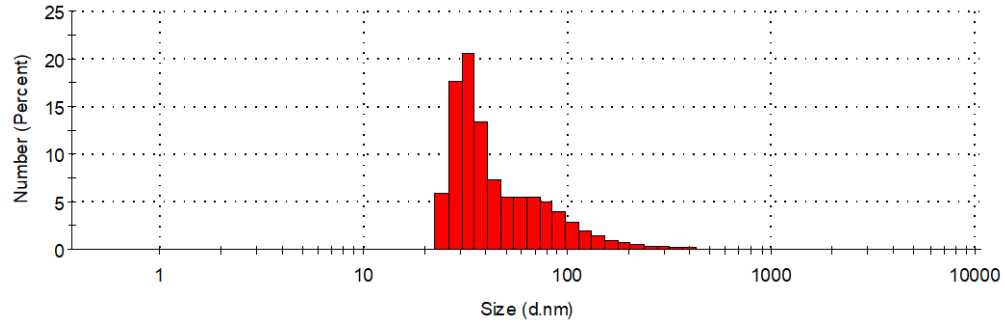

Figure S20. Hydrodynamic size distribution of CDs-AA (Number %).

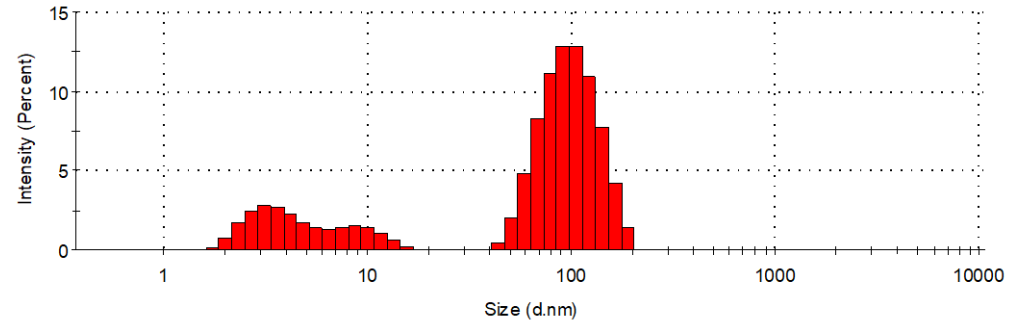

Figure S21. Hydrodynamic size distribution of CDs-PAMAM 1:1 (Intensity %).

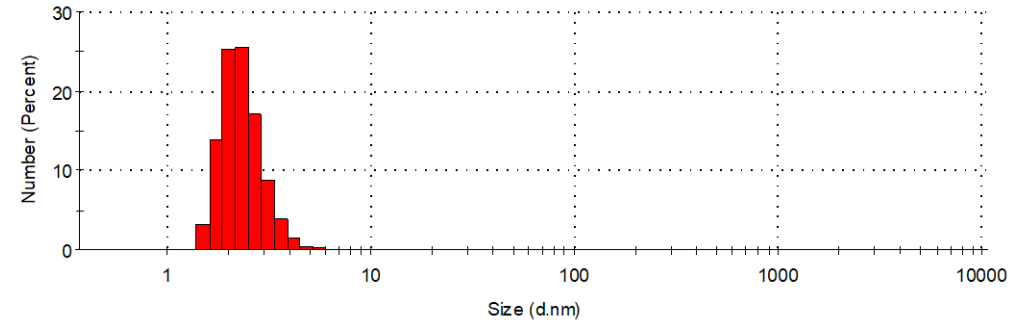

Figure S22. Hydrodynamic size distribution of CDs-PAMAM 1:1 (Number %).

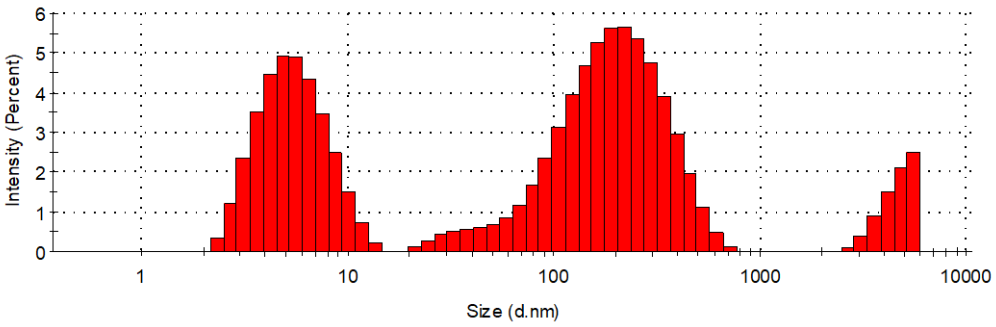

Figure S23. Hydrodynamic size distribution of CDs-PAMAM 2:1 (Intensity %).

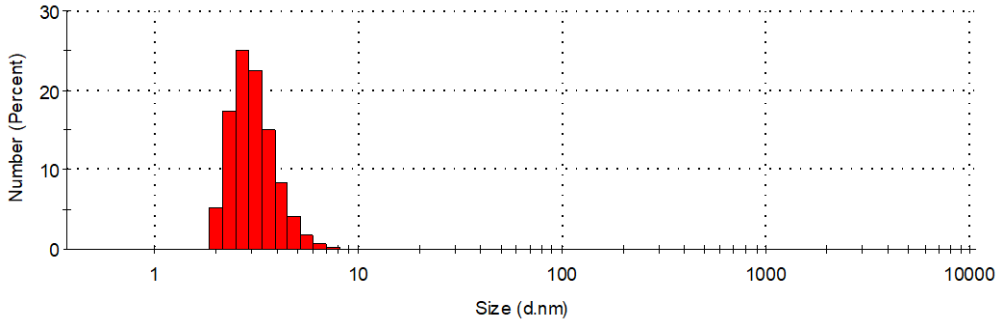

Figure S24. Hydrodynamic size distribution of CDs-PAMAM 2:1 (Number %).

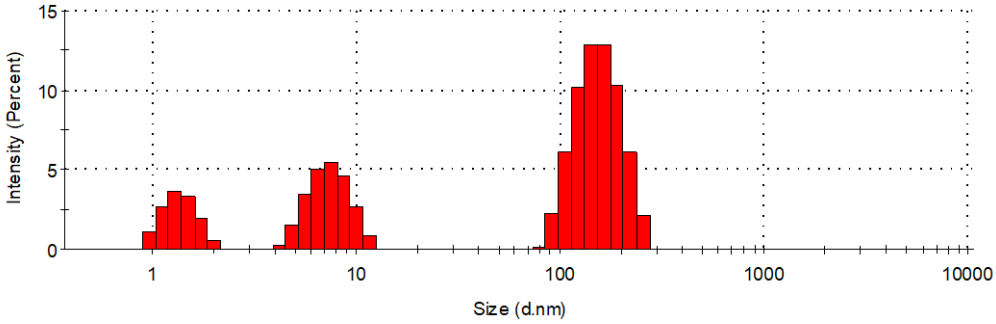

Figure S25. Hydrodynamic size distribution of CDs-PAMAM 1:2 (Intensity %).

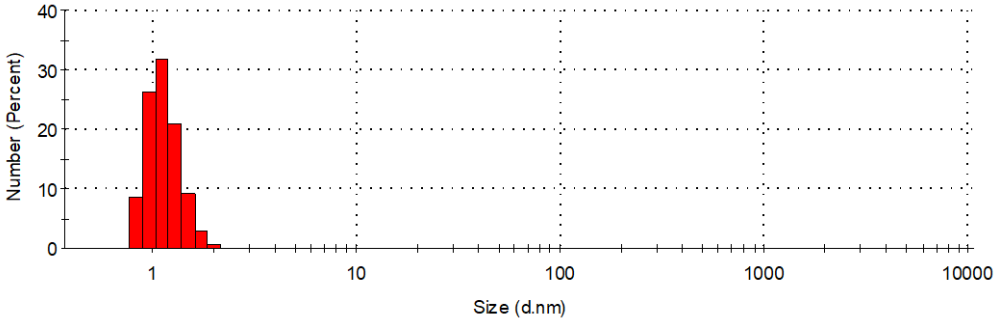

Figure S26. Hydrodynamic size distribution of CDs-PAMAM 1:2 (Number %).

1.4 Fluorescence QY

The QY was determined using the slope method[1], with pyrene in cyclohexane as the fluorescent reference. The procedure was the following:

1. Preparation of 4-5 samples each of Pyrene and carbon dots in cyclohexane and water respectively, having different absorbances between 0.01-0.1 at the excitation wavelength of 317 nm.
2. Measurement of the fluorescence spectrum from each sample using an excitation wavelength of 317 nm.
3. Calculation of the integrated fluorescence intensity from the spectrum using FL WinLab software.
4. Plot of the integrated fluorescence intensity against absorbance of the solutions.

Calculation of the fluorescence quantum yield using equation of the slope method. Q_R, quantum yield of the reference molecule; m, slope of the line; n^2, refraction index of the solvent.

$$Q = Q_R \left(\frac{m}{m_R}\right)\left(\frac{n^2}{n^2_R}\right)$$

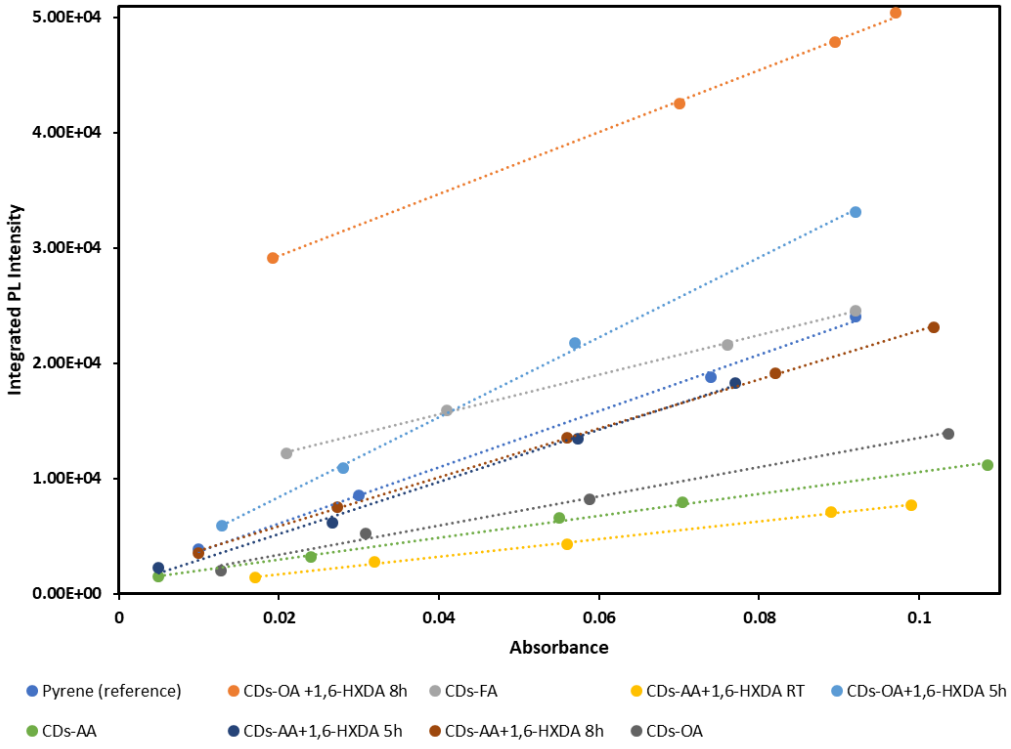

Figure S27. Slope of all types of CDs prepared including pyrene (reference).

Table S5. Slope and respective QY for all the CDs approaches.

Sample	Slope	QY (%)
Pyrene (reference)	243316	32
CDs-FA	172366	19.7
CDs-AA	94691	10.8
CDs-AA+1,6-HXDA 5 h	225394	25.8
CDs-AA+1,6-HXDA 8 h	212433	24.3
CDs-AA+1,6-HXDA RT	76517	8.74
CDs-OA	126910	14.5
CDs-OA+1,6-HXDA 5 h	346311	39.6
CDs-OA+1,6-HXDA 8 h	269575	30.8

1.5 pH Effect (Photographs, Absorption and Emission)

The pH effect on the absorption and emission of CDs-FA, CDs-AA, and CDs-RT was obtained using pH values between 1,3,5,7,9, and 11. From figures S28-S36 are the results from the studies.

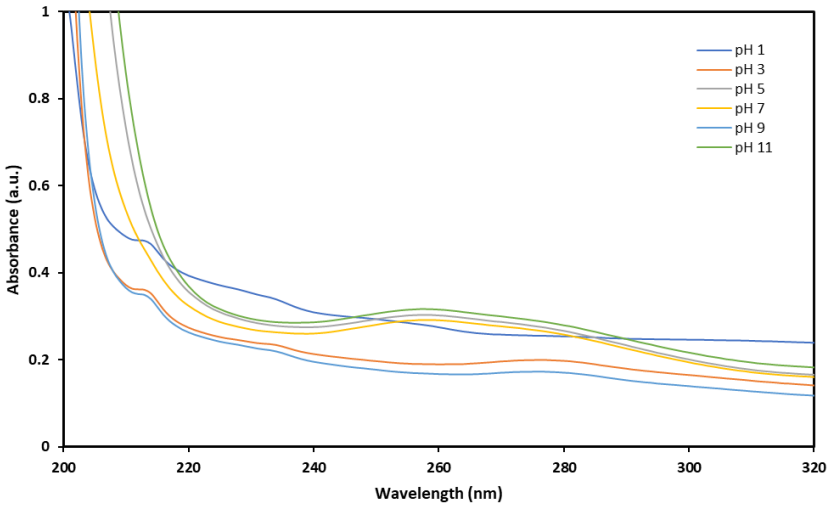

Figure S28. UV-Vis spectra of CDs-FA at different pH environments.

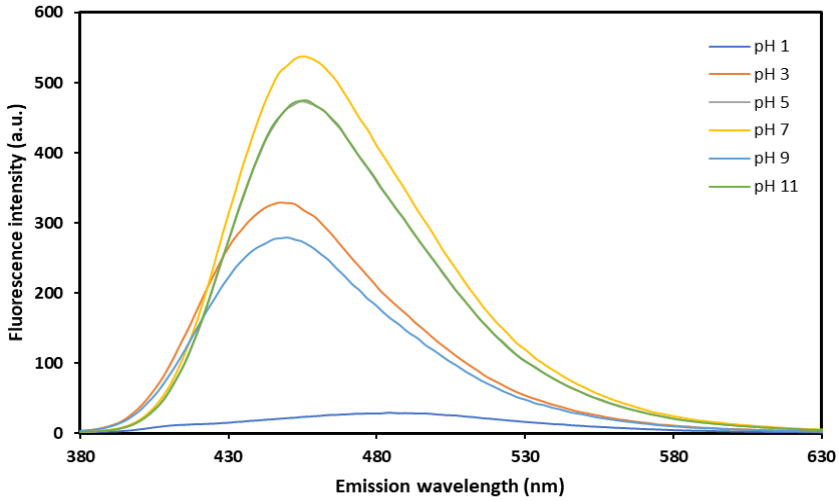

Figure S29. Emission spectra of CDs-FA at different pH environments, using a fixed 360 nm excitation wavelength.

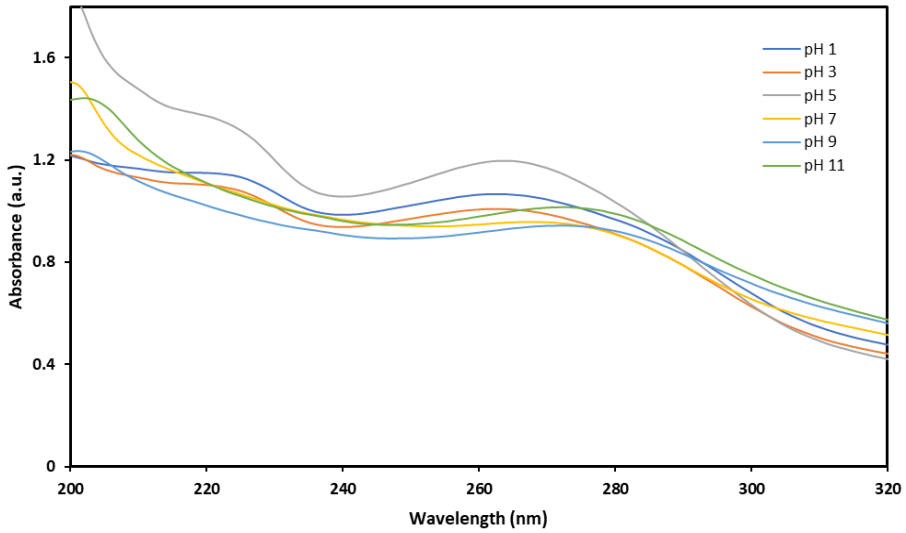

Figure S30. UV-Vis spectra of CDs-AA at different pH environments.

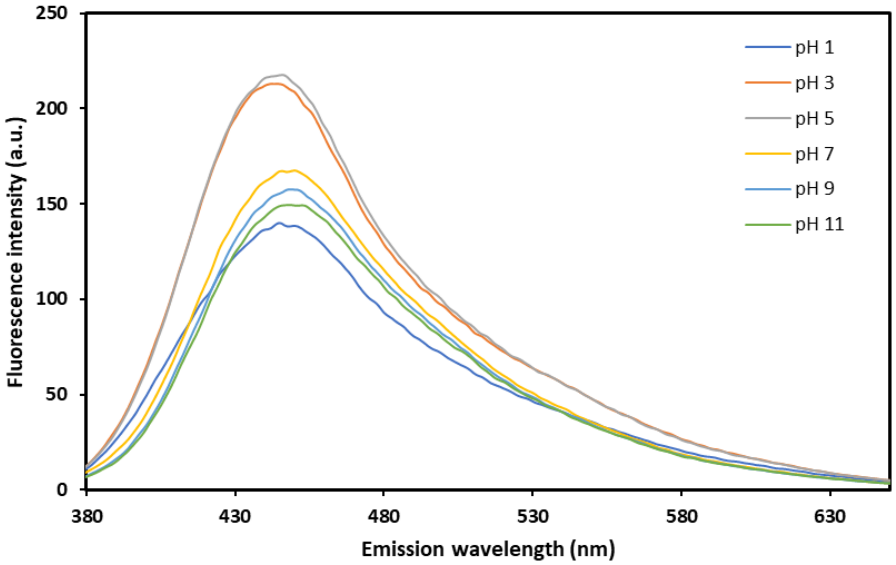

Figure S31. Emission spectra of CDs-AA at different pH environments, using a fixed 360 nm excitation wavelength.

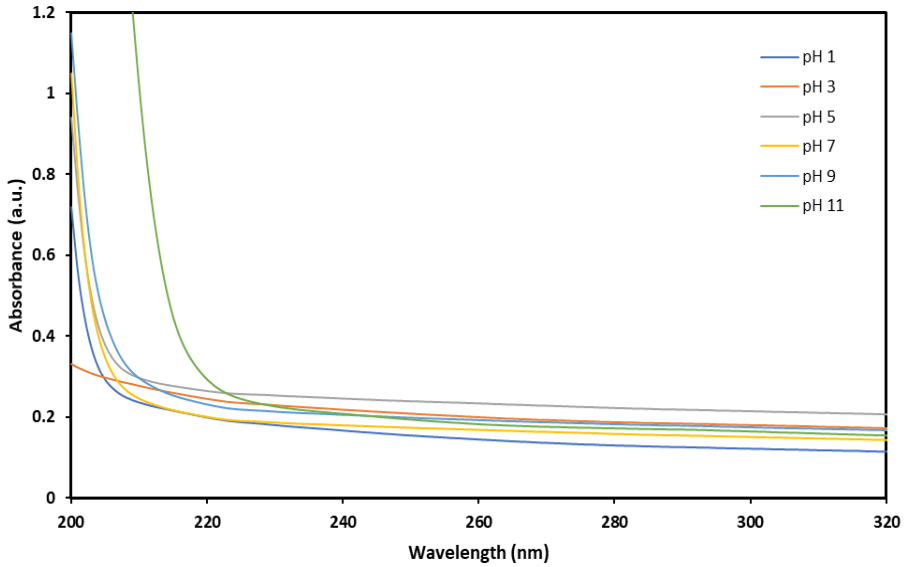

Figure S32. UV-Vis spectra of CDs-RT at different pH environments.

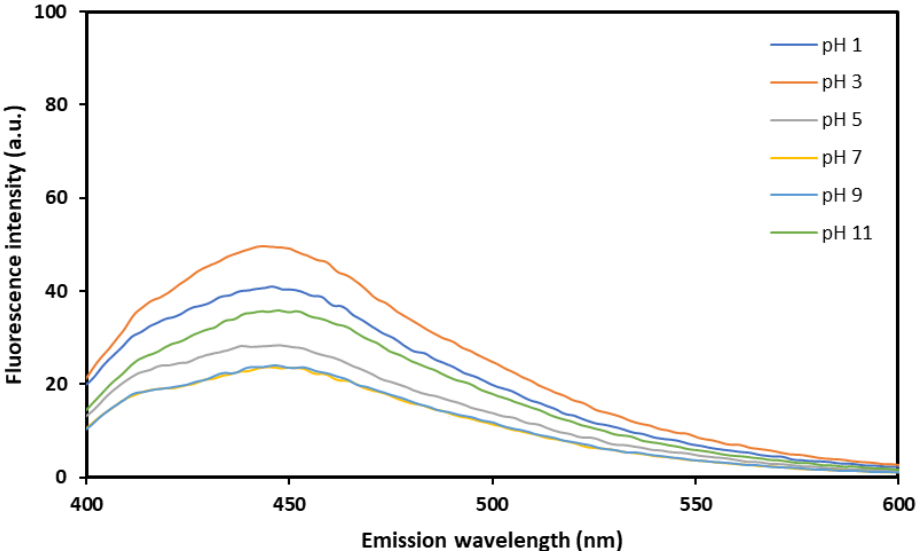

Figure S33. Emission spectra of CDs-RT at different pH environments, using a fixed 360 nm excitation wavelength.

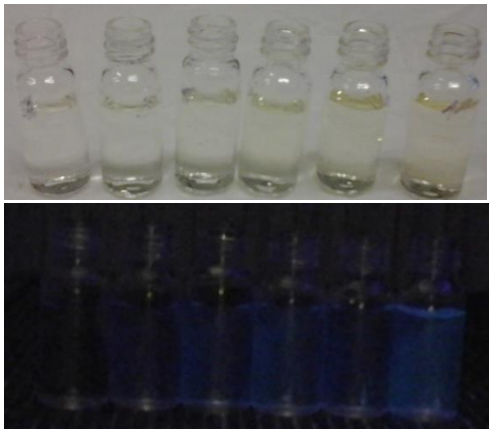

Figure S34. Photographs of CDs-FA at different pH environments at ambient light and under 366 nm excitation. From left to right: pH 1,3,5,7,9 and 11.

Figure S35. Photographs of CDs-AA at different pH environments at ambient light and under 366 nm excitation. From left to right: pH 1,3,5,7,9 and 11.

Figure S36. Photographs of CDs-RT at different pH environments at ambient light and under 366 nm excitation. From left to right: pH 1,3,5,7,9 and 11.

1.6 CDs-PAMAM Interaction (Emission and Photographs)

The following are the results from CDs-PAMAM interaction, comprising the emission spectra for the different ratios used and photographs at ambient and 366 nm excitation (figures S37-S41).

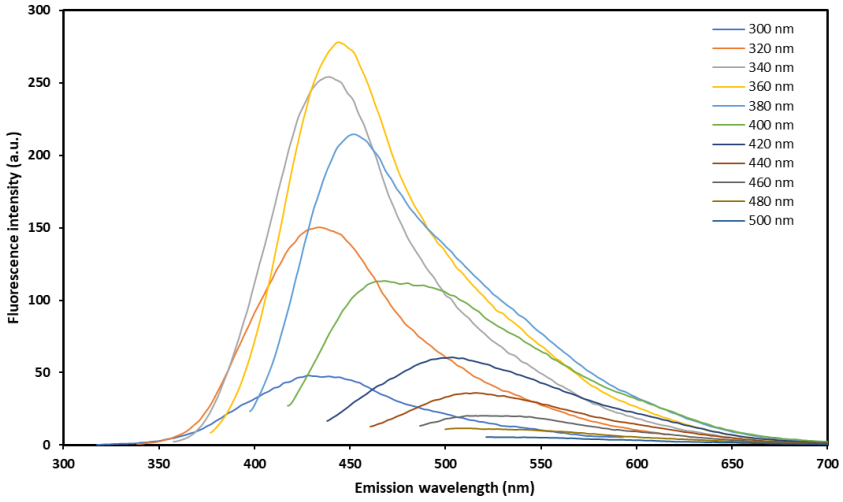

Figure S37. CDs-AA emission spectra using 300-500 nm excitation, with 20 nm increments.

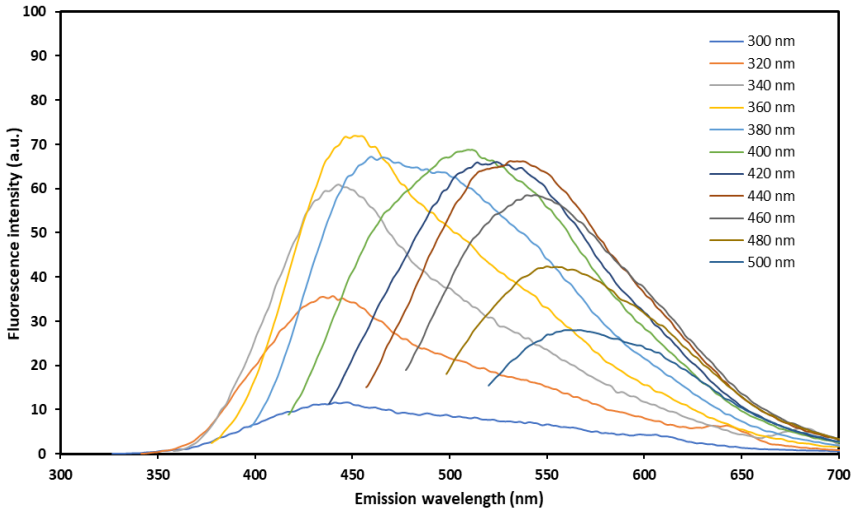

Figure S38. CDs-PAMAM-NH_2 1:1 emission spectra using 300-500 nm excitation, with 20 nm increments.

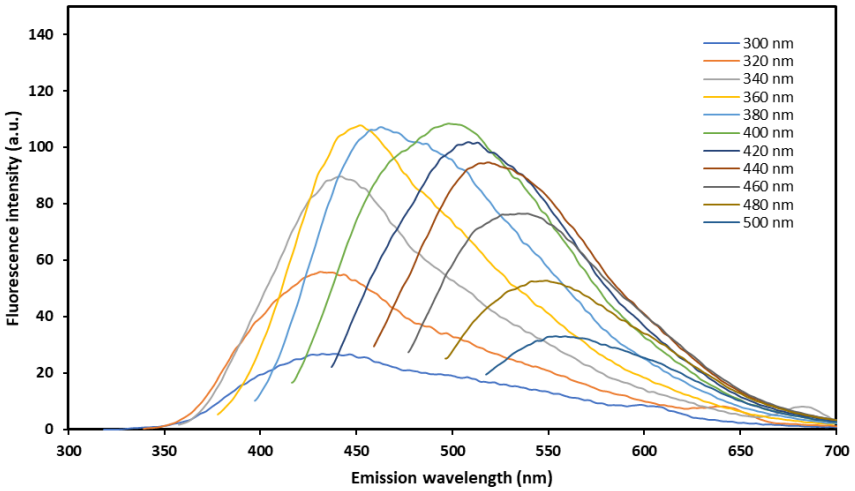

Figure S39. CDs-PAMAM-NH_2 1:2 emission spectra using 300-500 nm excitation, with 20 nm increments.

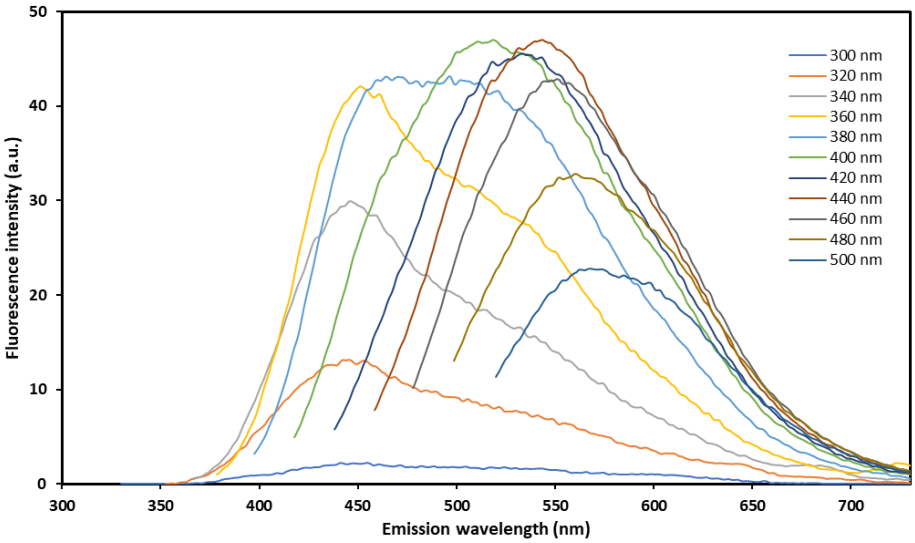

Figure S40. CDs-PAMAM-NH_2 2:1 emission spectra using 300-500 nm excitation, with 20 nm increments.

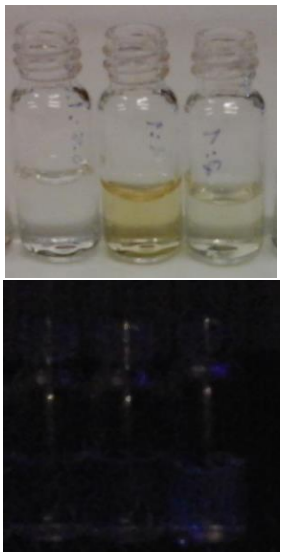

Figure S41. Photographs of CDs-PAMAM-NH_2 interaction at ambient light and after 360 nm excitation. From left to right: 1:1, 2:1 and 1:2 ratios.

2. Theory

Lastly, the instrumentation theory used for the work is presented. This section contains principles of UV-Vis and Fluorescence Spectroscopy, Infra-red Spectroscopy, Dynamic light scattering, NMR Spectroscopy, and TEM.

2.1 Spectroscopy and UV-Vis Spectroscopy

The electromagnetic spectrum is the interval of all possible electromagnetic radiation. The spectrum goes from the low-frequency waves (radio waves) to the high-frequency waves (gamma-rays). In the electromagnetic spectrum, there are distinct types of energy, *e.g.* radio waves, microwaves, infrared, visible, ultra-violet, x-rays, gamma-rays, and even cosmic rays.

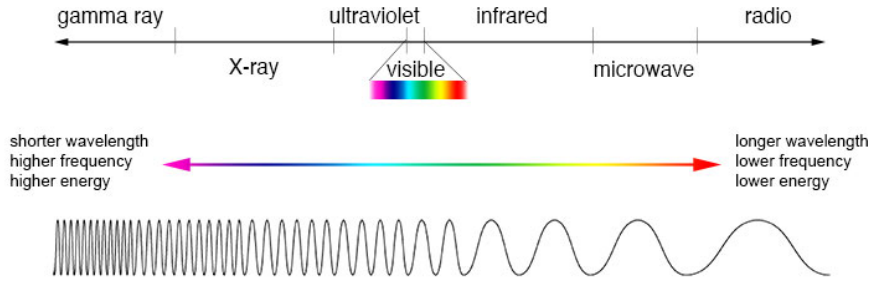

Figure S42. Illustration of an electromagnetic spectrum.

Spectroscopy is a term used for the interaction between matter and the electromagnetic radiation. As mentioned above, there are diverse types of energy, and according to its quantity, it produces a certain action into mater. The radio waves are responsible for nuclear spin transitions, the microwave radiation for the rotational movement, infrared produces molecular vibrations, ultraviolet triggers electronic transitions, and lastly, X-rays ionize matter[2].

Ultraviolet-visible spectroscopy refers to a spectroscopic technique that measures the absorption between the ultraviolet-visible range and is guided by the principle of electronic transitions.

The UV-Vis spectrophotometer is the apparatus used to measure the absorption of UV-vis radiation by a material. It is composed by the following components: lamp, monochromator, sample holder, detector, and recorder. A lamp of deuterium and tungsten are used to irradiate the sample, one responsible for the ultraviolet light and the other for the UV-visible rays, and the monochromator acts as a filter and selects gradually the bands of radiation intended to be used. Once the radiation hits the sample, a detector will be used to amplify the signal and to measure the difference between the transmitted light of the sample and the incident beam, with the further registration of the information[2].

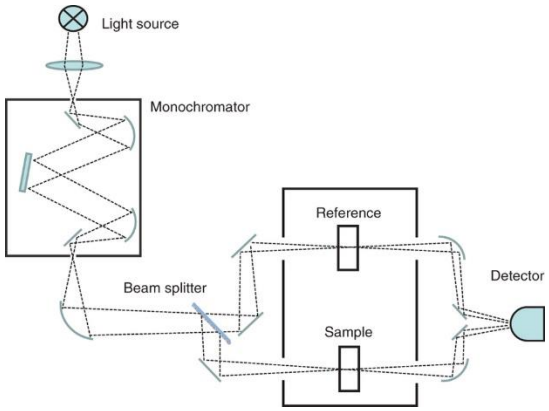

Figure S43. Schematic representation of components of a UV-Vis spectrophotometer[2].

UV-Vis Spectroscopy allows the quantitative analysis of a sample, which is based on the measurement of the absorbance. The Beer-Lambert rule is a law commonly applied for this type of analysis, and it is guided by the equation: $A = \varepsilon bc$, where ε is the molar absorptivity, b is the beam path and c, the concentration of the sample. The law relates the absorption of light by a material with the concentration of this in solution[2].

The UV-vis spectra are normally registered by absorbance vs. wavelength, but they can also be presented as molar absorptivity vs. wavelength. When analysing an absorption spectrum, it is important to have a few terms well clear. A chromophore is a group that carries a certain level of unsaturation (*e.g.,* C=C and C=O) as well as conjugated or non-conjugated systems; the chromophore is responsible for the colour of the molecule. An auxochrome is a group of atoms on a molecule responsible for the intensification of the colour, by modifying the ability of the chromophore to absorb light. Often, these groups (*e.g.*, OH and -NH_2) hold a pair of unbounded electrons and when connected to the chromophore change the wavelength of absorption as well as the absorbance[2].

2.2 Fluorescence Spectroscopy

Luminescence is a designation used to describe the emission of light by a substance due to the existence of excited electronic states created by the different physical stimulus, for instance: absorption of light, mechanical friction, or chemical action. Luminescence can be divided into two groups: fluorescence and phosphorescence.

Fluorescence is the capacity of a material to emit light after absorbing radiation from the electromagnetic spectrum. Whereas phosphorescence is another type of light emission, that arises due to the "forbidden" energy state transitions in quantum mechanics, resulting in slow light emission. Fluorescence and phosphorescence can be explained by the Jablonski diagram (figure S44), an electron is often in his ground state (lowest level of energy) when absorbs light goes to higher levels of energy (the excited state). In the excited state, the electrons lose energy through an internal conversion process; electron relaxation arises due to the interaction with the surrounding molecules (dissipation of energy by heat or vibration), when the electron returns to the ground state emits light, the so-called fluorescence. While phosphorescence, electrons in the excited state can undergo a spin conversion, going from an excited singlet state to a triplet state, this is called intersystem crossing. Since the transition from a triplet to a singlet state is "forbidden", the process of light emission does not occur immediately. Another remark from the Jablonski diagram is the singularity labeled as Stokes shift; this concept says that the energy of emission is smaller than the energy of absorption, it´s associated with the process of internal conversion, due to the rapid decay to the lowest vibrational state of S_1, solvent effects and the decay to higher vibrational levels of S_0, resulting in energy loss. Subsequently, the emission wavelength is always higher than the excitation wavelength[3].

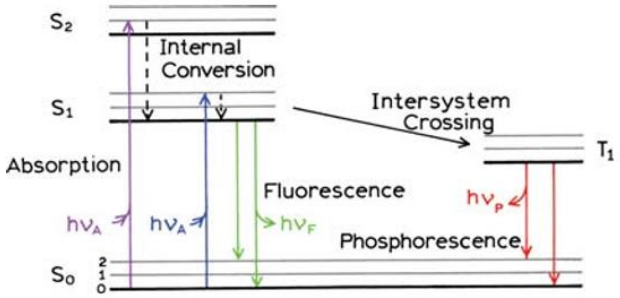

Figure S44. The Jablonski diagram.
The fluorescence and phosphorescence process[3].

The success of a fluorophore depends on two crucial characteristics, the quantum yield (QY) and the fluorescence lifetime. The QY is the number of emitted photons divided by the relative number of absorbed

photons. The fluorescence lifetime is the average time that a molecule spends in the excited state before return to the ground state. The higher the value of quantum yields the higher it's fluorescence intensity.

Additionally, another important aspect when dealing with fluorescence is the quenching effect. The quenching effect is a decrease in the fluorescence intensity, and there are two distinct types of quenching: collisional quenching and static quenching. The collisional quenching happens by a diversity of reasons: collisions with the surrounding particles, absorption of light by other molecules, and formation of complexes. It is described by the Stern-Volmer equation:

$$\frac{F_0}{F} = 1 + K[Q] = 1 + k_q \tau_0 [Q]$$

Where F_0, is fluorescence intensity without the quencher and F, the fluorescence intensity with the quencher, K stands for Stern-Volmer quenching constant, k_q is the bimolecular quenching constant, τ_o is the unquenched lifetime, and *[Q]* is the concentration of the quencher. Some chemical species can perform as quenchers, *e.g.,* oxygen, halogens, and amines. The quenching mechanism is unclear, but an electron transfer process, spin-orbital coupling, and intersystem crossing of the triplet state emerge as great possibilities.

Beyond collisional quenching, there is the static quenching, and it is mentioned as a process of formation of non-fluorescent species by conjugation with the quenchers, and it does not rely on diffusion or molecular collisions. An additional aspect is that intensity decreases can also occur by competition between another fluorescent molecule for light absorption.

Fluorescence spectroscopy is used to measure the emission of light by a substance. The fluorescence spectrometer is the apparatus used to record the emission. Consists on the following components: a light source, excitation/emission monochromator, sample holder, and detector. The importance of each component in the fluorescence spectrometer will be discussed in detail.

Light sources are important because they provide radiation and diverse types of lamps are used for instance: xenon, mercury, and quartz-tungsten lamps, among others. Xenon lamps are the most broadly used, being versatile and providing a relatively continuous light output from 250-700 nm.

Monochromators are vital components that mechanically select the excitation wavelength. The conversion of white light into the coloured light is a process accomplished using a prism or a diffraction grating. The fluorescence spectrometer uses a diffraction grating. The slit is another vital constituent, changing its width allows the control of light be hitting the cuvette.

Light can be in the polarized or unpolarized form, the major difference is that polarized light has the electric field oscillating in one direction, while the other has the electric field oscillating in all directions, and so the polarized light needs to be used to guarantee the same type of light passes through the cuvette and subsequently being detected, and for that the fluorescence spectrometer contains a polarizer[3].

In a fluorescence spectrometer, the sample is irradiated by a light source, a Xenon lamp. The diffraction grafting, or prism will convert white light into coloured light, and the excitation slit, depending on the width will focus the beam with a certain wavelength. The polarizer will select the polarized light from the unpolarized light and ensure that the sample is irradiated only with light in one direction. The emitted light is measured at an angle of 90 degrees about the excitation beam and thus, avoiding the interference of transmitted light (remaining light of excitation). A second monochromator is positioned to catch the emitted light and picks the complementary wavelength of emission.

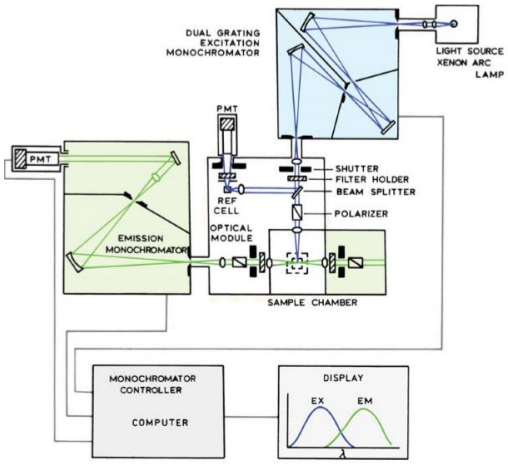

Figure S45. Schematic representation of the components of a Fluorescence Spectrometer[3].

2.3 Infra-Red Spectroscopy

Infrared Spectroscopy is an analytical tool used typically to identify the functional groups of organic compounds. Infrared radiation, when absorbed by matter, triggers molecular vibration. Molecular vibrations are seen in an IR spectrum only if they change the dipolar moment of a given molecule. When a group of atoms vibrates, the dipolar moment changes and the bigger the alteration, the greater is the intensity of absorption. Every functional group in a molecule has their specific amount of energy to vibrate, and thus the differences in absorption allow the identification of different functional groups. The stretching and the bending vibrations are two vibration forms. A given group of atoms can stretch in the symmetrical or asymmetrical form, and the bending vibrations can be in-plane or out-of-plane. In-plane vibrations are rocking and scissoring whereas the out-of-plane are the wagging and twisting forms. Stretching vibrations occur at high energy levels, meaning higher wavenumbers, while the bending vibrations happen at low energy levels, meaning lower wavenumbers[4].

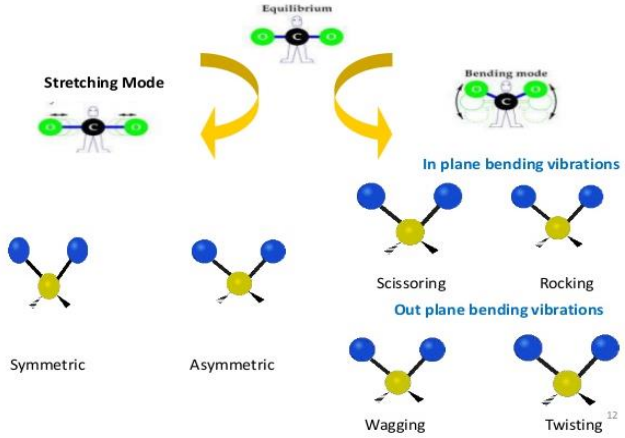

Figure S46. Types of vibration in IR spectroscopy[4].

An infrared spectrum is a graphical representation corresponding to the % of transmittance as a function of wavenumber. The wavenumber is used to represent the x-axis of an IR spectrum since it is directly proportional to the energy, so the higher the energy, the greater the wavenumber. An infrared spectrum can be divided into two main regions: the functional group and the finger print region. Importantly, there are characteristic areas in the spectrum that correspond to certain functional groups. The most common functional groups are: -OH (3600 cm^{-1}), N-H (3400 cm^{-1}), C=O (1715 cm^{-1}), C=C (1650 cm^{-1}) and C-O (1100 cm^{-1}), and the presence of a certain functional group is as important as its absence[4].

Infrared spectroscopy is used to measure the absorption of energy by functional groups in an organic molecule. The FT-IR spectrometer is composed by a radiation source, interferometer, sample compartment, detector, amplifier, and a displayer. The source of IR radiation comes from an inert solid that is electrically heated to emit infrared light. The Michelson interferometer is the core of the IR spectroscopy, and it is used to split one beam of light into two so that the paths of the beams are different, and then the interferometer recombines the beams towards the detector. Lastly, the signal detected is amplified and converted from raw data to an actual IR spectrum using the Fourier transform (mathematical process)[4].

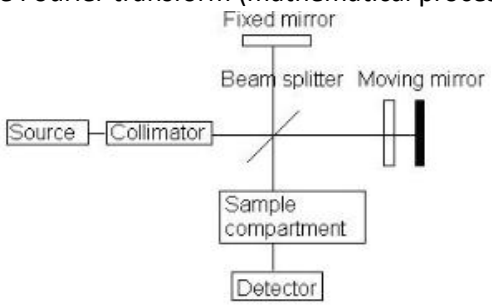

Figure S47. Infrared spectrometer diagram[93].

2.4 Dynamic Light Scattering

Dynamic Light Scattering or Photon Correlation Spectroscopy is an analytical tool used to measure the hydrodynamic size and the ξ-potential of particles in suspension. It is composed by the following components: laser beam, sample holder, a detector (photomultiplier), and an autocorrelator.

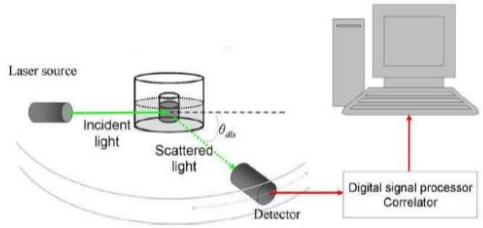

Figure S48. Schematic illustration of dynamic light scattering.

In a typical DLS measurement, a laser beam composed by, *e.g.* He-Ne is activated towards the cuvette with the particles in suspension, particles move randomly at different speeds, the larger particles will move slowly while the smaller faster. The particles, when hit by the laser beam, will scatter light, with further detection and the processing of information occurring in an autocorrelator. The autocorrelator compares the signal (intensity vs. time) with its signal but at a delay time, and when the two are superimposed a perfect correlation is achieved, once the signals start to separate, the correlation decreases exponentially. The value of the decay will be used to calculate the diffusion coefficient of the particle. Afterward, the equation of Stokes-Einstein: $D=K_BT/6\pi\eta R_H$ will be used to determine the hydrodynamic diameter of the particle. In the Stokes-Einstein equation, D means diffusion coefficient, K_B the Boltzmann constant, η is the viscosity of the suspension, and R_H is the hydrodynamic radius of the particle[5].

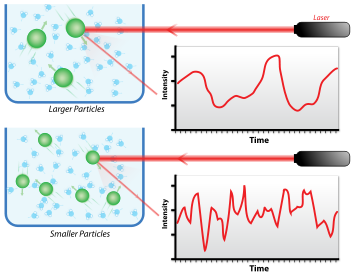

Figure S49. Schematic representation of the signal detected after being scattered by the particles[5].

The ξ-potential is a designation used to measure the stability of the particles in suspension. Ions are often present in liquids when particles with a certain charge are in solution, ions of the opposite charge will be attracted to them, the ones closely attracted are in the diffuse layer, the Stern potential. Near to the first layer of ions, will remain other ions interacting with the 1st layer, the region is known as the slipping plane, and it is called the ξ-potential. The value of the zeta-potential is a key indicator of the stability of the particles and values between ± 5 mV are indicative of rapid flocculation, whereas values above ± 30 mV are suggestive of favourable stability for the particles[5].

The ξ-potential is measured by applying an electric field across the dispersion, particles with a certain charge will migrate with a certain speed to the opposite direction of the field, the velocity is directly proportional to the ξ-potential[6].

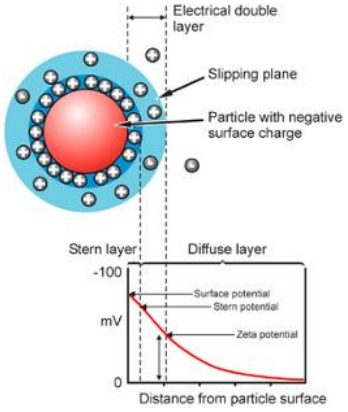

Figure S50. ξ-potential schematic diagram[6].

2.5 NMR Spectroscopy

Nuclear magnetic resonance spectroscopy is one of the most powerful tools to determine the chemical structure of organic compounds. The principles of NMR spectroscopy can be explained by quantum mechanisms and classical physics.

Subatomic particles such as: electrons, protons, and neutrons can be imagined as spinning in their axes, and atoms, *e.g.* ^{12}C have paired spins and so meaning no overall spin. The spin of the nuclei can be determined by knowing the number of protons and neutrons. Atoms can behave like magnets; they just need an odd number of protons or neutrons. Due to its charge and spin, the nuclei can behave as a magnet, and the proton´s spin can be oriented either in the lower or higher state of energy, known as the α-state and β-state, respectively. Once an external magnetic field is applied, the nuclei tend to orient themselves so that the lower state of energy prevails. After radiation in the radiofrequency is used to change the position, and the absorption of energy during this change marks the basis of NMR[7].

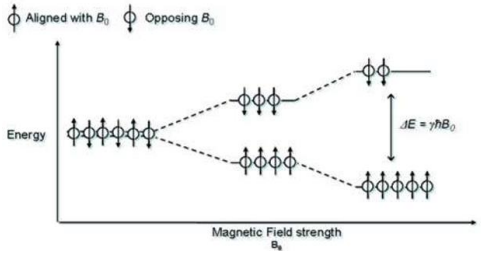

Figure S51. Schematic illustration of the spin alignment as a function of magnetic field strength[7].

Magnetic shielding is a central concept in NMR spectroscopy, and if all protons absorbed the same amount of energy in a magnetic field, not much information is obtained. Nonetheless, protons are surrounded by electrons, acting as shields to protect the protons, from an external magnetic field. The circulating electrons

oppose the external magnetic field by creating their induced magnetic field. The protons in a molecule, depending on their chemical environment are said to be shielded at various levels. For example, the molecule: CH_3-OH has 4 protons, three of them are more shielded (-CH_3 group) thus absorbing at higher fields, whereas the O-H proton is less shielded and so, absorbing at lower fields. In a typical NMR spectrum, this molecule would present two signals, one with a lower chemical shift (-CH_3) and the other with a higher chemical shift (-OH)[7].

In a typical NMR spectrum, the number of signals composing the spectrum shows how many kinds of protons are present, the location of the signals shows how shielded or deshielded the protons are. The intensity of the signals shows the number of protons on the adjacent atoms. The chemical shifts in the NMR spectrum are expressed in parts per million (ppm).

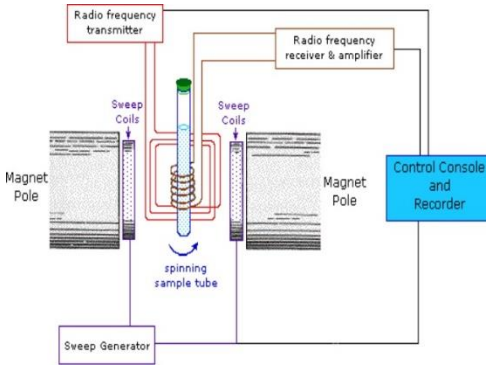

Figure S52. Scheme of the components of an NMR apparatus[7].

2.6 TEM

Transmission electron microscopy is a powerful microscopic technique used to visualize the topography, morphology, size, and the crystallographic nature of materials. This technique uses a beam of electrons emitted towards the sample. The instrument uses a source of illumination that consists of a filament or a cathode that emit electrons at the top of the cylindrical column. Since electrons can be scattered by collisions with air molecules, air must be pumped out by vacuum. The electrons generated are then accelerated towards the sample by using a nearby anode, electrons that pass through the sample are said to be transmitted and are used to generate an image. The limit of resolution of this technique is around 0.2 nm, and in some special conditions, it´s even possible to see an individual atom[8].

The sample preparation of many materials requires different procedures such as fixation, staining, dehydration, embedding, and sectioning.

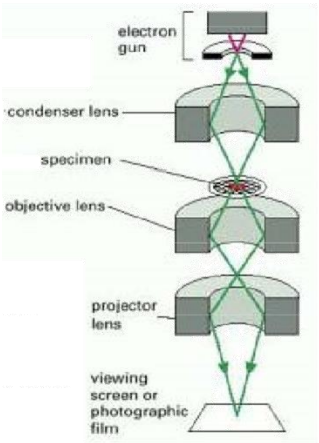

Figure S53. Schematic representation of the interior of a TEM machine[8].

3. Supporting References

1. Allen, M.W.; Measurement of Fluorescence Quantum Yields. **2010.** Thermo Fischer Scientific, Madison, WI, USA
2. Christian, D.G. Analytical Chemistry. 4th Edition, John Wiley & Sons, New York, 2009 ISBN: 978-0471885740
3. Lacowicz, J.R. Principles of Fluorescence Spectroscopy. 3rd Edition. Springer, New York, NY, USA 2006 ISBN 978-0-387-31278-1
4. George, W.O.; McIntyre, P.S.; Mowhorpe, D.J.; Infrared Spectroscopy. John Wiley & Sons, United Kingdom. 1991 ISBN: 9780471913832
5. Zetasizer Nano Series User Manual, Malvern Instruments, Ltd, United Kingdom, 2004
6. Pecora, R. Dynamic Light Scattering measurement of nanometer particles in liquids. *J. Nanopart. Res.* **2000**, *2*, 123-131 https://doi.org/10.1023/A:1010067107182
7. Gunther, H. NMR Spectroscopy, John Wiley & Sons, New York, 1996
8. Sigle, W.; Analytical Transmission Electron Microscopy. *Annu. Rev. Mater. Res*. **2005**, *35*, 239-314 https://doi.org/10.1146/annurev.matsci.35.102303.091623

PEst-OE/QUI/UI0674/2013

M1420-01-0145-FEDER-000005

Centro de Química da Madeira - CQM^{+} (Madeira 14-20)

Cofinanciado por: